Structural and functional interaction between domains in CFTR

Dissertation

submitted for the degree of
Doctor of Natural Sciences (Dr. rer. nat.)

presented by

Inna Jakšeković

at the

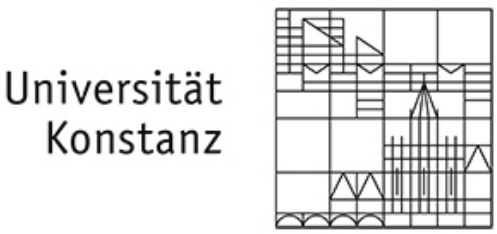

Faculty of Sciences
Department of Biology

First referee: Prof. Dr. H.-J. Apell
Second referee: Prof. Dr. D. C. Gadsby

Date of the oral examination: 17.11.2014

Contents

Abstract

This work is related to structural and functional aspects of cystic fibrosis transmembrane conductance regulator (CFTR), a chloride channel whose dysfunction causes cystic fibrosis. The aim of the project was to test predictions made by structural models for CFTR about interactions between amino acid residues during the gating cycle.

The residues hypothesized to interact were studied with a cysteine-specific crosslinking approach: after their mutation to cysteine, the properties of resulting mutant CFTR were assayed upon the treatment with the cysteine-specific crosslinker bismaleimidoethane (BMOE).

Electrophysiological experiments suggest crosslinking between residues T164 and L1059, I266 and A969 (supported by biochemical evidence), and between G971 and S1049, implying a possible intramolecular interaction these residues are involved in. Crosslinking between F508C and R1070C might occur, too. Experiments with the pair G178/V260 did not give evidence of possible crosslinking between these residues or conformational changes of CFTR leading to the channel closure upon the crosslinker influence.

During erlectrophysiological experiments, intermittent fluctuations of the whole cell conductance were observed upon sulfhydryl-specific reagents, which could be related to possible activation of Ca^{2+}-dependent Cl^- channels (CaCC).

The approach applied in this work can provide evidence of structural proximity and functional interaction of amino acid residues belonging to different structural units of a protein, which information is essential for planning of future experiments and determining of drug discovery targets.

Zusammenfassung

Diese Arbeit beschäftigt sich mit strukturellen und funktionellen Aspekten des Cystic Fibrosis Transmembrane Conductance Regulators (CFTR), eines Chloridkanals, dessen Dysfunktion Mukoviszidose verursacht. Das Ziel des Forschungsprojekts war es, die Vorhersagen von Strukturmodellen über Wechselwirkungen zwischen Aminosäureresten in CFTR während des Gating-Zyklus zu testen.

Die Paare von Aminosäuren, die vermutlich an solchen Wechselwirkungen beteiligt sind, wurden mithilfe der Cystein-spezifischen Vernetzung untersucht: nach der Mutation zum Cystein wurden die Eigenschaften der resultierenden CFTR Mutanten unter der Behandlung des Cystein-spezifischen Vernetzungsmittels BMOE beobachtet.

Elektrophysiologische Experimente lassen eine Vernetzungsreaktion für die Paare von Aminosäuren T164/L1059, I266/A969 (unterstützt durch biochemische Beweise) und G971/S1049 vermuten, was eine mögliche intramolekulare Wechselwirkung zwischen diesen Aminosäuren impliziert. Experimente mit Aminosäureresten F508/R1070 lassen ebenso vermuten, dass die Vernetzungsreaktion auch zwischen F508C und R1070C stattfinden könnte. Bei Mutanten G178C und V260C scheint das Vernetzungsmittel keinen Einfluss auf Konformationsänderungen zu haben, die zur Kanalschließung führen.

Während elektrophysiologischen Messungen haben sulfhydrylspezifische Reagenzien eine kurze Schwankung der Zellleitfähigkeit verursacht, die mit einer möglichen Aktivierung von Ca^{2+}-abhängigen Cl^{-}-Kanälen (CACC) in Verbindung stehen könnte.

Die verwendete Vorgehensweise kann strukturelle Nähe und funktionelle Wechselwirkung zwischen Aminosäuren aus verschiedenen Struktureinheiten eines Proteins nachweisen, was entscheidende Information für die Planung von zukünftigen Experimenten und zur Zielbestimmung der Wirkstoffforschung liefert.

List of figures

List of abbreviations

ΔF508	deletion of phenylalanine in position 508
ABC	ATP-binding cassette
APS	ammonium persulfate
BMOE	bismaleimidoethane
CAVD	congenital absence of the vas deferens
CF	cystic fibrosis
CFTR	cystic fibrosis transmembrane conductance regulator
DMSO	dimethyl sulfoxide
ECL	extracellular loop
endoH	endoglycosidase H
ER	endoplasmic reticulum
HEPES	4-(2-hydroxyethyl)-1-piperazineethanesulfonic acid
ICL	intracellular loop
LB	lysogeny broth
NBD	nucleotide binding domain
PBS	phosphate buffered saline
PKA	cAMP-dependent protein kinase
PMSF	phenylmethanesulfonylfluoride
PVDF	polyvinylidene difluoride

RPM	revolution per minute
TEMED	tetramethylethylenediamine
TMD	transmembrane domain
wt	wild type

1. Introduction

1.1 CFTR and its physiological role

The cystic fibrosis transmembrane conductance regulator (CFTR) is a protein whose malfunction leads to cystic fibrosis (CF), a human autosomal-recessive hereditary disease causing progressive disability and early death.

The name *cystic fibrosis* refers to the characteristic 'fibrosis' (tissue scarring) and cyst formation within the pancreas, first described in the 1930s by Dorothy Andersen (Andersen 1938). Another name for CF, mucoviscidosis, was given in 1945 by Sidney Farber (Farber 1945), who recognized the role of sticky mucus as a cause of many of the symptoms (lat. *mucus* and *viscidus*, viscous). CF is most common in populations of European descent, where it occurs in about 1 in 3,200 newborns (Hamosh, et al. 1998), but is found in all ethnic groups (Brown and Schwind 1999). CF is linked to a single specific gene, which encodes the CFTR protein and is located on chromosome 7. To date, over one thousand mutations of the CFTR gene have been described; approximately 1 of 25 Europeans is a carrier of a CF causing mutation, and the most common one is the loss of phenylalanine in position 508 (ΔF508 mutation).

CFTR is expressed in epithelial cells of many organs, including the respiratory and digestive tracts (Zeitlin, et al. 1992), and also in cardiomyocytes (Levesque, et al. 1992), mastocytes (Kulka, et al. 2002), endothelia (Tousson, et al. 1998) and some other cells. As a chloride channel, CFTR delivers chloride anions out of the cell down their electrochemical gradient. This ion flow enriches secretion of exocrine cells with chloride and therefore with water, which is crucial for the normal gland function and the proper condition of their secretion. Mutations of CF gene alter the CFTR folding; therefore, the protein fails to be delivered to the plasma membrane and degrades more quickly (Cheng, Gregory, et al. 1990). In absence of CFTR, the impaired chloride ion flow across

membranes leads to abnormally viscous secretion, which obstructs the gland ducts and lead to developing of CF symptoms (Thomas, Qu und Pedersen 1995, Qu, Strickland und Thomas 1997). At the moment, there is no cure for CF, and most individuals with CF die young from lung infection and failure, although modern treatment increased the life expectancy from less than 10 years in the 1960s to an average of 30 to 40 years nowadays.

Beside CF, impaired CFTR function is associated with other disorders, such as congenital absence of the vas deferens (CAVD), disseminated bronchoectasis and chronic pancreatitis (Welsh, et al. 1995). Hyperactive CFTR is responsible for polycystic kidney disease and secretory diarrhoea (Sullivan, Wallace and Grantham 1998, Gabriel, et al. 1994).

Aside from the chloride anions, this channel is also known to be able to transport bicarbonate (Tang, Fatehi und Linsdell 2009) and thiocyanate (Fragoso, et al. 2004). Additionally to its channel function, CFTR is reported to regulate other proteins, such as the epithelial sodium channel ENaC (Stutts, et al. 1995), sodium-bicarbonate transporters (Shumaker, et al. 1999), and aquaporins (Cheung, et al. 2003).

It was first uncertain whether CFTR is a chloride channel, or whether it functions only to regulate such a chloride channel; hence the name: cystic fibrosis transmembrane conductance regulator. However, studies of recombinant CFTR soon provided compelling evidence that CFTR is an apical membrane chloride channel. First, CFTR was expressed in cells that do not normally contain chloride channels (Anderson, Rich, et al. 1991, Bear, Duguay, et al. 1991), and expression of CFTR generated a chloride current activated by cAMP agonists. Second, similarity was shown between the biophysical properties and regulation of chloride currents in cells expressing recombinant CFTR, in epithelial cells expressing endogenous CFTR, in the apical membrane of secretory epithelia (Hanrahan 1993). Third, mutation of specific residues in CFTR altered the anion selectivity sequence of chloride currents (Anderson, Gregory, et al. 1991). Fourth, when recombinant CFTR was purified and reconstituted into planar lipid bilayers, it formed chloride channels with properties essentially identical to those in native epithelia (Bear, Li, et al. 1992). The causal relationship between CFTR mutation and defective chloride transport in CF was

confirmed later by introduction of intact CFTR genes to the epithelial cells of CF patients, which corrected chloride conductivity (Rich, Anderson, et al. 1990).

1.2 CFTR as an ABC protein

1.2.1 ABC transporters superfamily

The CFTR gene was discovered and sequenced in 1989 (Riordan, et al. 1989). The primary amino acid sequence of CFTR identified it as a member of the ATP-binding cassette (ABC) transporters superfamily (Hyde, et al. 1990), which members utilize the energy of ATP hydrolysis to transport substrates across cell membranes, show similar domain organization and have common structural elements (Higgins 1992, Childs and Ling 1994, Dean and Allikmets 1995).

The term "ABC transporters" was introduced in 1992 (Higgins 1992). The characteristic feature of these proteins is a structural element called "ATP-binding cassette": highly conserved through the superfamily cytoplasmic domains, which bind ATP (nucleotide-binding domains, NBDs). Homology of NBDs through the superfamily allows identication of new ABC proteins based on their amino acid sequence.

The ABC transporters superfamily is one of the largest and most ancient protein families, widely represented in prokaryotes and eukaryotes (Jones and George 2004, Ponte-Sucre 2009). Thousands of members are known to date, and 48 of them in humans (Dean and Annilo 2005), which ones are divided into seven subfamilies (A-G), according to the phylogenetic analysis (Dean 2002). CFTR belongs to the C subfamily and is named ABCC7.

ABC proteines utilize the energy of ATP hydrolysis to transport various substrates across extra- and intracellular membranes, such as metabolites and drugs, or carry out non-

transport-related processes such as translation of RNA and DNA repair, and are involved in development of such conditions as multiple drugs resistance and hereditary diseases (Davidson, et al. 2008, Goffeau, Hertogh und Baret 2004).

ABC transporters are divided into subtypes based on their function. Importers, which are present only in prokaryotes, deliver substrates into the cell. These substrates include ions, amino acids, peptides, sugars, and other cell nutrients. Exporters, which are present in both prokaryotes and eukaryotes, transport substrate, such as toxins and drugs, from the cell. Another subgroup of ABC proteins is involved in translation and DNA repair processes (Davidson, et al. 2008). It is accepted that ABC transporters have four common domains: two transmembrane domains (TMDs) and two cytoplasmic nucleotide-binding domains (NBDs) (Figure 1).

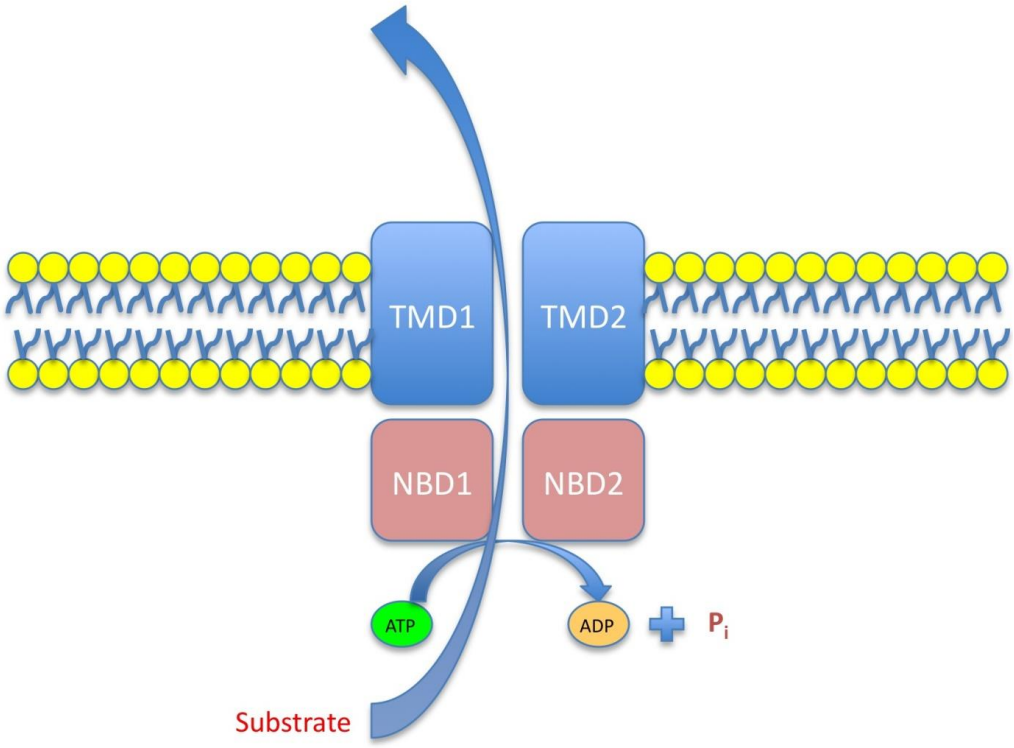

Figure 1. Domain structure of ABC transporters.

Two transmembrane domains (TMDs) bind and transport a substrate; two nucleotide-binding domains (NBDs) bind and hydrolyze ATP.

TMDs specifically bind a substrate, and NBDs bind and hydrolyze ATP. ATP hydrolysis is coupled to the transport of the substrate, although the exact mechanism of this coupling still remains unclear. NBDs of ABC transporters are homologous throughout the family and have several highly conserved motifs, which participate in processes of ATP binding and hydrolysis.

These motifs (Figure 2) include the nucleotide-binding "P-loop" ("Walker-A" motif), the "ABC signature sequence" (LSGGQ motif, or "C-loop", "Walker-C"), which contacts the nucleotide in the ATP-bound state, the "Walker-B" motif that hydrolyses ATP, the "Q-loop" that is thought to contact the TMD; the "D-loop" that contacts with the opposite NBD, the "A-loop" that participates in the nucleotide binding, and the "switch motif" that contributes catalytic reaction (Hyde, et al. 1990, Zaitseva, et al. 2005, Ambudkar, et al. 2006). TMDs of ABC transporters are highly hydrophobic and consist of multiple membrane-spanning α-helical segments. In CFTR, they form the channel pore. The amino acid sequences of TMDs from different ABC transporters reveal little or no significant similarity.

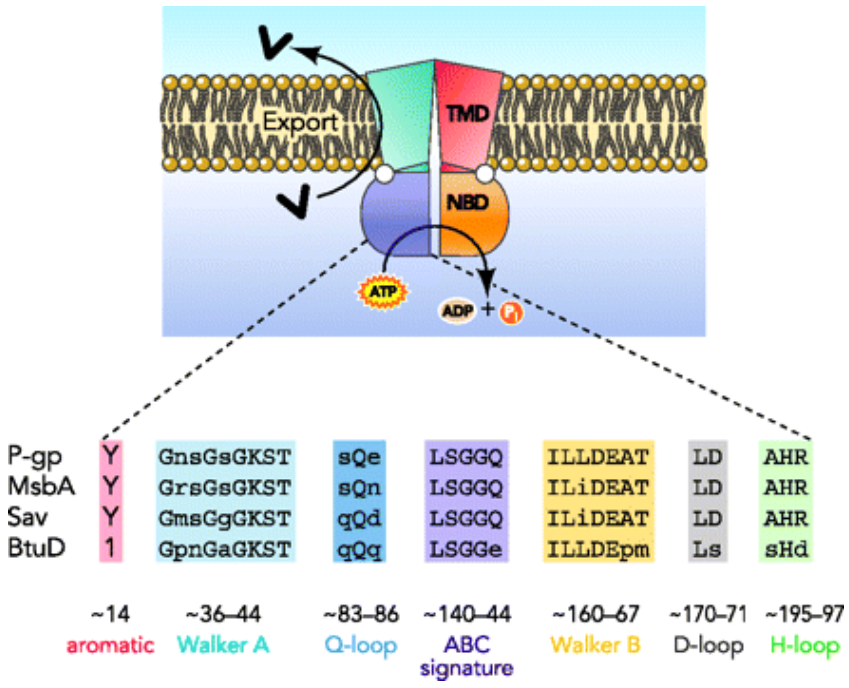

Figure 2. Highly conserved motifs in NBDs of ABC transporters (Linton 2007).

Some ABC transporters have additional domains that serve other specific functions. For example, CFTR is the only member of the family, which has an additional R-domain ("R" stands for "regulatory"). This domain is situated in the cytoplasm, contains multiple phosphorylation sites, and serves a regulatory function (Cheng, Rich, et al. 1991, Rich, Gregory, et al. 1991): gating of CFTR is dependent on phosphorylation of this domain by protein kinase A (PKA) (Anderson, Berger, et al. 1991).

ABC proteins change their conformations during the transport cycle between "inward facing" and "outward facing" (Dawson und Locher 2006, Ward, et al. 2007) (Figure 3). The inward facing conformation exposes the substrate to the intracellular side, and the outward facing conformation to the extracellular side.

In CFTR, the outward- and inward- facing conformations would correspond to the open and closed state of the channel, respectively.

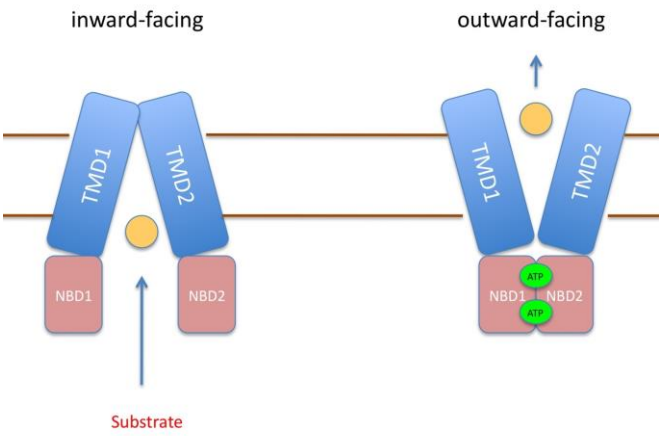

Figure 3. Two conformations of ABC proteins.

The inward facing conformation (left) exposes the substrate to the intracellular side, the outward facing one (right) to the extracellular side. The substrate transport direction is shown for exporters.

The occurance of these two conformations is supported by known X-ray structures of the various ABC transporters, which identified these both orientations of TMDs. The

ATP-bound state appears to be the outward facing, and the nucleotide-free state inward facing (K. Locher 2009, Rees, Johnson und Lewinson 2009). This also supports the idea that ATP binding in NBDs drives conformational changes in TMDs.

1.2.2 Domain structure of CFTR

Five domains of CFTR, four of which are common for all ABC proteins (two TMDs and two NBDs), and the regulatory R-domain are shown on Figure 4.

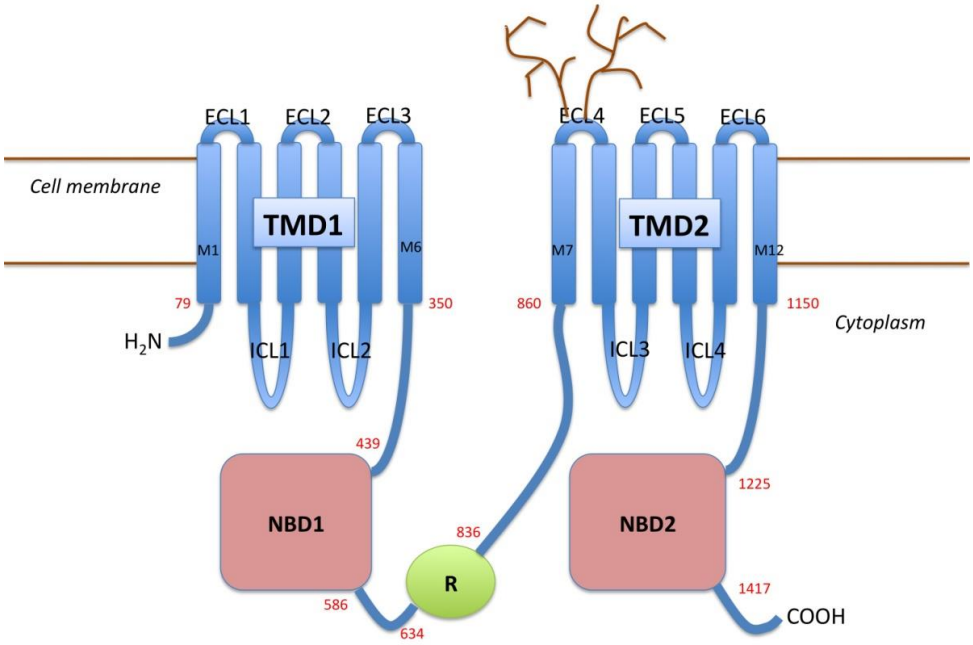

Figure 4. Proposed topology of CFTR domains.

TMDs comprise membrane-spanning α-helices (M1-M12), extracellular (ECLs) and intracellular (ICLs) loops. NBDs and the R-domain are located in the cytoplasm, as well as the N- and C-terminus. Red numbers mark positions of residues corresponding to the originally proposed approximate domain boundaries (Riordan, et al. 1989, Chen, et al. 2001, Cui, et al. 2006).

Each TMD consists of 6 transmembrane helices, three extracellular loops (ECLs) and two intracellular loops (ICLs). ECL4 contains two N-linked glycosylation sites. Each ICL has a single helix, which is parallel to the cell membrane and was suggested to be responsible for the NBD-TMD coupling, therefore it is called “the coupling helix” (Hollenstein, Dawson and Locher, Dawson, Hollenstein and Locher 2007).

Electron crystallography of 2D CFTR crystals revealed its overall architecture (Rosenberg, et al. 2004). However, this protein was refractory to solve its structure using X-ray crystallography, and high-resolution structures are not yet available for the whole CFTR, although such structures were obtained for murine and human NBD1 (Lewis, Buchanan, et al. 2004, Lewis, Zhao, et al. 2005, Thibodeau, et al. 2005, Atwell, et al. 2010, H. A. Lewis, C. Wang and X. Zhao, et al. 2010), and for human NBD2 (DOI:10.2210/pdb3gd7/pdb) and some other members of the ABC transporters, such as P-glycoprotein (Aller, et al. 2009), the bacterial multidrug ABC transporter Sav1866 from *Staphylococcus aureus* (Dawson and Locher 2006), the vitamin B12 transporter BtuCD from *E. coli* (Locher, Lee and Rees 2002), the bacterial ABC lipid flippase MsbA (Ward, et al. 2007).

The lack of a high-resolution structure for CFTR forces to use other approaches to gain structural information about this protein. Possible structures of a protein can be suggested by computer-built homology models, which are based on the known structure of the protein homologues.

Proteins with homologous amino acid sequences show similarity in their three-dimensional structure; therefore, known domain architecture of other ABC transporters can serve as a basis of structural models for CFTR. Such homology models can be used as a tool to generate hypotheses to be tested, and experiments can confirm whether the homology model reflects a real structure of the protein. This strategy has already given insight into the structure and function of CFTR (Mense, et al. 2006, Mendoza und Thomas 2007, Serohijos, et al. 2008, Huang, et al. 2009, Norimatsu, et al. 2012).

Such models for CFTR helped to answer a question prompted by the crystal structure of a bacterial ABC transporter Sav1866 (Dawson und Locher 2006): according to

this structure, the molecular architecture of Sav1866 can be described with a “domain-swap” model (Figure 5 b), where each NBD forms connections with both TMDs. An alternative would be a “side-by-side” model (Figure 5 a), which implies that each NBD interacts with only one TMD of the corresponding side of the molecule.

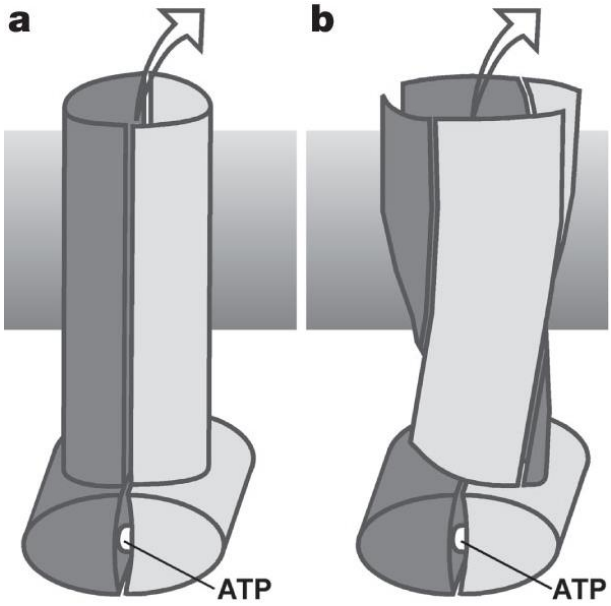

Figure 5. Two proposed models of domain-domain interaction.

Left (a) – “side-by-side” model, right (b) – “domain-swap” model (Dawson and Locher 2006).

The evidence which model corresponds to the domain structure of CFTR was obtained by a crosslinking method, an approach that joins chemically two points of the protein molecule to test whether they are neighboring. A homology model of CFTR based on the known structure of Sav1866 (Figure 6) suggested residues proposed to interact, and biochemical crosslinking experiments confirmed intramolecular contacts of NBDs with ICLs of TMDs from the opposite half of CFTR (Serohijos, et al. 2008, He, et al. 2008), confirming that the domain swapping described by Dawson and Locher also occurs in CFTR.

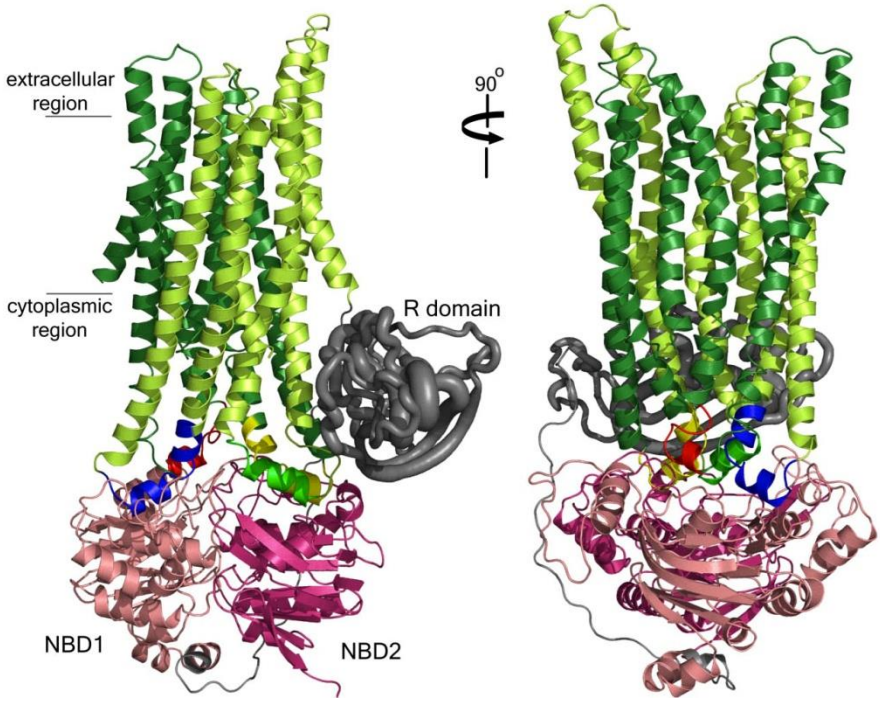

Figure 6. Homology model for CFTR based on the Sav1866 structure (Serohijos, et al. 2008).

Domains are colored: TMD1 dark green, TMD2 light green, NBD1 light red, NBD2 dark red and R-domain grey.

This kind of domain architecture is found in other ABC proteins as well: the crystal structure of the heterodimeric ABC transporter TM287–TM288 (TM287/288) from *Thermotoga maritima* in its inward-facing state (Figure 7) demonstrates that the coupling helices of ICL2 and ICL4 interact with the NBD of the opposite subunit (Hohl, et al. 2012).

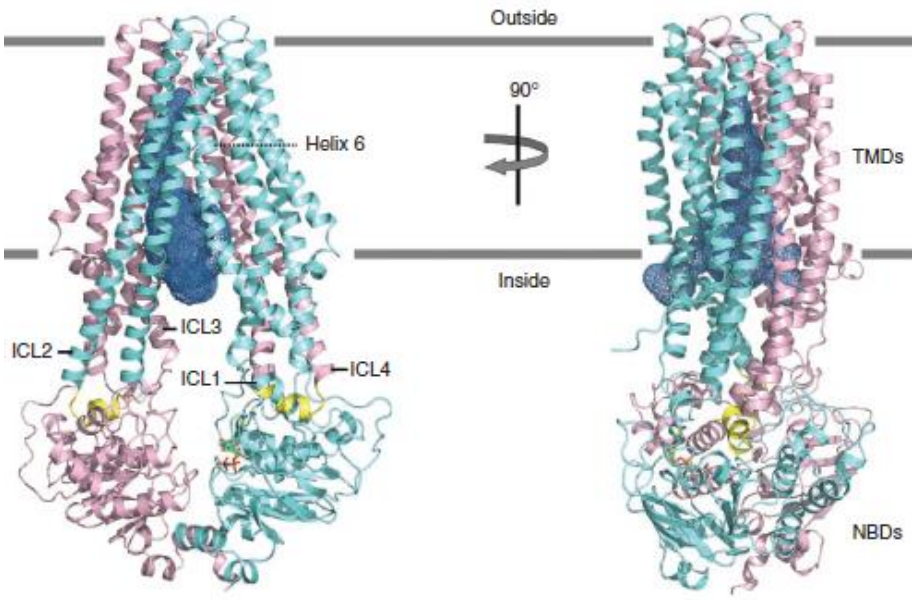

Figure 7. Structure of TM287/288 viewed along a membrane plane (Hohl, et al. 2012).

TM287 and TM288 are colored cyan and pink, respectively. Coupling helices of ICL2 and ICL4 interacting with NBDs are colored yellow. The inward-facing cavity is shown as a blue mesh.

1.2.3 CFTR as an ion channel

CFTR is the only known channel among the ABC transporters. Channels and transporters are thought to have different mechanism of function determined by their structure: transporters bind a substrate and move it across the membrane during conformational changes followed by this binding; and channels contain a pore, which allow ions to diffuse down their electrochemical gradient. However, CFTR appear to have structural properties of an ABC transporter, though functions as a channel, which suggests that these functional properties developed during evolution (Gadsby 2009, Miller 2010).

CFTR functions as a cAMP-activated ATP-gated anion channel with linear current

to voltage relationship in symmetrical Cl^- concentrations (Berger, Anderson, et al. 1991, Drumm, et al. 1991).

Gating of the CFTR channel depends on the R-domain phosphorylation and is driven by ATP binding and hydrolysis. The R-domain is usually phosphorylated by protein kinase A (PKA) (Anderson, Berger, et al. 1991), although it can be phosphorylated by other protein kinases, for example, protein kinase C (Berger, Travis and Welsh 1993).

According to the currently accepted model for the gating cycle of CFTR (Figure 8), NBDs bind two molecules of ATP between the Walker A motif of one NBD and the LSGGQ motif of the other (Vergani, et al. 2005, Rees, Leslie and Walker 2009). This interaction promotes the switch to the outward-facing conformation, opening of the gate in the TMDs and chloride anions to flow down their electrochemical gradient through the pore (Tabcharani, et al. 1991, Linsdell 2006).

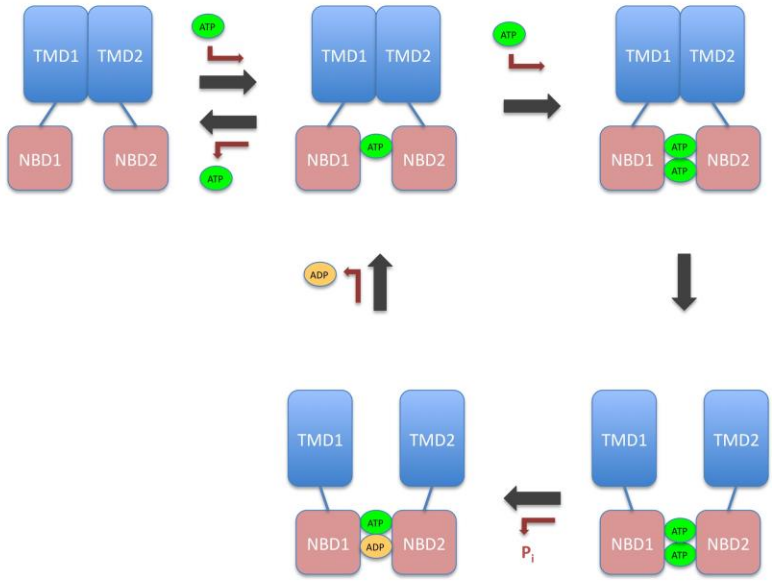

Figure 8. Gating of CFTR.

Binding of two ATPs between NBDs promotes opening of the gate in the TMDs. ATP hydrolysis leads to the gate closure.

ATP hydrolysis leads to disruption of the NBD1/NBD2 interface, this disruption produces a signal somehow transmitted to TMDs, where it causes the gate closure. Structural changes occurring while opening/closing the gate are not known yet. It has been proposed that structural rearrangements of TMD could open a pathway for anions (this rearrangement would correspond to the switch between inward- and outward-facing conformations of other ABC transporters); another possibility would mean the removal of an intramolecular barrier for ions, similarly to other ion channels (Wang und Linsdell 2012).

1.2.4 Biochemistry of CFTR

CFTR is a 1480 amino acid long glycoprotein with a molecular mass of ≈160 kDa. This protein is initially synthesized in the endoplasmic reticulum membrane as an immature form, which is core-glycosylated and has the size of ≈140 kDa; the majority (60-80%) of CFTR fails to mature and degrades in proteasomes (Ward, Omura and Kopito 1995). In the Golgi apparatus cisternae, the precursor forms the mature ("fully glycosylated") molecule that contains complex oligosaccharide chains (Cheng, Gregory, et al. 1990, Kopito 1999). This is the form of CFTR that is present on the cytoplasmic membrane. Many known mutations in CFTR impair the maturation of CFTR and trafficking to the plasma membrane, (Gregory, et al. 1991, Cotten, Ostedgaard and Carson 1996, Seibert, Linsdell, et al. 1996, Sheppard, et al. 1996).

So on a Western blot, CFTR can be seen as 3 bands (Figure 9), which reflect different maturation steps: a 150-170 kDa band represents the mature fully glycosylated form (band C); a band at 135 kDa (band B) is the core glycosylated fraction. A band at 130 kDa (band A) represents unglycosylated protein. Depending on maturation of a certain mutant, some bands can be less visible or even absent (so, mutant Δ508 on Figure 9 is represented by only band B, corresponding to the core glycosylated form of the protein and reflecting inability of this mutant to mature).

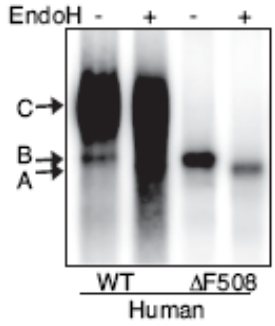

Figure 9. Example of a Western blot for CFTR.

Bands A, B, and C are indicated by arrows. The blot demonstrates fully glycosylated (band C), core glycosylated (band B) and unglycosylated (band A) human CFTR (wild type (wt) and Δ508) before and after Endoglycosidase H (endoH) treatment. Fully glycosylated wt CFTR is not endoH-sensitive (Ostedgaard, et al. 2007).

1.3 Aim of this work

Although much is known about the biological role of CFTR and regulation of its activity, there are still many questions about its structure and function to be answered, such as the pore location, the role of the R-domain in the gating control, the mechanism of NBD-TMD coupling, the role of coupling helices of ICLs in the gating signal transfer from TMDs to NBDs, and the conformational changes occurring during the gating cycle. These questions are especially difficult to answer because no high-resolution structure of the entire CFTR protein is available yet, but they are crucial for the development of novel therapeutic approaches for CF and other CFTR-related diseases.

If certain pairs of residues can be chemically crosslinked, it means that a conformation exists, which brings these residues close together. If a covalent-binding crosslinker is used, these two points of the protein stay connected after crosslinking even during intramolecular rearrangements of after denaturation. In this case, the presence or

absence of crosslinking can be detected, for example, by protein electrophoresis as an appearance of the additional band, representing the product of crosslinking (Figure 10). The additional band is especially easy to distinguish from the bands representing non-crosslinked proteins when the protein sequence is split into two halves, each of them containing one of points to be connected. But even if non-split protein constructs are used, the additional crosslinking band is still visible due to different mobility of the crosslinked molecule during electrophoresis (Serohijos, et al. 2008).

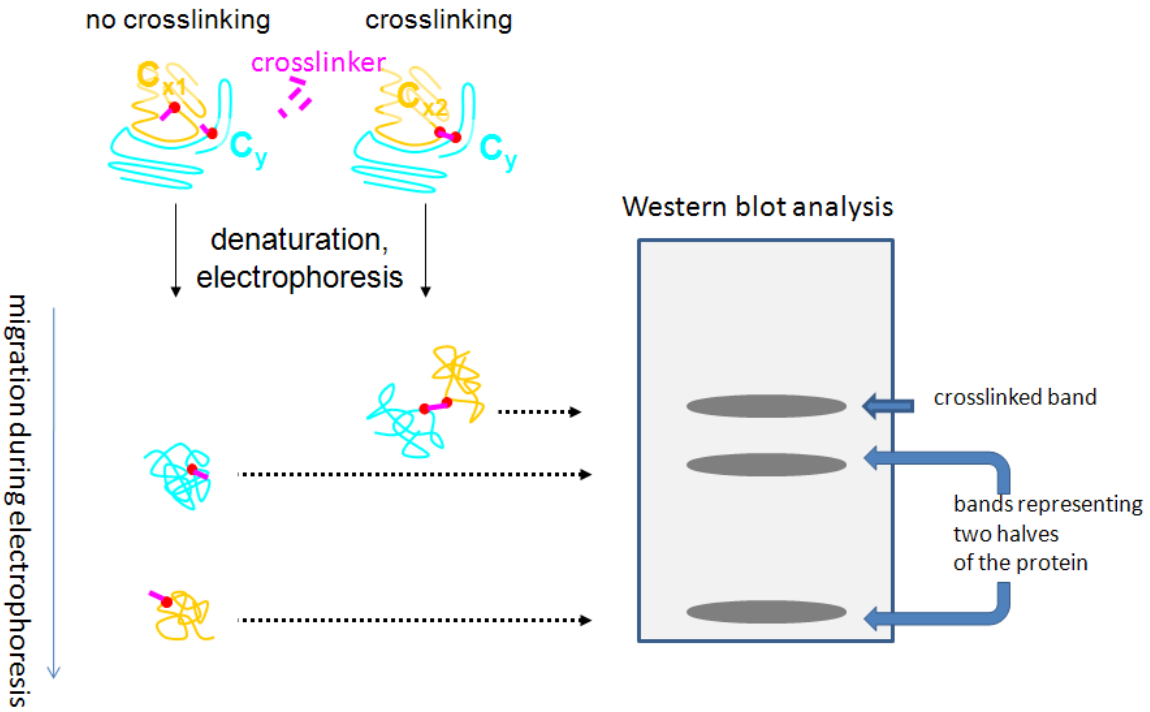

Figure 10. Illustration of a biochemical crosslinking experiment.

Two part of the protein (blue and yellow), once crosslinked, stay together. The presence/absence of crosslinking can be detected by gel electrophoresis: non-crosslinked and crosslinked proteins migrate separately.

This approach has already brought some insight into the CFTR domains interplay: application of cysteine-specific bifunctional crosslinkers on *Xenopus* oocytes expressing CFTR with introduced pairs of target cysteines demonstrated that NBDs of CFTR interact with each other in a "head-to-tail" configuration (Mense, et al. 2006).

The goal of the crosslinking experiments on CFTR presented in this work was to study possible interactions between coupling helices of ICLs and NBDs (Figure 11).

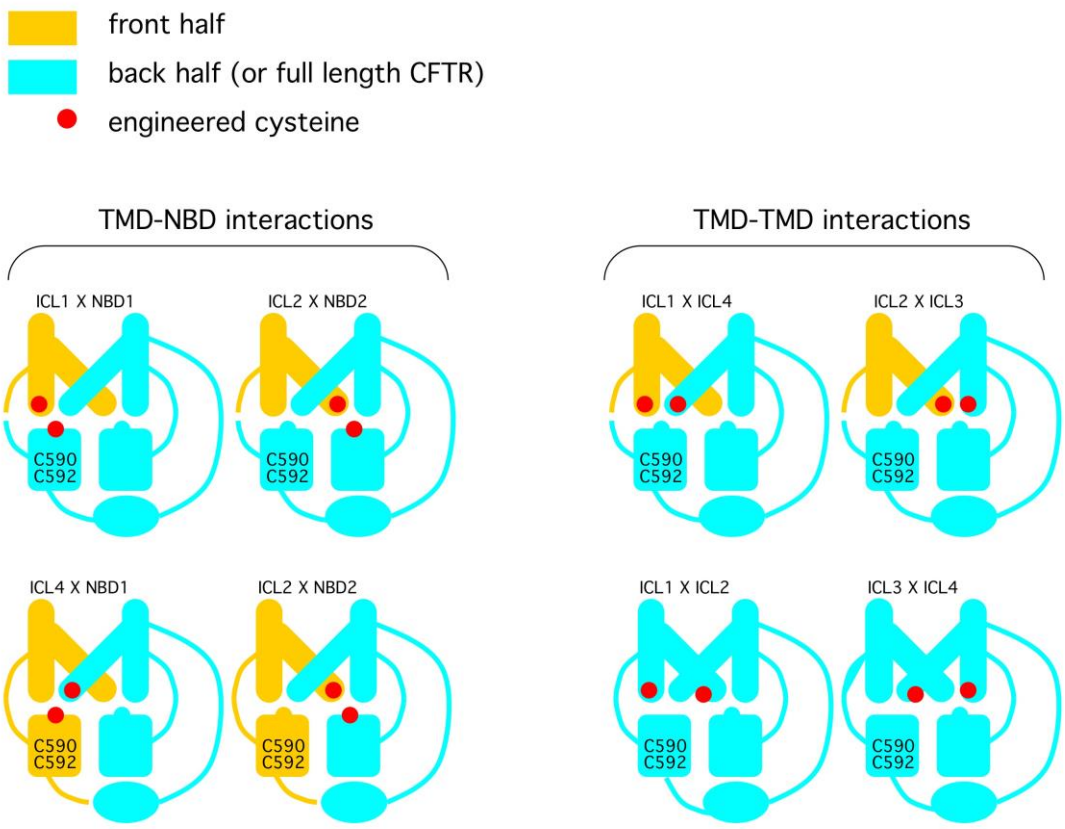

Figure 11. Possible domain interactions in CFTR according to the "domain-swap" model.

Two parts of CFTR are shown in yellow (front half) and blue (back half). Upside-down Y-letters represent TMDs, rounded rectangles – NBDs, the ellipse – R domain.

The cysteine-specific crosslinking strategy requires some prerequisites: native CFTR cysteines should be removed to avoid their reaction with the crosslinker; target residues should be mutated to cysteine. Then a crosslinker can be applied attempting to join these cysteines. A membrane-permeant bismaleimide based crosslinking reagent bismaleimidoethane (BMOE) allows performing a crosslinking of cytoplasmic target cysteines *in vivo* (Figure 12). Its molecule has a "spacer arm" between two maleimide groups, which allows joining two cysteines within an intramolecular distance of 8 Å.

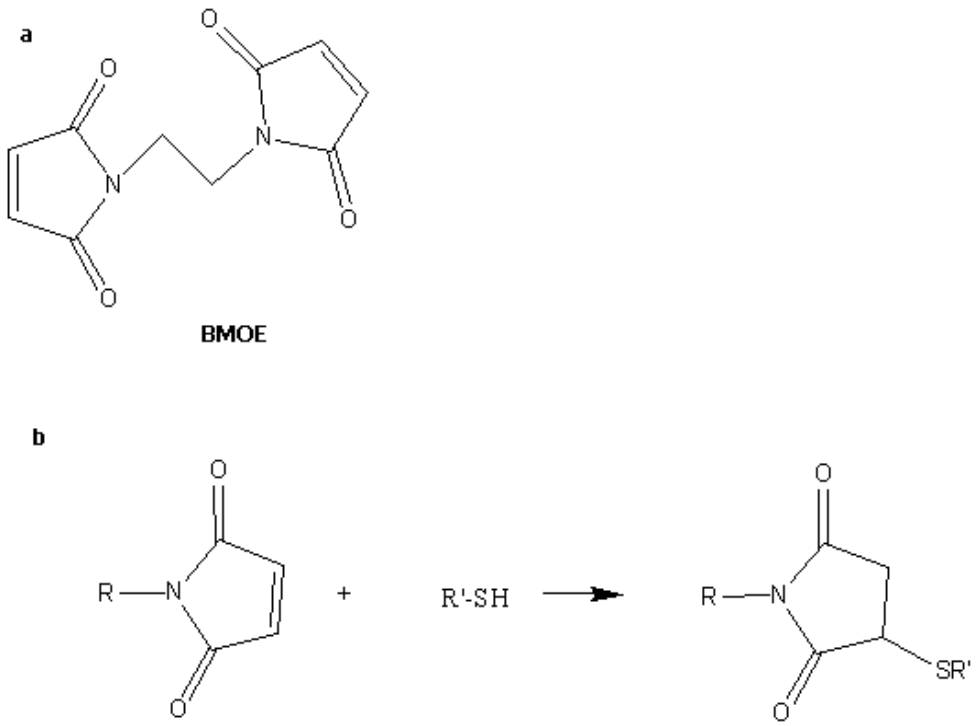

Figure 12. Crosslinker bismaleimidoethane (a) and the reaction of crosslinker with the target molecule (b).

As phosphorylation of CFTR by PKA activates the channel, application of stimulating PKA activity reagents, such as forskolin and 3-isobutyl-1-methylxanthine (IBMX), increases the whole cell conductance of CFTR-expressing cells. So, the whole-cell conductance measured before and after forskolin stimulation reflects the presence of functional CFTR in the cell membrane.

A suitable technique for such measurements is two-electrode voltage-clamp (TEVC), which is a sensitive and relatively simple electrophysiological method (Stühmer 1992). TEVC measures current across the cell membrane at a given membrane potential. This technique can assay functional expression of CFTR and the influence of different factors on CFTR function. For instance, the channel conductance changes upon the crosslinker influence can reflect possible intramolecular events caused by a formation of a

covalent bond between two cysteine residues. This approach has been successfully used in the laboratory to study interaction between residues F508 and L1065 (Jaksekovic, et al. 2008).

The goal of this work was to study possible structural and functional interactions between NBDs and TMDs of CFTR with a crosslinking approach, which allows finding points of inter- and intradomain interaction in CFTR during the gating cycle. A subset of residues likely to participate in such interactions was selected using a homology model for CFTR (Figure 13) based on the known structure of the bacterial transporter Sav1866 and representing CFTR in its outward-facing conformation (Gulyas-Kovacs, Lockless and Gadsby 2007), which corresponds to the open state of the CFTR channel.

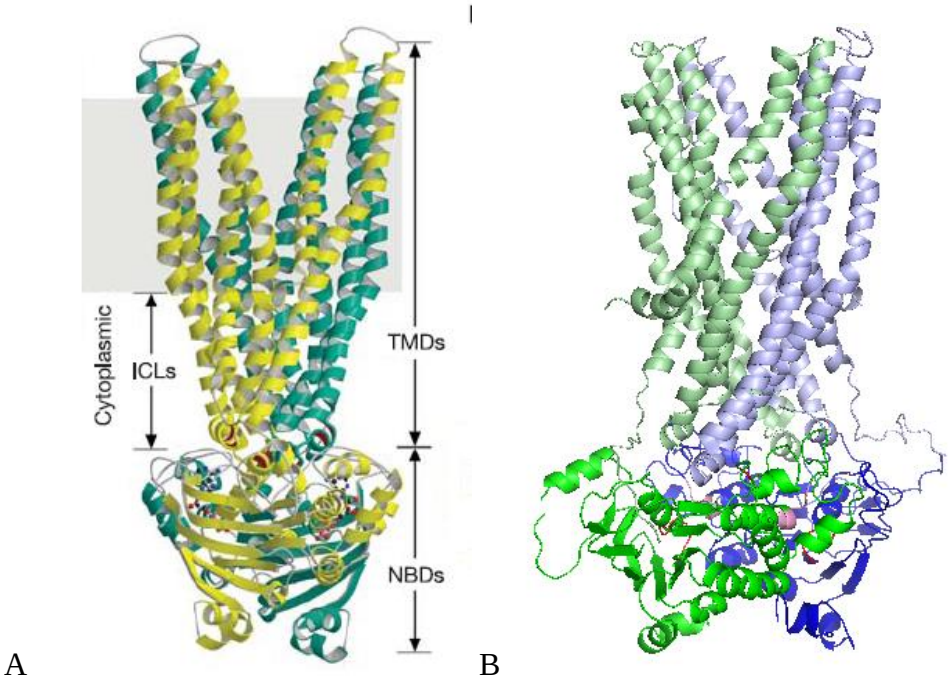

Figure 13. Homology model of CFTR based on the Sav1866 structure.

A. Sav1866 structure (Dawson und Locher 2006). Two different subunits colored yellow and turquoise. B. Homology models of CFTR (Gulyas-Kovacs, Lockless and Gadsby 2007). TMD1 (pale green), TMD2 (pale blue), NBD1 (bright green) and NBD2 (bright blue) are presented.

Some of these residues are shown on Figure 14, which demonstrates the intracellular view on TMDs (Figure 14 A), as well as two NBD/TMD interfaces (Figure 14 B, C). Residues belonging to each interface are shown in different colors.

On the ICL1/ICL4 interface, residues T164 and L165 from ICL1 and residue L1059 from ICL4 appear to be in close proximity to each other (Figure 14 A, blue). The homology model predicts also a possible close contact of residues I266, E267 and A969 on ICL2/ICL3 interface (Figure 14 A, yellow), residues S176, I177, G178, Q179 and V260 on ICL1/ICL2 interface (Figure 14 A, red), residues G970, G971, I972, S1049, F1052 and T1053 on ICL3/ICL4 interface (Figure 14 A, green).

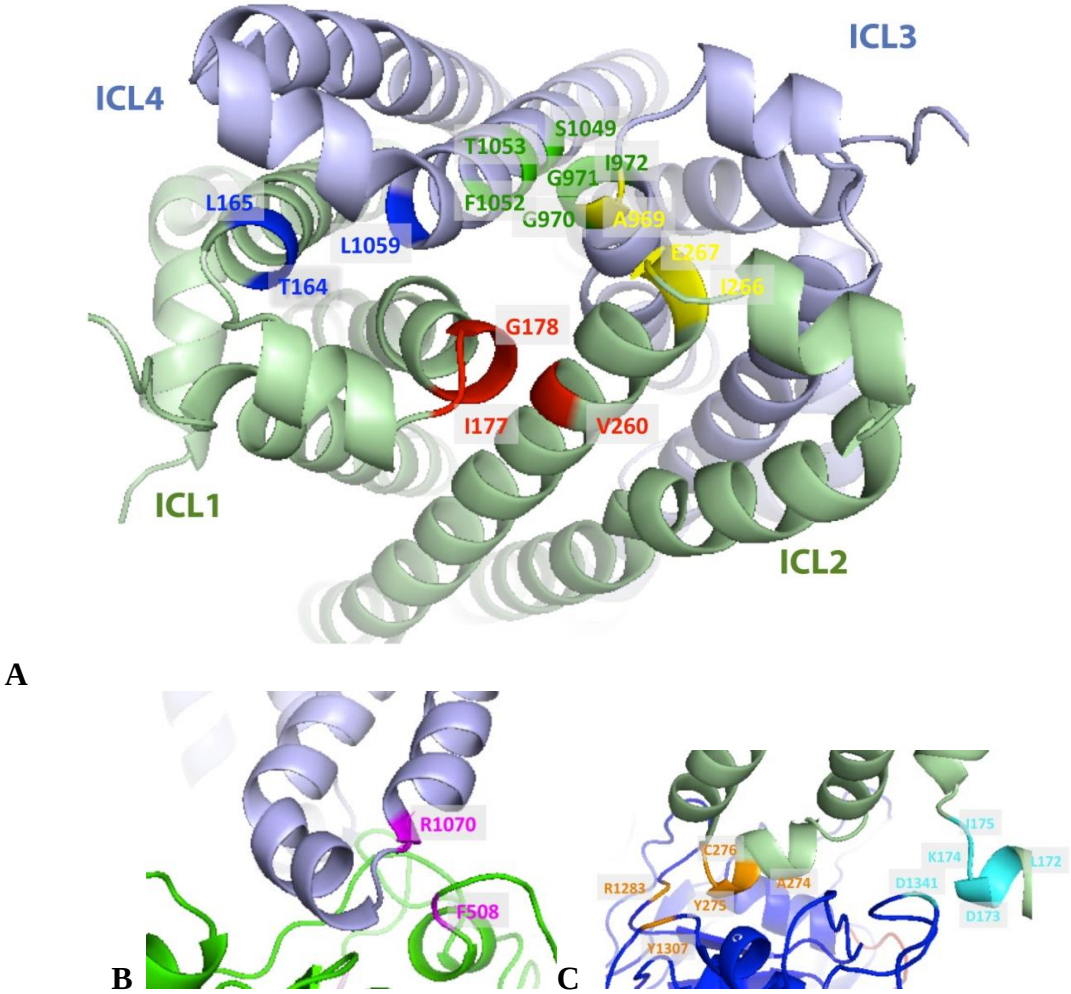

Figure 14. Residues proposed to be involved in intramolecular interactions based on a homology model for CFTR (Gulyas-Kovacs, Lockless and Gadsby 2007).

The homology model for CFTR (Figure 13) is based on the known structure of the bacterial transporter Sav1866 and representing CFTR in its outward-facing conformation (Gulyas-Kovacs, Lockless and Gadsby 2007), which corresponds to the open state of the CFTR channel. Parts of TMD1 (pale green), TMD2 (pale blue), NBD1 (bright green) and NBD2 (bright blue) are shown. A. TMDs, cytoplasmic view. Residues belonging to ICL1/ICL2 interface are marked red, to ICL2/ICL3 interface yellow, to ICL3/ICL4 interface green, and to ICL4/ICL1 interface blue. B. Residues belonging to NBD1/TMD2 interface are marked magenta. C. Two clusters of residues belonging to NBD2/TMD1 interface are marked orange and cyan.

Possible interactions between NBDs and ICLs predicted by this homology included the one between F508 and R1070 on TMD2/NBD1 interface. Close spatial proximities of

the residues L172, D173, K174, I175 from TMD1 (ICL1) and D1341 from NBD2 (Figure 14 B), as well as A274, Y275, C276 from TMD1 (ICL2) and R1283 and Y1307 from NBD2 were also suggested (Figure 14 C).

Figure 15 shows another homology model of CFTR (Mornon, Lehn und Callebaut 2008), which is also based on the experimental structure of the bacterial transporter Sav1866.

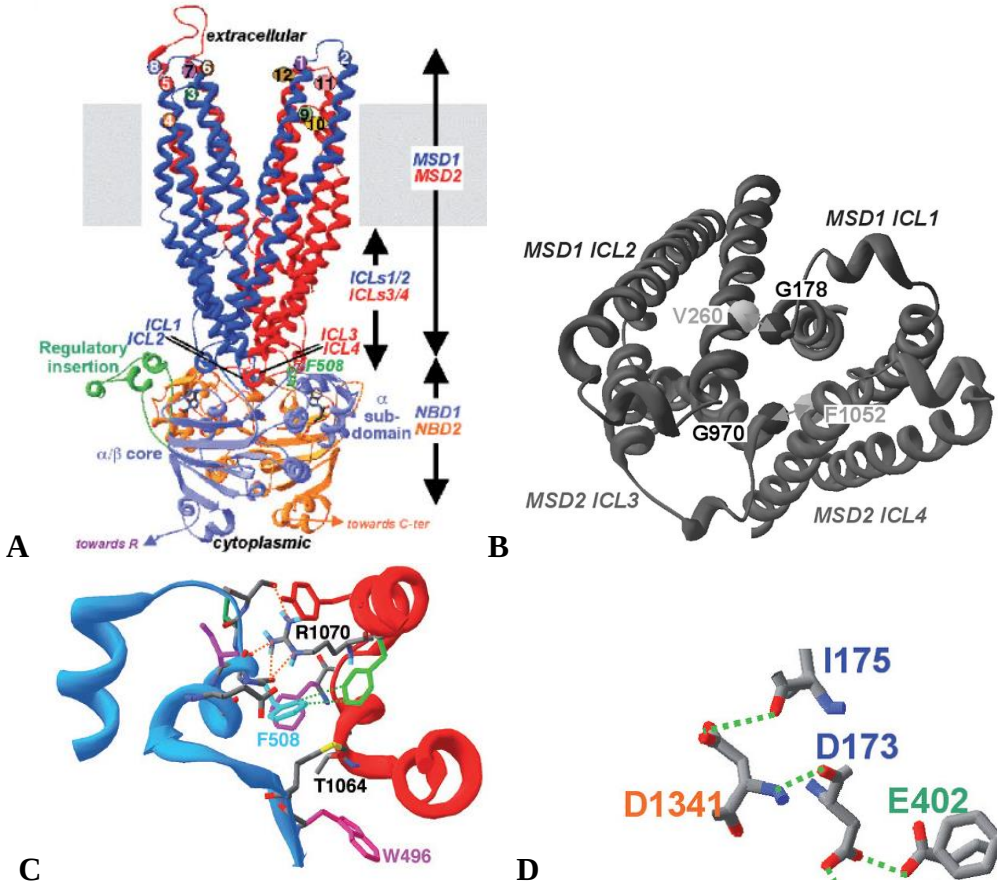

Figure 15. Intramolecular interactions predicted by the homology model of CFTR (Mornon, Lehn und Callebaut 2008).

A. Homology model of CFTR. TMD1 and NBD1 are colored dark and light blue, respectively. TMD2 and NBD2 are colored red and orange, respectively. B. TMDs, cytoplasmic view. Residues on TMD/TMD interfaces proposed to interact. C. Residues proposed to interact belonging to NBD1/TMD2 interface. D. Residues proposed to interact belonging to NBD2/TMD1 interface.

This model suggests interactions of the following residues belonging to TMD/TMD and TMD/NBD interfaces: G178 from ICL1, which possibly builds a contact with V260 from ICL2; two possibly interacting residues from TMD2 are G970 (ICL3) and F1052 (ICL4) (Figure 15 B). Within the NBD/TMD interfaces, a possible interacting partner for F508 from NBD1 is R1070 belonging to TMD2 (Figure 15 C). A formation of a hydrogen bond is predicted between residues and D173 and D1341 (Figure 15 D). There is also a proposed contact between Y275 from ICL2 and Y1307 from NBD2.

The interaction between residues L172 and D1341 was predicted by another homology model of CFTR and supported by crosslinking data (He, et al. 2008). The cited work also demonstrated biochemical evidence of the interaction between residues C276 and Y1307.

A pair of engineered cysteines at positions N105C in TM287 (a residue corresponding to D173 from ICL1 of CFTR according to the mentioned above multiple sequence alignment) and T486C in TM288 (a residue corresponding to D1341 in human CFTR according to the multiple sequence alignment performed in the laboratory by Dr. W. Labeikowsky) forms disulfide bonds in the outward-facing state of the protein, which was expected from the homology model of TM287/288 created on the basis of the outward-facing Sav1866 structure (Hohl, et al. 2012).

Mutations of some of the mentioned residues were found in patients with CF: L165, Q179C, Y275, L1059, Y1307 (http://www.genet.sickkids.on.ca), I175 (Romey, et al. 1994), I177 (http://www.genet.sickkids.on.ca), G178 (Zielenski, Bozon, et al. 1991), F508 (Riordan, et al. 1989), G970 (Seibert, Linsdell, et al. 1996), F1052 (Gelfi, et al. 1994), R1070 (Shrimpton, Borowitz and Swender 1997), R1283 (Cheadle, Meredith and al-Jader 1992); and in patients with CAVD: T1053 (http://www.genet.sickkids.on.ca), which might reflect the role of these residues in the proper domain assembly and the channel function.

The mentioned homology models suggest likely inter- and intradomain interactions, which allowed choice of the target residues for experiments presented in this work. The plan of experiments included mutation of these residues to cysteines and application of the cysteine-specific crosslinker to allow sufficiently close target positions to be connected by

a covalent bond. The properties of such crosslinked CFTR channels can then be studied to assay how the covalent bond formation between two engineered cysteines influences the channel function.

2. Material and Methods

2.1 Construction of CFTR mutants

2.1.1 Selection of amino acid residues

Appropriate pairs of target amino acid residues were selected based on the homology models for CFTR in the outward-facing conformation (Figure 13, Figure 15). Oligonucleotide primers for site-directed mutagenesis (Table 1) were designed with Lasergene SeqBilder Software (DNASTAR, Madison, WI, USA). For some interfaces, several residues were mutated to allow later selection based on their expression levels as assessed in preliminary TEVC experiments; the residues chosen for more detailed study are marked bold in Table 1.

The corresponding oligonucleotide primers were obtained from GeneLink™ facility (Gene Link, Inc., Hawthorne, NY, USA). As a native cysteine C276 was replaced in the cysteine-depleted template to serine (Mense, et al. 2006), this residue was mutated back to cysteine ("mutant S276C").

Engineered cysteines were introduced into appropriate cysteine-depleted CFTR backgrounds (see the following section) by the PCR site-directed mutagenesis (QuikChange, Stratagene, La Jolla, CA, USA) using the pGHE vector.

Table 1. Point mutations and corresponding oligonucleotide primers

mutant	Forward primers	Reverse primers
T164C	gtttagtttgatttataagaagTGTttaaagctgtcaagccgtg	cacggcttgacagctttaaACActtcttataaatcaaactaaac
L165C	gtttgatttataagaagactTGTaagctgtcaagccgtg	cacggcttgacagcttACAagtcttcttataaatcaaac
L172C	gctgtcaagccgtgttTGTgataaaataagtattggacaac	gttgtccaatacttattttatcACAaacacggcttgacag
D173C	gctgtcaagccgtgttctaTGTaaaataagtattggacaac	gttgtccaatacttattttACAtagaacacggcttgacagc
K174C	gctgtcaagccgtgttctagatTGTataagtattggacaac	gttgtccaatacttatACAatctagaacacggcttgacagc
I175C	gccgtgttctagataaaTGTagtattggacaacttgttagtctcc	ggagactaacaagttgtccaatactACAtttatctagaacacggc
S176C	gccgtgttctagataaaataTgtattggacaacttgttagtctcc	ggagactaacaagttgtccaatacAtattttatctagaacacggc
I177C	gccgtgttctagataaaataagtTGTggacaacttgttagtctcc	ggagactaacaagttgtccACAacttattttatctagaacacggc
G178C	gttctagataaaataagtattTGTcaacttgttagtctcctttcc	ggaaaggagactaacaagttgACAaatacttattttatctagaac
Q179C	gataaaataagtattggaTGTcttgttagtctcctttcc	ggaaaggagactaacaagACAtccaatacttattttatc
V260C	gggaagatcagtgaaagacttTGTattacctcagaaatgatcgag	ctcgatcatttctgaggtaatACAaagtctttcactgatcttccc
I266C	gtgattacctcagaaatgTGCgagaacatccaatctgttaaggcc	ggccttaacagattggatgttctcGCAcatttctgaggtaatcac
E267C	gtgattacctcagaaatgatcTGCaacatccaatctgttaaggcc	ggccttaacagattggatgttGCAgatcatttctgaggtaatcac
A274C	catccaatctgttaagTGCtactcctgggaagaagcaatgg	ccattgcttcttcccaggagtaGCActtaacagattggatg
Y275C	catccaatctgttaaggccTGCtcctgggaagaagcaatgg	ccattgcttcttcccaggaGCAggccttaacagattggatg
S276C	catccaatctgttaaggcctacTGCtgggaagaagcaatgg	ccattgcttcttcccaGCAgtaggccttaacagattggatg
F508C	ccattaaagaaaatatcatcTGTggtgtttcctatg	cataggaaacaccACAgatgatattttctttaatgg
N965C	gcacctatgtcaaccctcTGCacgttgaaagcaggtggg	cccacctgctttcaacgtGCAgagggttgacataggtgc
A969C	caaccctcaacacgttgaaaTGCggtgggattcttaatagattc	gaatctattaagaatcccaccGCAtttcaacgtgttgagggtt
G970C	ccctcaacacgttgaaagcaTGTgggattcttaatagattctcc	ggagaatctattaagaatcccACAtgctttcaacgtgttgaggg
G971C	caacacgttgaaagcaggtTGTattcttaatagattctcc	ggagaatctattaagaatACAacctgctttcaacgtgttg
I972C	ccctcaacacgttgaaagcaggtgggTGTcttaatagattctcc	ggagaatctattaagACAcccacctgctttcaacgtgttgaggg
S1049C	ctggaatctgaaggcaggTGTccaattttcactcatcttg	caagatgagtgaaaattggACAcctgccttcagattccag
F1052C	ctgaaggcaggagtccaattTGCactcatcttgttacaagc	gcttgtaacaagatgagtGCAaattggactcctgccttcag
T1053C	ggcaggagtccaattttcTGTcatcttgttacaagcttaaaagg	ccttttaagcttgtaacaagatgACAgaaaattggactcctgcc
L1059C	cactcatcttgttacaagcTGTaaaggactatggacacttcgtgcc	ggcacgaagtgtccatagtcctttACAgcttgtaacaagatgagtg
R1070C	ggacacttcgtgccttcggaTGCcagccttactttgaaactctg	cagagtttcaaagtaaggctgGCAtccgaaggcacgaagtgtcc
R1283C	caataactttgcaacagtggTGTaaagcctttggagtgatacc	ggtatcactccaaaggctttACAccactgttgcaaagttattg
Y1307C	gaaaaaacttggatcccTGTgaacagtggagtgatc	gatcactccactgttcACAgggatccaagtttttc
D1341C	gggaagcttgactttgtccttgtgTGTgggggctctgtcttaagt	acttaagacagagcccccACAcacaaggacaaagtcaagcttccc

2.1.2 Choice of a template

Cysteine-depleted CFTR. For cysteine-specific crosslinking experiments, the target residues should be replaced with cysteines. As CFTR have 18 native cysteines, which may constitute a problem as a possible substrate for a reaction with cysteine-specific reagents, I used a cysteine-depleted "background" to introduce engineered cysteines. This background has already been obtained and used in the laboratory: all 18 native CFTR cysteines were removed and replaced with serines (or leucines or valines for C590 or C592) (Mense, et al. 2006). It turned out that mutation of C590 and C592 nearly abolished CFTR maturation in *Xenopus* oocytes. Therefore these native cysteines remained unmutated to enhance protein expression, and almost all experiments of the present work were performed using CFTR with two native cysteines C590 and C592.

The exception was the mutation of F508: replacement of this residue with cysteine abolished CFTR maturation and required to leave more native cysteines unmutated to rescue protein expression.

Split vs. full-length CFTR. For biochemical experiments, a reasonable choice is a template, in which the whole CFTR sequence is split in two sequences so that the residues to be crosslinked belong to different domains. If two residues from different "halves" of CFTR are crosslinked, these "halves" migrate together during electrophoresis, and the difference between molecular weights of the separated halves and the whole molecule allows better visualization of the crosslinking product on Western blot. CFTR constructs split between TMD1 and NBD1 (residues 633 and 634) (Csanády, Chan und Seto-Young, et al. 2000, Mense, et al. 2006) and between NBD1 and TMD2 (residues 389 and 390) were already tested in the laboratory, and these constructs were used also in this work as templates.

Wild-type background for the F508C mutant. Mutation F508C was introduced into the N-terminal 1-633 native (wild type) part of the CFTR sequence, as the cysteine-free background combined with this mutation completely abolished CFTR expression and did not allow performing the experiments.

Following cysteine-depleted CFTR constructs were used as a background for the site-directed mutagenesis:

- mutations T164C, L165C, L172C, D173C, K174C, I175C, I266C, E267C, A274C, Y275C, S276C were introduced (each separately) into the N-terminal cysteine-free fragment of the CFTR amino acid sequence from 1 to 389 residue (**1-389 0C** background), which was coexpressed with the corresponding C-terminal half to obtain the whole CFTR, namely with the C-terminal half 390-1480 containing two native cysteines, C590 and C592 (**390-1480 2C** background), which served as a background for mutations A969C, L1059C, R1283C, Y1307C and D1341C;

- mutation F508C was introduced into the N-terminal **1-633** native (wild type) part of the CFTR sequence, as the cysteine-free background combined with this mutation completely abolished CFTR expression and did not allow performing experiments. This part of the protein was then coexpressed with the C-terminal cysteine free part 634-1480 (**634-1480 0C** background); the latter one was used as a background for mutation R1070C;

- mutations S176C, I177C, G178C, Q179C, V260C, N965C, G970C, G971C, I972C, S1049C, F1052C and T1053C were introduced into the full-length cysteine-depleted CFTR sequence with two native cysteines, C590 and C592 (**1-1480 2C** background).

2.1.3 Site-directed mutagenesis: experimental protocols

The mutants were obtained by site-directed mutagenesis (QuikChange, Stratagene, La Jolla, CA, USA). For each cycling reaction, 10 µl of reaction buffer (100 mM KCl, 100 mM $(NH_4)_2SO_4$, 200 mM tris-(hydroxymethyl)aminomethane) hydrochloride (Tris-HCl), 20 mM $MgSO_4$, 1% polyethylene glycol p-(1,1,3,3-tetramethylbutyl)-phenyl ether (Triton® X-100), 1 mg/ml nuclease-free bovine serum albumin (BSA)), 10 ng of template DNA, 125 ng of each oligonucleotide primer (forward and reverse), 2 µl of dNTP mixture (10 mM dATP, 10 mM dCTP, 10 mM dGTP, 10 mM dTTP, 0.6 mM Tris-HCl), 5 µl of DMSO, 2 µl of PfuTurbo polymerase (QuikChange, Stratagene, La Jolla, CA, USA) and water to 100 µl final volume were mixed in an Eppendorf tube and placed in the thermal cycler for the cycling reaction. The reaction parameters are shown in Table 2.

Table 2. Parameters of the cycling reaction

Number of cycles	Temperature	Time
1	95°C	30 s
12-18	95°C	30 s
	55°C	1 min
	68°C	1 min/kBase of plasmid length

After the reaction was completed, 2 µl of 10 U/µl *Dpn* I restriction enzyme (New England Biolabs, Ipswich, MA, USA) were added to the reaction mixture and incubated at 37°C for 1 hour to digest the parental DNA.

To precipitate the obtained DNA, 250 µl of absolute ethanol, 10 µl of 3 M sodium acetate (pH 5.5) and 1,5 µl of GlycoBlue™ Coprecipitant (Ambion, Inc., Austin, TX,

USA) were added; the mixture was frozen at –80ºC for 15-20 min and then centrifuged at 10,000 RPM and 4 ºC for 15 min. The resulting pellet was washed 2 times with 70 % ethanol, dried at 37ºC and dissolve in 10 µl H_2O.

For the transformation, MAX Efficiency® DH5α™ Competent Cells (Invitrogen, Carlsbad, CA, USA) were thawed on ice and aliquoted in 45 µl samples in pre-chilled Falcon 2059 polypropylene tubes. After the incubation with 5 µl of the PCR product on ice for 30 min, a heat shock was performed by placing the tube for 30 seconds at 37°C and then on ice for 2 minutes.

After that, 950 µl of SOC-medium (2% tryptone (Sigma-Aldrich Co., St. Louis, MO, USA), 0.5% yeast extract (Sigma-Aldrich Co., St. Louis, MO, USA), 10 mM NaCl, 2.5 mM KCl, 10 mM $MgCl_2$, 10 mM $MgSO_4$, 20 mM glucose) were added to each sample and shaken at 225–250 RPM for 1 hour at 37°C. After the following centrifugation at 2000 RPM for 1 min, the resulting pellet was plated on LB–ampicillin agar (Sigma-Aldrich Co., St. Louis, MO, USA) and stored overnight at 37ºC.

The resulting colonies were placed in Falcon tubes with 5 ml lysogeny broth (LB) with ampicillin, shaken for 1 hour at 37ºC and centrifuged at 3000 RPM and 4ºC. The supernatant was removed, and the pellets were used for the DNA preparation with QIAprep Miniprep Kit (Qiagen, Venlo, Netherlands).

The mutations were confirmed by automated DNA sequencing at Genewiz, Inc. (South Plainfield, NJ, USA).

The resulting cDNA constructs were linearized using the NheI restriction enzyme (New England BioLabs, Inc., Ipswich, MA, USA) and transcribed with the T7 mMessage mMachine RNA kit (Ambion, Inc., Austin, TX, USA) to obtain the corresponding cRNA.

2.2 Expression of mutant CFTR in *Xenopus* Oocytes

2.2.1 Experimental protocol

Xenopus laevis oocytes are routinely used for protein expression and electrophysiological studies. For the following experiments, the oocytes were isolated from adult female frogs by partial ovariectomy under tricaine (3-aminobenzoic acid ethyl ester) anaesthesia (0.17% water solution) and defolliculated by treatment with ~500 u/ml collagenase (Collagenase Type I GIBCO, Invitrogen, Carlsbad, CA, USA) in oocyte Ringer (OR2) solution (82.5 mM NaCl, 2 mM KCl, 1 mM $MgCl_2$, 5 mM 4-(2-hydroxyethyl)-1-piperazineethanesulfonic acid (HEPES), pH 7.5) for about 2 hours at room temperature.

Then oocytes of stage V–VI, which are preferred because of their size (1-1.4 mm), stability and ability to express proteins, were selected and incubated at 18°C for several hours in $OR2^{++}$ solution (OR2 with 1.8 mM Ca^{2+} and 50 mg/ml gentamycin (GIBCO, Life Technologies, Carlsbad, CA, USA)) before injection.

The amount of injected cRNA was 5-50 ng per oocyte in a constant total volume of 50 nl. The injection was performed by injector "NANOJECT" (Drummond Scientific, Broomall, PA, USA). Injection pipettes were pulled with a vertical puller (PP83 Narishige, Tokio, Japan) from glass capillaries (3-000-203-G/X; Drummond Scientific, Broomall, PA, USA). The pipette's tips were broken to an internal diameter of 10–20 μm, which size provides efficient injection and is not damaging for the oocytes.

The oocytes were further incubated at 18˚C for 2-5 day before they were used for experiments.

As a control, some oocytes were injected with an equal volume of water (Nuclease-free water, Ambion, Austin, TX, USA).

2.3 Two-electrode voltage-clamp (TEVC) recording

2.3.1 Theoretical background

The voltage clamp method measures ion flow across a cell membrane as an electric current at a given voltage. This technique was developed by Cole (Cole 1949) and Hodgkin *et al*. (Hodgkin, Huxley and Katz 1952) for the squid giant axon and later evolved in many variants applied to other cells.

For instance, two-electrode voltage-clamp (Stühmer 1992) is used for whole-cell recordings in electrophysiological studies of membrane proteins. This method allows measurement of the whole-cell current provided by ion channels while keeping the membrane potential on a controlled level. Membrane voltage is clamped at a certain level by injecting current into the cell. These procedures are performed with two different electrodes (Figure 16): a voltage electrode measures membrane potential, and current is injected through a current electrode. Channel activity resulting in membrane current changes is followed by a corresponding current injection and detected by the amplifier connected to the current electrode, whose output is monitored and recorded. So, the method allows sensitive measurement of changes in electrophysiological properties of membrane proteins expressed by the cell.

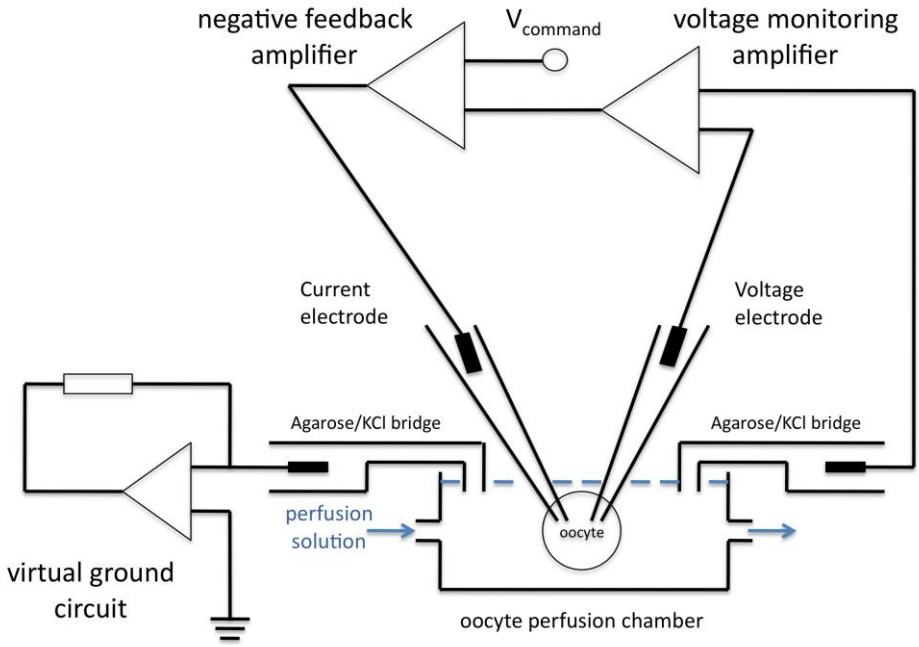

Figure 16. Scheme of a TEVC recording setup.

Black rectangles denote Ag/AgCl pellets. The oocyte with the expressed tested construct is placed in an experimental chamber filled with a perfusion solution. The chamber is connected via two bridges filled with agarose/3M KCl and containing Ag/AgCl pellets (bath electrodes). One of these electrodes is connected to the voltage-measuring amplifier, the second one to the virtual ground circuit. The second input of the voltage-measuring amplifier is connected to the Ag/AgCl pellet in the voltage recording glass microelectrode. The measured voltage is fed into one of the inputs of the negative feedback amplifier, where it is compared with the command voltage fed into the second input of this amplifier. The output of the amplifier is connected to the Ag/AgCl pellet in the current microelectrode and, together with the output of the virtual ground circuit, is monitored and recorded (Dascal 2000).

2.3.2 Experimental protocols

For TEVC measurements, oocytes were placed in a recording chamber, impaled with two microelectrodes for the voltage and current measurement and continuously superfused at room temperature. The microelectrodes were pulled with a horizontal puller (P-2000, Sutter Instrument Co., Novato, CA, USA) from glass capillaries (3-000-210-G; Drummond Scientific, Broomall, PA, USA) and filled with 3 M KCl. Voltage microelectrodes had resistance of about 2 MΩ, and current ones had resistance of 1–1,5 MΩ. The current electrode was shielded by wrapping in aluminium foil to 1-2 mm to the tip end. The chamber was connected to virtual ground circuitry through Ag/AgCl electrodes in 2.5% agar/3 M KCl bridges. Current was measured by a voltage-clamp amplifier (OC-725A oocyte clamp; Warner Instrument Corp., CT, USA), filtered at 50 Hz by an eight-pole Bessel filter (Frequency Devices, Inc., IL, USA), digitized at 100 Hz using a Digidata 1200 board (Axon Instruments, Inc., Foster City, CA, USA) with PatchMaster software (HEKA Elektronik, Lambrecht/Pfalz, Germany) and analyzed by IgorPro 6.01 software (WaveMetrics, Inc., Lake Oswego, OR, USA). Resting current was measured while oocytes were superfused with OR2 solution, and forskolin-induced current was measured during superfusion with 40 μM forskolin (Figure 17) and 1 mM IBMX solution in OR2, prepared from stock solutions in DMSO (40 mM forskolin and 1 M IBMX).

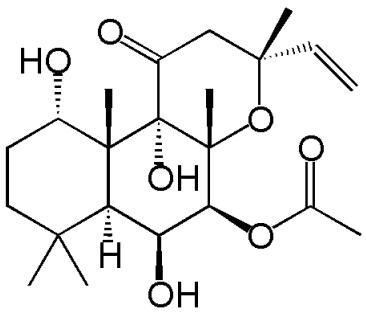

Figure 17. Forskolin.

An example of the TEVC recording is shown on Figure 18. This example demonstrates, how the whole cell conductance increases upon the forskolin stimulation (500-1000 s from the start), and returns back to its initial level upon the washout with OR2 solution. The increased conductance after the application of forskolin reflects the expression of mature CFTR on the cell surface.

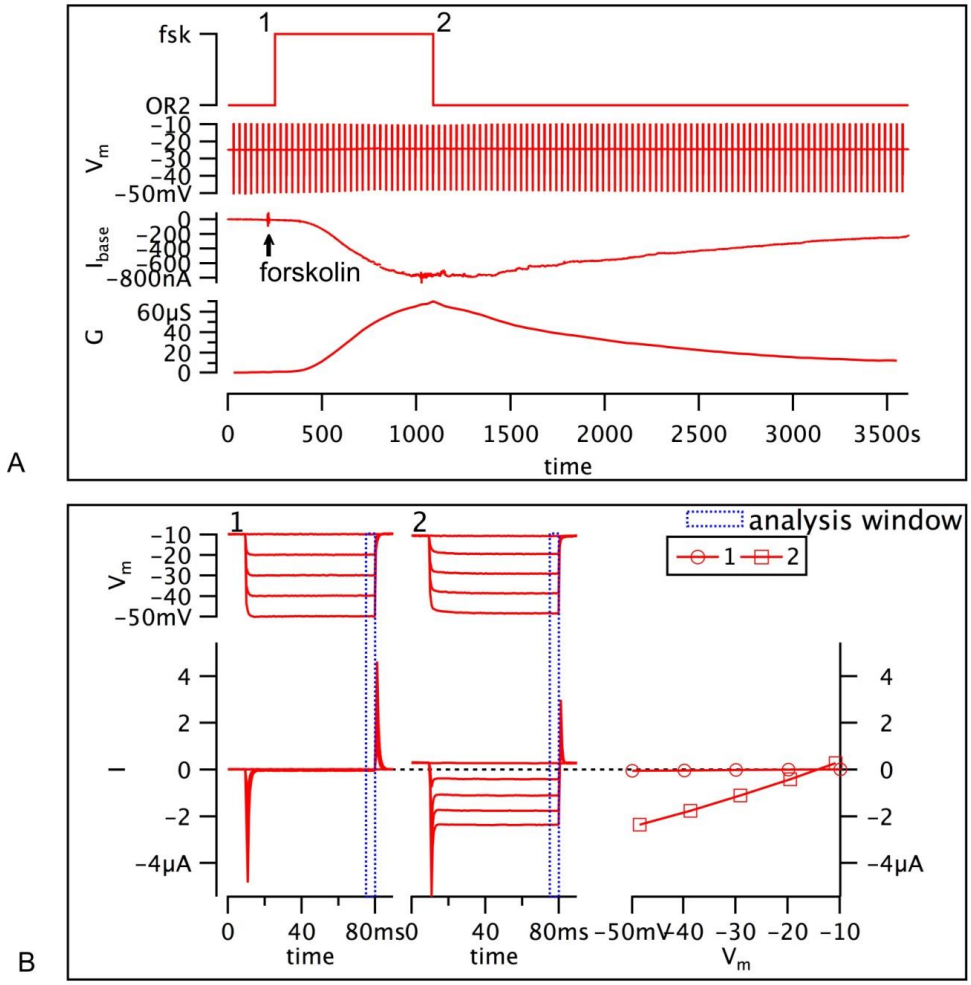

Figure 18. Example of TEVC recording.

A. Voltage steps, current and conductance changes upon the forskolin stimulation. B. Voltage steps applied before and after stimulation with forskolin (left); two current-voltage (IV) curves (right) compare the conductance under basal (circles) and forskolin-stimulated (squares) conditions; the conductance amplitude after stimulation monitors the expression level of CFTR, in this case the higher conductance confirms CFTR expression.

This response on the forskolin application is a useful tool to detect the functional CFTR in the cell membrane and therefore to evaluate the quality of the mutant expression, and this assay was therefore used in preliminary experiments to select mutants for the detailed study, because only a sufficient expression level of the channel allows detection and evaluation of conductance changes under the crosslinker influence.

Crosslinker influence on the current was assayed during the superfusion with 300 μM bismaleimide based crosslinking reagent bismaleimidoethane (BMOE, Figure 12) (Pierce Biotechnology, Rockford, IL, USA). The BMOE solution was prepared in OR2 from the 25 mM stock solution BMOE in DMSO solution. In control experiments, a monofunctional cysteine-specific reagent N-ethylmaleimide, NEM (Figure 19) (Sigma-Aldrich Co., St. Louis, MO, USA) was used in the same concentration as BMOE (300 μM solution in OR2 prepared from 25 mM stock solution in DMSO).

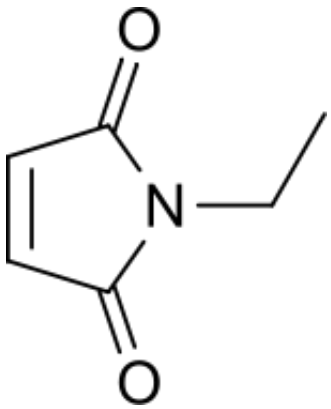

Figure 19. N-Ethylmaleimide.

During the measurements, voltage was held at –10mV, and voltage steps (70 ms steps from –50 to –10 mV, in 10 mV increments) were applied. Currents were averaged near the ends of voltage steps, and plotted against voltage, and conductance was calculated from linear fits of the IV curves.

To assay electrophysiological properties of the mutant CFTR under the crosslinker influence, I used two perfusion protocols.

The first protocol aimed to test how the channel responds on the forskolin stimulation being pre-treated with the crosslinker. For this purpose, BMOE was added to the OR2 perfusion solution about 3-5 min from the start of the recording and applied for about 15 min. After the BMOE treatment, the combination of forskolin and IBMX was added to the perfusion solution. The second protocol aimed to test the influence of the crosslinker on the forskolin-induced conductance of CFTR pre-stimulated with forskolin/IBMX solution. First, oocytes were superfused with forskolin/IBMX solution; when the whole cell conductance stopped to increase upon the forskolin stimulation, the crosslinker BMOE was added to the perfusion solution.

These protocols were also used in preliminary experiments, which aimed to choose one pair of possibly interacting residues for a certain inter- or intradomain surface. When the double-cysteine mutant demonstrated a sufficient expression level, but after the BMOE application showed no or little forskolin response, or when the BMOE application decreased conductance, it suggested a possible interaction between these residues, and these mutants were selected for more detailed experiments.

2.4 Oocyte plasma membrane preparation

2.4.1 Experimental protocol

Oocytes were injected with 5-20 ng cRNA per oocyte and stored for CFTR expression 2-5 days at 18˚C in $OR2^{++}$ solution.

After that, two samples of 25–35 oocytes for each tested mutant were selected: one sample for crosslinking and another one for the control. Samples were equilibrated in 4 ml OR2 solution in 35-mm Petri dishes for 10 min at room temperature.

Then crosslinking was performed by adding 25 µl of 300 mM BMOE solution in DMSO to each crosslinking sample and 25 µl of DMSO to each control sample. After 15 minutes incubation at room temperature, the oocytes were transferred with a pipette into Eppendorf tubes with 500 µl ice-cold lysis buffer (400 mM KCl, 5 mM 4-(2-hydroxyethyl)-1-piperazineethanesulfonic acid (HEPES), 100 µM protease inhibitor cocktail set I (CALBIOCHEM, La Jolla, CA, USA), 100 µM phenylmethanesulfonylfluoride (PMSF), pH 7.0 (adjusted with KOH). The buffer for crosslinking samples contained additionally 25 mM L-cysteine to stop the crosslinking reaction.

Samples were lysed by sonication (Branson Digital Sonifier 450, Branson, Danbury, CT, USA) at 10% of amplitude 2 times for 10 seconds. The homogenate of lysed oocytes was centrifuged at 1600 RPM for 10 min to spin down cell debris. The supernatant was diluted 1:2 in phosphate buffered saline (PBS), containing 137 mM NaCl, 2.7 mM KCl, 10 mM Na_2HPO_4 and 1.7 mM KH_2PO_4, and centrifuged at 90000 RPM for 45 min.

The resulting pellet was resuspended by pipetting in 120-150 µl PBS and stored at –80˚C or used immediately for Western Blot analysis.

2.5 Protein electrophoresis and Western blot analysis

2.5.1 SDS-PAGE

2.5.1.1 Experimental protocol

Polyacrylamide gel electrophoresis (PAGE) allows separation of biological macromolecules according to their electrophoretic mobility, which depends on the length, conformation and charge of the molecule. Sodium dodecyl sulfate (SDS) is an anionic detergent, which denatures proteins and coats them with a negative charged cover, so the SDS-PAGE separates proteins on a polyacrylamide gel in an electric field according their molecular size (Laemmli 1970).

For the biochemical analysis of crosslinking, membrane preparation samples (25 µl for each sample) were denatured upon addition of 5 µl 6X reducing loading buffer (250 mM TRIS-HCl pH 6.8, 10 % SDS, 50 % glycerol, 0.4 % bromophenol blue, 12 % mercaptoethanol) for 30 min at room temperature.

After the denaturation, the samples were separated on 6.5% SDS-polyacrylamide mini gels. Gels were prepared in mini Bio-Rad PAGE apparatuses for 1 mm gel thickness. For the resolving gel, tetramethylethylenediamine (TEMED) and ammonium persulfate (APS) solutions were added and mixed with an automatic pipette to avoid bubble formation. About 9 ml of resolving gel solution were poured into the form, 1-2 ml isobutanol were pipetted on top. After solidification of the resolving gel, isobutanol was removed, and the gel surface was washed with Tris-Cl buffer 4 times. Stacking gel solution with added TEMED and APS were poured on top of the resolving gel and the sample comb was inserted to form sample lanes.

For each gel, 10 ml resolving and 2.5 ml stacking gel solutions were prepared and degased in vacuum for 40-45 min to allow better polymerization of acrylamide. The

resolving gel solution contained 2.5 ml Tris-Cl buffer pH 8.8 (Bio-Rad Laboratories, Inc., Hercules, CA, USA), 3.25 ml acrylamide/bis (37.5/1) (Bio-Rad Laboratories, Inc.), 0,1 ml 10% sodium dodecyl sulfate (SDS) 5.75 ml H_2O; 0.05 ml 10% APS in ethanol and 3.35 µl TEMED were added for polymerization. The stacking gel solution contained 0.625 ml Tris-Cl buffer pH 6.8 (Bio-Rad Laboratories, Inc.), 0.25 ml acrylamide/bis (37.5/1), 0.025 ml 10% sodium dodecyl sulfate (SDS), 1.6 ml H_2O; 0.0125 ml 10% APS in ethanol and 1.25 µl TEMED were added for polymerization.

After the stacking gel solidification, 30 µl samples were loaded to each lane. Two lanes of each gel were loaded with a marker (Precision Plus Protein™ All Blue Standards, Bio-Rad Laboratories, Inc., Hercules, CA, USA) and a control sample (a membrane preparation from oocytes expressing wild type CFTR).

Electrophoresis was performed at 80 mA for the stacking gel and at 100-120 mA for the resolving gel.

The resulting gels were used for Western blot analysis.

2.5.2 Western blot analysis

2.5.2.1 Experimental protocol

After electrophoresis, the gels were placed in transfer buffer **(**25 mM Tris, 192 mM glycine, 1.3 mM SDS, 20% methanol) for 10 min. Proteins were transferred from the gel to a membrane by a semidry blot: a polyvinylidene difluoride (PVDF) membrane (Immun-Blot® PVDF Membrane, Bio-Rad, Hercules, CA, USA) was pre-wet with methanol; two sheets of filter paper were soaked with transfer buffer. A "sandwich" from filter paper, the PVDF membrane, the gel and filter paper on top was placed into a Bio-Rad semidry electrophoretic transfer cell (Trans-Blot® SD Semi-Dry, Bio-Rad, Hercules, CA, USA), where proteins were transferred at 20 V for 45 min.

The membrane was rinsed then with water and Tris-buffered saline (TBS) (20 mM Tris, 137 mM NaCl, pH 7.6) containing additionally 0.1% Polyoxyethylene (20) sorbitan monolaurate (Tween20, Thermo Fisher Scientific Inc., Rockford, IL USA) (TBS-T) for 10 min each, and blocked with 5% nonfat dry milk (CARNATION® NonFat Dry Milk, Nestlé USA, Glendale, CA, USA) solution in TBS-T at +4°C overnight.

For immunodetection, the membrane was incubated with a 1:2000-1:1000 dilution of a rabbit polyclonal anti-R-domain antibody G449 (kindly provided by Dr. Angus Nairn) in TBS-T at room temperature. After 1 hour of incubation, the membrane was rinsed 2-3 times for 20 min with TBS-T. Then the horseradish peroxidase-linked secondary antibody, goat anti-rabbit IgG (Sigma, St. Louis, MO, USA), was applied in dilution 1:10000 in TBS containing 5% nonfat dry milk. After 1 hour of incubation, the membrane was rinsed 2-3 times with TBS. Immunoreactive bands were visualized with an ECL Plus Western Blotting Detection System (Amersham, Piscataway, NJ, USA) and Amersham Hyperfilm™ (Amersham Biosciences). The resulting films were scanned at 16-bit grayscale resolution on a flatbed scanner (Epson Perfection 3200 Photo, Epson, Long Beach, CA, USA).

3. Results

Cysteine-depleted CFTR constructs carrying mutations of selected residues were obtained as described in 2.1 and tested by TEVC recording. These mutations included T164C, L165C and L1059C from ICL1/ICL4 interface; I266C, E267C and A969C on ICL2/ICL3 interface; S176C, I177C, G178C, Q179C and V260C on ICL1/ICL2 interface, N965C, G970C, G971C, I972C, S1049C, F1052C and T1053C on ICL3/ICL4 interface; L172C, D173C, K174C, I175C, A274C, Y275C, S276C, R1283C, Y1307C and D1341C on TMD1/NBD2 interface; F508C and R1070C on TMD2/NBD1 interface.

ICL1/ICL4 interface. Residue L165 was initially suggested as a target for crosslinking experiments to test its possible interaction with residue L1059. However, the L165C mutant did not show a sufficient expression level in *Xenopus* oocytes for performing TEVC experiments. This might reflect the importance of this residue for the CFTR maturation and the negative influence of its mutation on the channel maturation. Mutations of this residue are found in CF patients (http://www.genet.sickkids.on.ca).

A neighbouring residue T164 was then mutated to cysteine, and the expression level of this mutant was sufficient to perform crosslinking experiments, so the TEVC data were collected for the pair of residues T164 and L1059. Figure 20 demonstrates the distance between these residues predicted by the homology model for CFTR (Figure 13) based on the known structure of Sav1866 and representing CFTR in its outward-facing conformation (Gulyas-Kovacs, Lockless and Gadsby 2007), which corresponds to the open state of the CFTR channel.

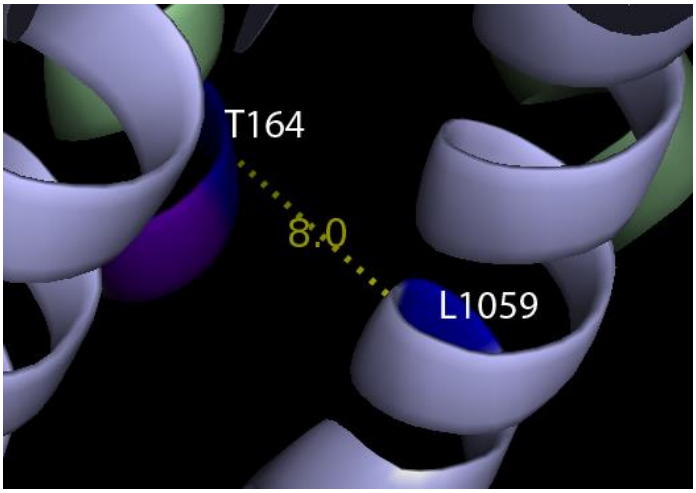

Figure 20. Distance (Å) between residues (Cα-atoms) T164 and L1059 predicted by the homology model for CFTR (Gulyas-Kovacs, Lockless and Gadsby 2007).

ICL2/ICL3 interface. Both mutants I266C and E267C demonstrated a sufficient expression level in *Xenopus* oocytes in preliminary experiments; the mutant I266C was selected for the further TEVC experiments. Figure 21 shows the distance between these residues predicted by the homology model for CFTR (Gulyas-Kovacs, Lockless and Gadsby 2007).

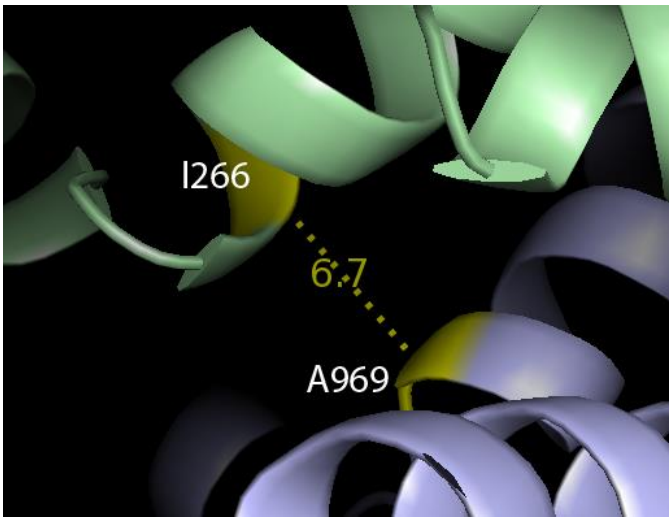

Figure 21. Distances (Å) between residues (Cα-atoms) I266 and A969 predicted by the homology model for CFTR (Gulyas-Kovacs, Lockless and Gadsby 2007).

ICL1/ICL2 interface. Mutants S176C, I177C, G178C, Q179C and V260C showed a sufficient expression level in *Xenopus* oocytes in preliminary experiments. Double-cysteine mutants G178C/V260C, Q179C/V260C demonstrated changes of the forskolin-induced conductance after BMOE application; the pair G178C/V260C was chosen for a more detailed study. Figure 22 illustrates the distance between these residues predicted by the homology model for CFTR (Gulyas-Kovacs, Lockless and Gadsby 2007).

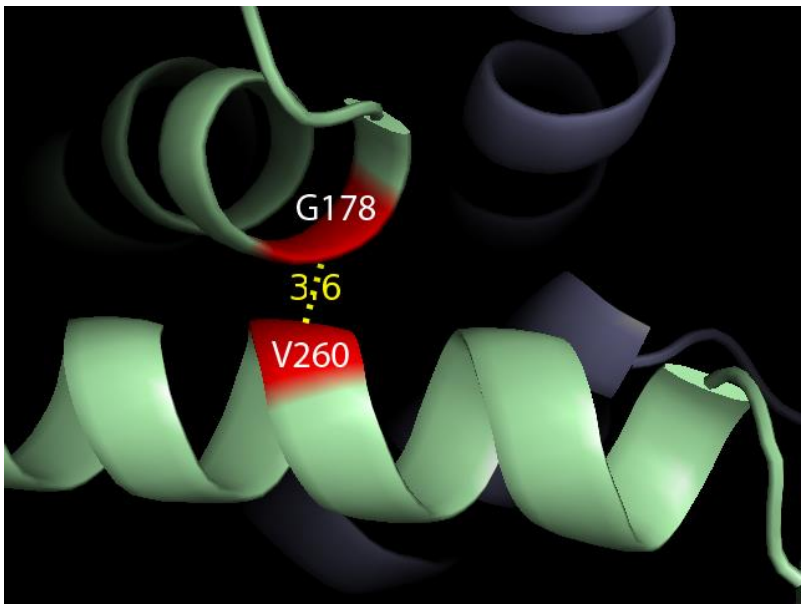

Figure 22. Distances (Å) between residues (Cα-atoms) G178 and V260 predicted by the homology model for CFTR (Gulyas-Kovacs, Lockless and Gadsby 2007).

ICL3/ICL4 interface. Mutants N965C, G970C, G971C, I972C, S1049C, F1052C and T1053C showed sufficient expression in *Xenopus* oocytes in preliminary experiments. These experiments also assayed the forskolin-induced conductance of the double-cysteine mutants N965C/S1049C, N965C/F1052C, N965C/T1053C, G970C/S1049C, G970C/F1052C, G970C/T1053C, G971C/S1049C, G971C/F1052C, G971C/T1053C, I972C/S1049C, I972C/F1052C and I972C/T1053C after the application of BMOE. The absence of the forskolin response after the crosslinker application for the pairs N965C/S1049C, N965C/F1052C, N965C/T1053C, G971C/S1049C, G971C/F1052C, and

G971C/T1053C suggested possible interactions between these residues. The full set of experimental data was collected for the pair G971/S1049. Figure 23 shows the distance between these residues predicted by the homology model for CFTR (Gulyas-Kovacs, Lockless and Gadsby 2007).

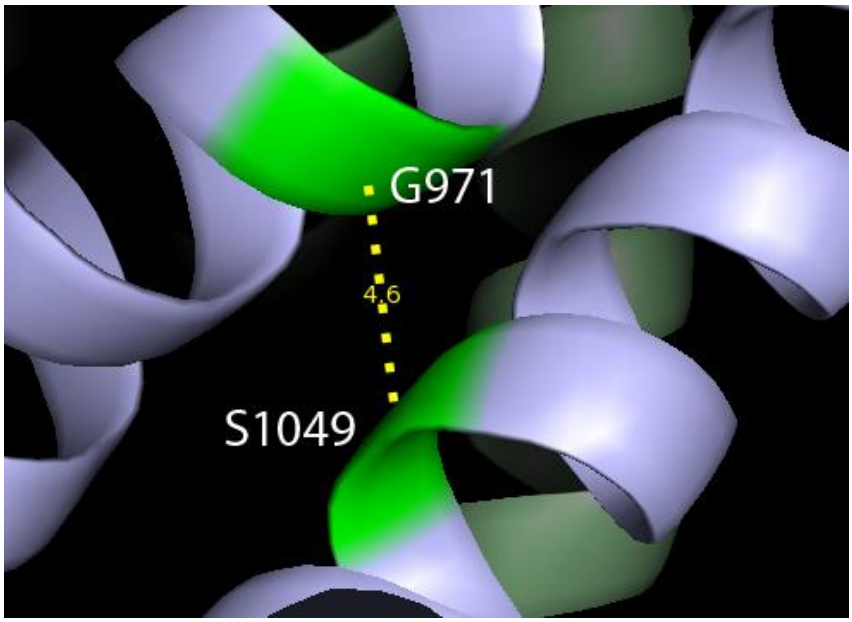

Figure 23. Distances (Å) between residues (Cα-atoms) G971 and S1049 predicted by the homology model for CFTR (Gulyas-Kovacs, Lockless and Gadsby 2007).

TMD2/NBD1 interface. Mutants F508C and R1070C both demonstrated a sufficient expression level in *Xenopus* oocytes to perform further TEVC experiments. Figure 24 shows the distance between these residues predicted by the homology model for CFTR (Gulyas-Kovacs, Lockless and Gadsby 2007).

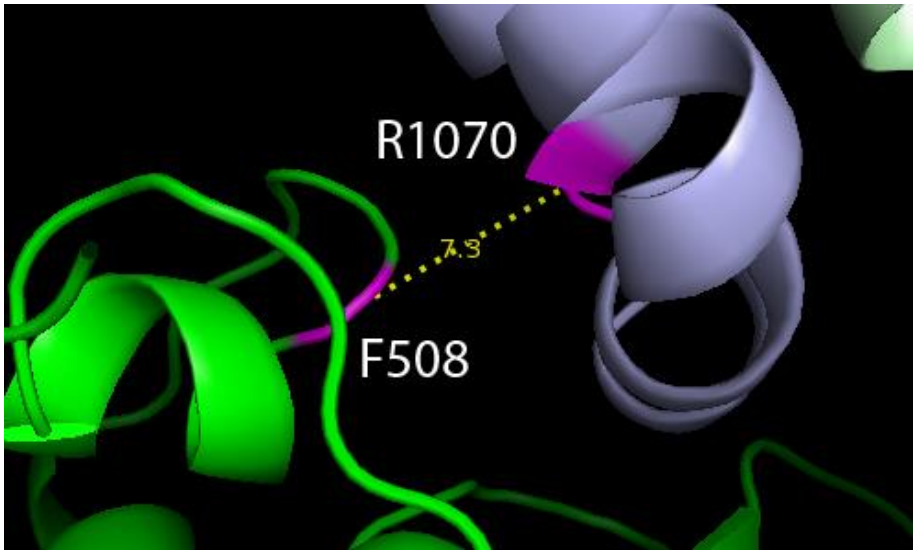

Figure 24. Distances (Å) between residues (Cα-atoms) F508 and R1070 predicted by the homology model for CFTR (Gulyas-Kovacs, Lockless and Gadsby 2007).

TMD1/NBD2 interface. Mutations L172C, D173C, K174C A274C, and Y275C diminished expression level of the cysteine-depleted CFTR (1-1480 2C background, see 2.1.2) in *Xenopus* oocytes, and mutations I175C, R1283C, Y1307C and D1341C almost completely depleted it. The insufficient expression did not allow selection of mutants for crosslinking experiments.

Consequently, the five selected mutant pairs for detailed analysis were: T164C/L1059C (ICL1/ICL4), I266C/A969C (ICL2/ICL3), G178C/V260C (ICL1/ICL2), G971C/S1049C (ICL3/ICL4) and F508C/R1070C (NBD1/ICL4). Their electrophysiological properties were studied with two perfusion protocols. The first protocol tested the forskolin response of channels pre-treated with the crosslinker, and the second one assayed the influence of the crosslinker on the forskolin-induced current. Examples of recordings are presented below, and the corresponding average conductance changes are summarized on graphs.

3.1 BMOE-induced conductance fluctuation

In TEVC experiments, BMOE caused an effect common for all tested constructs: brief intermittent fluctuations of the whole cell conductance (Figure 25). The effect took place also in oocytes expressing the background CFTR construct (both split and full-length) lacking engineered target cysteines, and retaining only two native cysteines C590 and C592 (or also C76, C128, C225, C276, C343, C491, and C524 in the N-terminal part for the F508C mutation, see 2.1.2) and even in control intact (injected with water, see 2.2) oocytes. This effect typically started within the first five minutes of the BMOE application, lasted up to ten minutes and tended to disappear by the end of this period. The fluctuation of the conductance was usually observed in TEVC experiments performed with the first perfusion protocol (see 2.3.2), when BMOE was applied before the forskolin stimulation (170 out of 243 experiments); however, if the BMOE application took place after the forskolin-induced current reached its maximum, the effect, though rarer, could also be seen in some experiments (11 out of 154 experiments, see, for example, Figure 47 C, Figure 52 C, D).

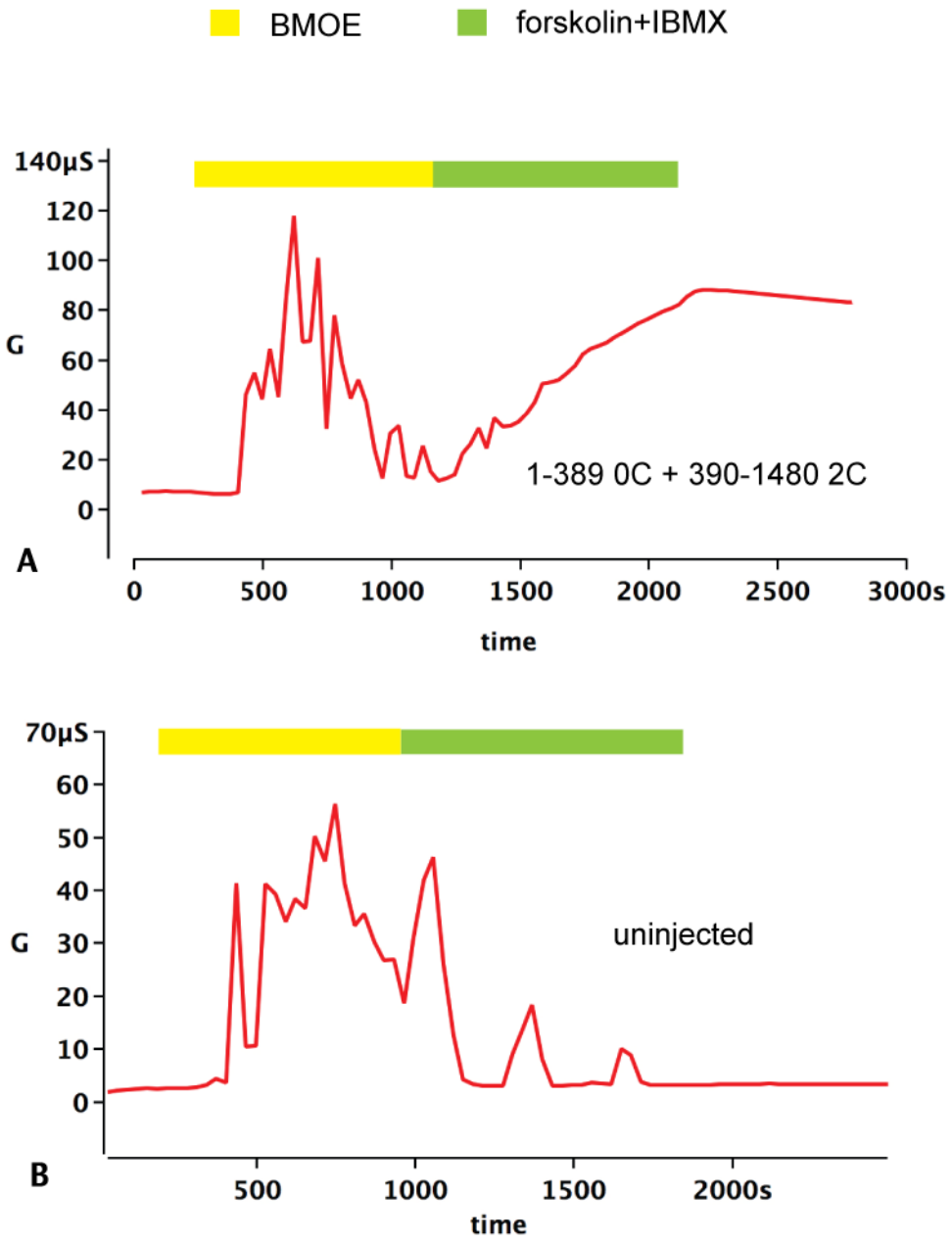

Figure 25. BMOE effect on the whole-cell conductance.

Examples of TEVC recordings for the background construct 1-389 0C + 390-1480 2C (A) and for the intact oocytes (B). Red traces show the changes of the whole cell conductance. During the experiments, the oocytes were perfused with the crosslinker solution (the perfusion period is marked as a yellow bar above the trace) before the forskolin stimulation (a green bar above the trace). The crosslinker application caused conductance fluctuations (Fig.25 A: 400-1500 s, Fig. 25 B: 400-1500 s of the recording).

Application of DMSO, the solvent used for BMOE stock solutions, in the same ~1% concentration as in the BMOE perfusion solution, did not cause this effect (0 out of 9 experiments, Figure 26).

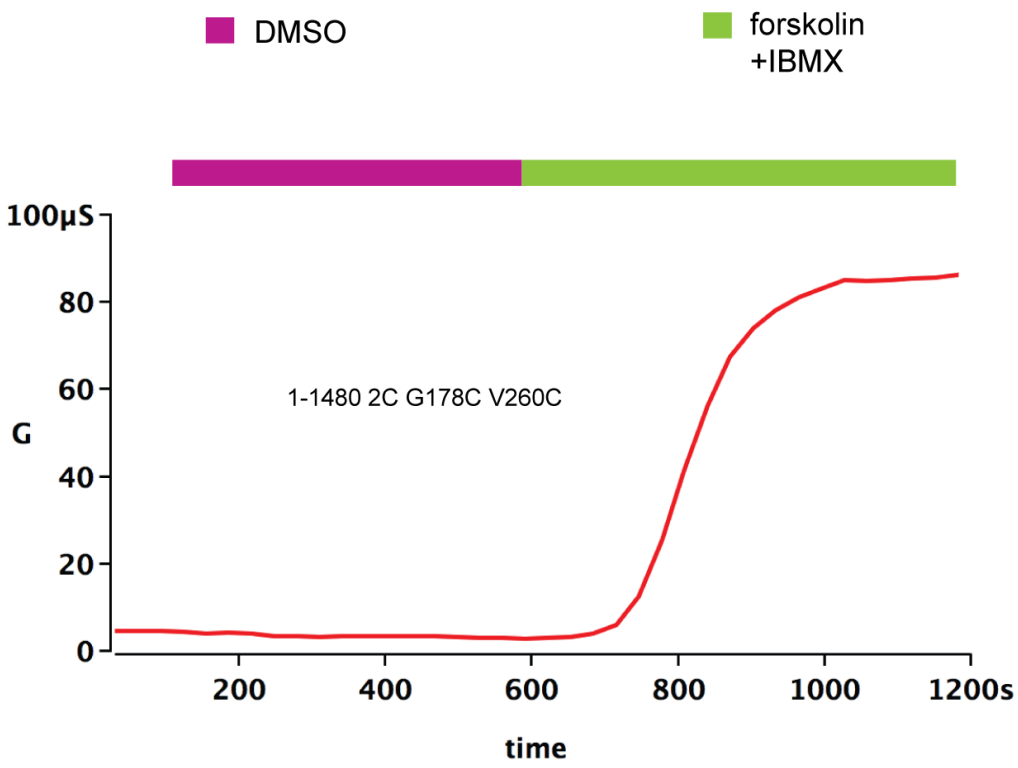

Figure 26. DMSO in ~1% concentration does not cause conductance fluctuations.

Application of ~1% DMSO (the corresponding time period is marked as a magenta bar) did not cause conductance fluctuations. The TEVC measurement was performed with the oocytes expressing CFTR carrying G178C and V260C mutations.

Application of N-Ethylmaleimide (NEM), an alkylating reagent that reacts with sulfhydryls (Figure 19), caused conductance fluctuations similar to those observed upon the BMOE influence (Figure 27). This suggests that the observed conductance changes could be caused by chemical reactions with sulfhydryl groups of either CFTR or also other proteins (as this effect was observed also in intact oocytes) influencing endogenous oocyte conductance (perhaps Ca-activated Cl^- channels (Miledi 1982)).

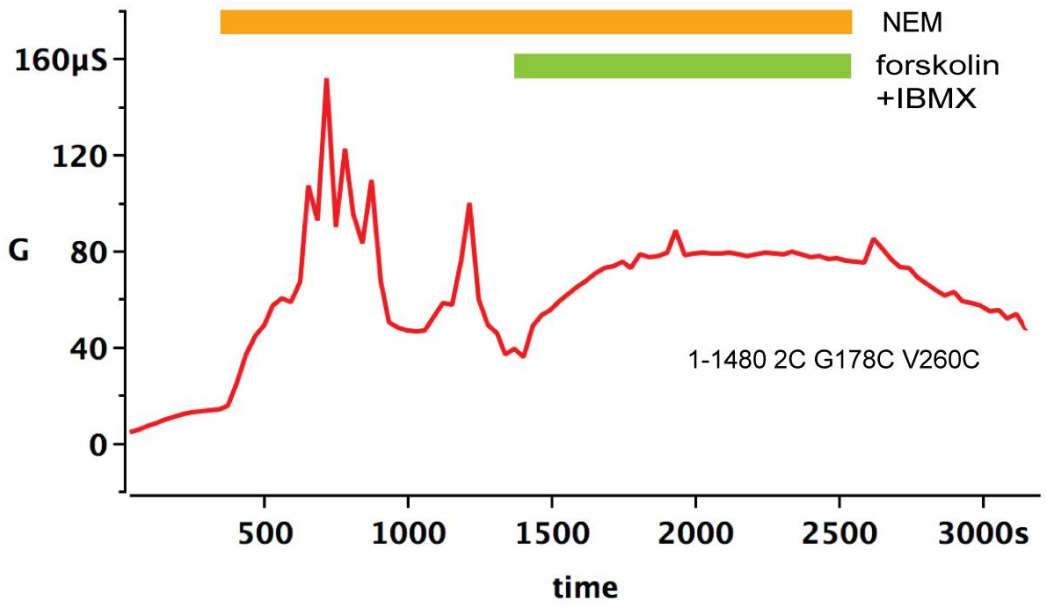

Figure 27. Conductance changes caused by the application of N-Ethylmaleimide (NEM).

Conductance changes of the oocytes expressing the 1-1480 2C G178C V260C construct upon the NEM application (300 µM solution in OR2 prepared from 25 mM stock solution in DMSO) can be observed in the interval 600-1500 s of the recording.

3.2 Probing of possible interactions between cytoplasmic helical extensions from the transmembrane helices

3.2.1 TMD1/TMD2 interfaces

According to the homology model for CFTR (Figure 14A), the interface between cytoplasmic helical extensions from the transmembrane helices of TMDs includes residue T164, which belongs to ICL1 and are proposed to interact with L1059 from ICL4. This interface also includes residue I266 from ICL2, which is proposed to interact with A969 from ICL3.

3.2.1.1 Experimental data collected for the pair of residues T164 and L1059

Positions of residues T164 and L1059 are demonstrated in Figure 28. They were mutated to cysteines in the split CFTR background: the T164C mutation was introduced into the N-terminal cysteine-free fragment of the CFTR amino acid sequence from 1 to 389 residue (1-389 0C background), the L1059C mutation was introduced into the C-terminal half 390-1480 containing two native cysteines, C590 and C592 (390-1480 2C background).

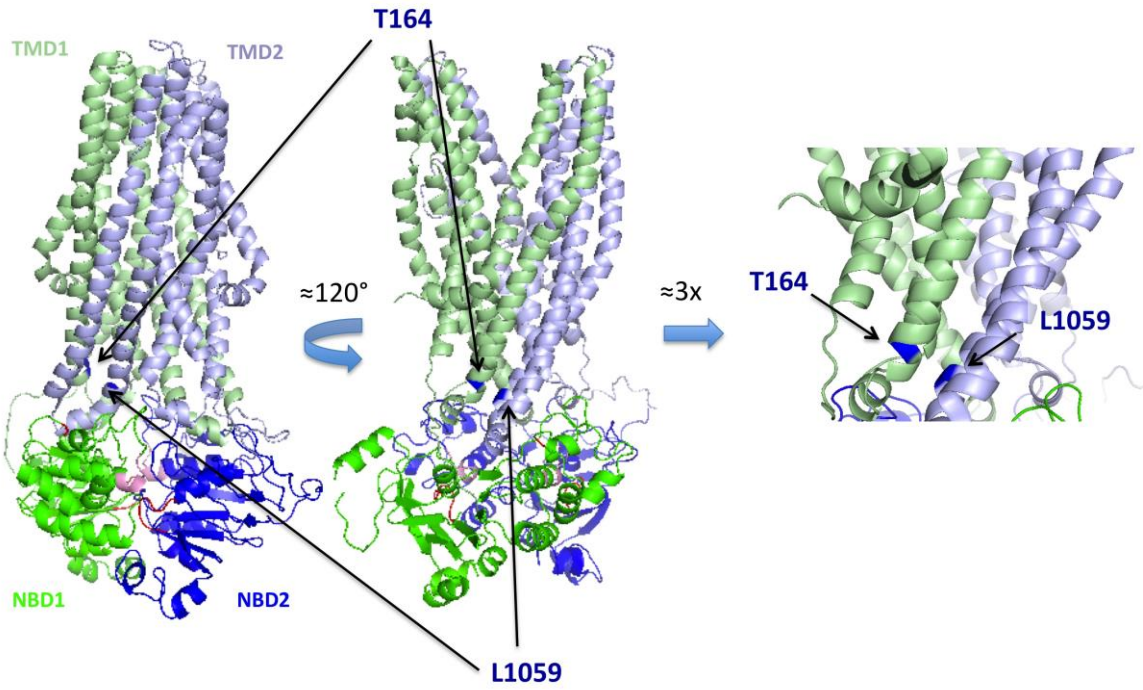

Figure 28. Positions of amino acid residues T164 and L1059 predicted by the homology model.

Side views of the homology model show TMD1 (pale green), TMD2 (pale blue), NBD1 (bright green) and NBD2 (bright blue). Residues T164 and L1059 are marked blue.

Figure 29 demonstrates examples of conductance traces obtained during TEVC recordings using the first perfusion protocol, which tested how the channels respond on the forskolin stimulation being pre-treated with the crosslinker. BMOE was added to the OR2 perfusion solution after about 3-5 min from the start of the recording and applied for about 15 min. After the BMOE treatment, the combination of forskolin and IBMX was added to the perfusion solution.

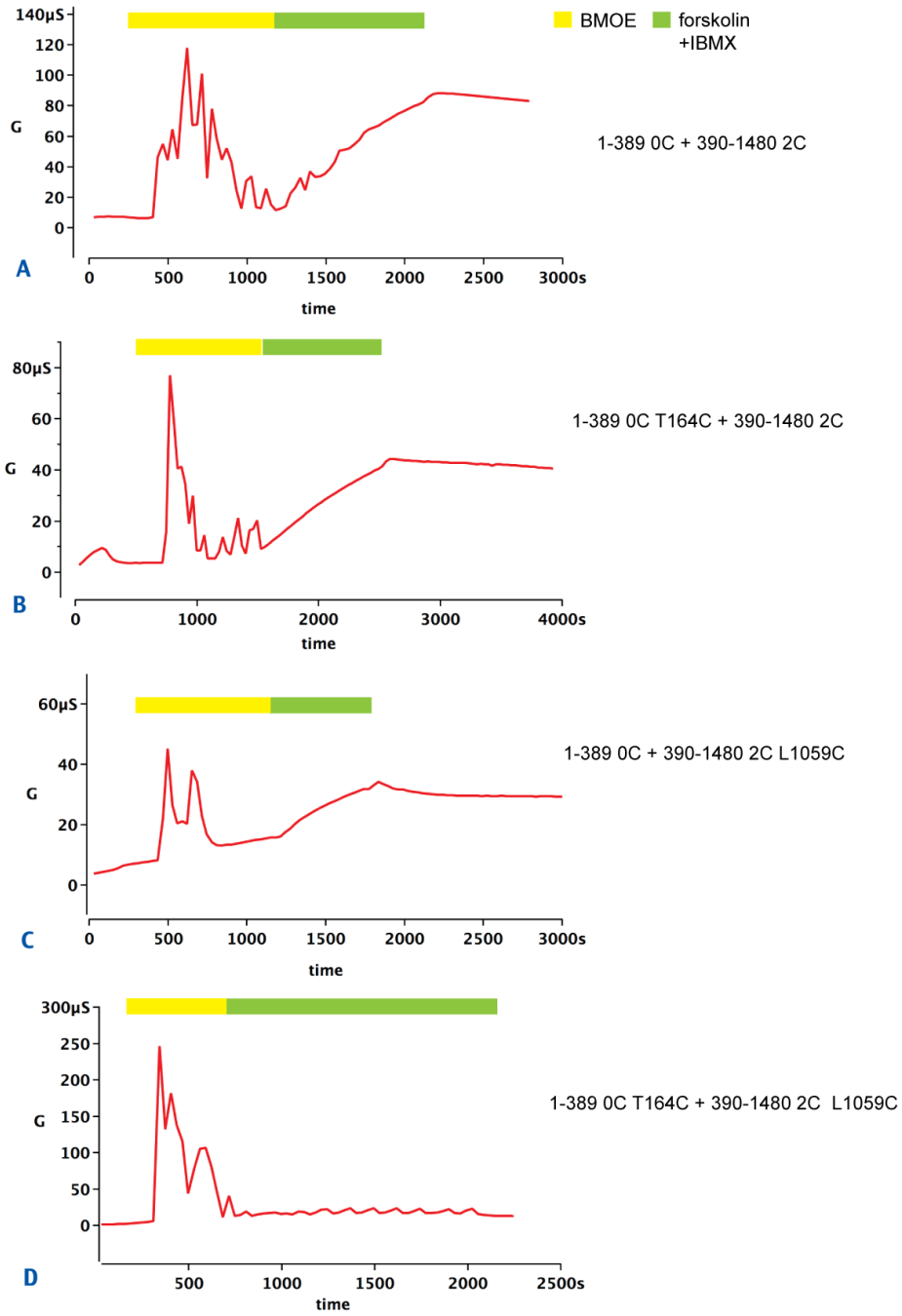

Figure 29. Response on the forskolin stimulation of CFTR pre-treated with BMOE. Examples of TEVC recordings for the pair of tested residues T164 and L1059.

Red traces show the changes of the whole cell conductance (G) for the background construct (A), single-cysteine mutants T164C (B) and L1059 (C), and the double-cysteine mutant T164C L1059C (D), recorded for 35-40 min. During the experiments, the oocytes were superfused with the crosslinker solution (the perfusion period is marked as a yellow bar above the trace) before the forskolin stimulation (perfusion period is marked as a green bar above the trace).

After the BMOE pre-treatment, application of forskolin and IBMX caused a continuous increase of the whole cell conductance for the background construct and both single-cysteine mutants (Figure 29 A: 1200-2100 s, Figure 29 B: 1500-2500 s, Figure 29 C: 1200-1800 s); but for the double-cysteine mutant, the conductance did not change significantly (Figure 29 D: 750-2000 s). The observed conductance changes are summarized on Figure 30. The diagram represents a ratio of the whole-cell conductance of these pre-treated with BMOE cells after and before the stimulation with forskolin. So, the size of the bars reflects the relative conductance increase under the forskolin influence.

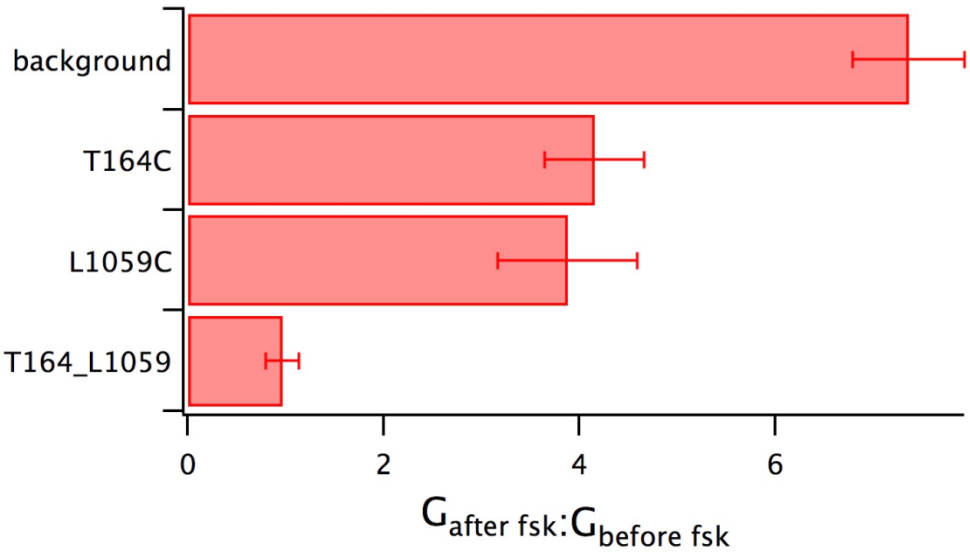

Figure 30. Effect of BMOE pre-treatment on the whole-cell conductance for the pair of tested residues T164 and L1059.

Each bar of the diagram represents a ratio of the whole-cell conductance of the pre-treated with BMOE oocytes after the forskolin stimulation ($G_{after\ fsk}$) and before this stimulation ($G_{before\ fsk}$) averaged for 3-6 oocytes for each expressed construct. Error bars reflect the standard error of the mean.

Forskolin increased the whole-cell conductance significantly stronger ($P<0.01$) for the oocytes expressing the background construct (7-8 times, Figure 30, top bar) than for oocytes expressing the mutant constructs. The whole-cell conductance upon the forskolin influence rose about four times for the single-cysteine mutants (Figure 30, bars 2 and 3 from the top) and did not change for the double-cysteine mutant (Figure 30, the bottom bar).

The second protocol tested the crosslinker influence on the conductance of channels pre-stimulated with forskolin/IBMX. Examples of the traces are shown in Figure 31.

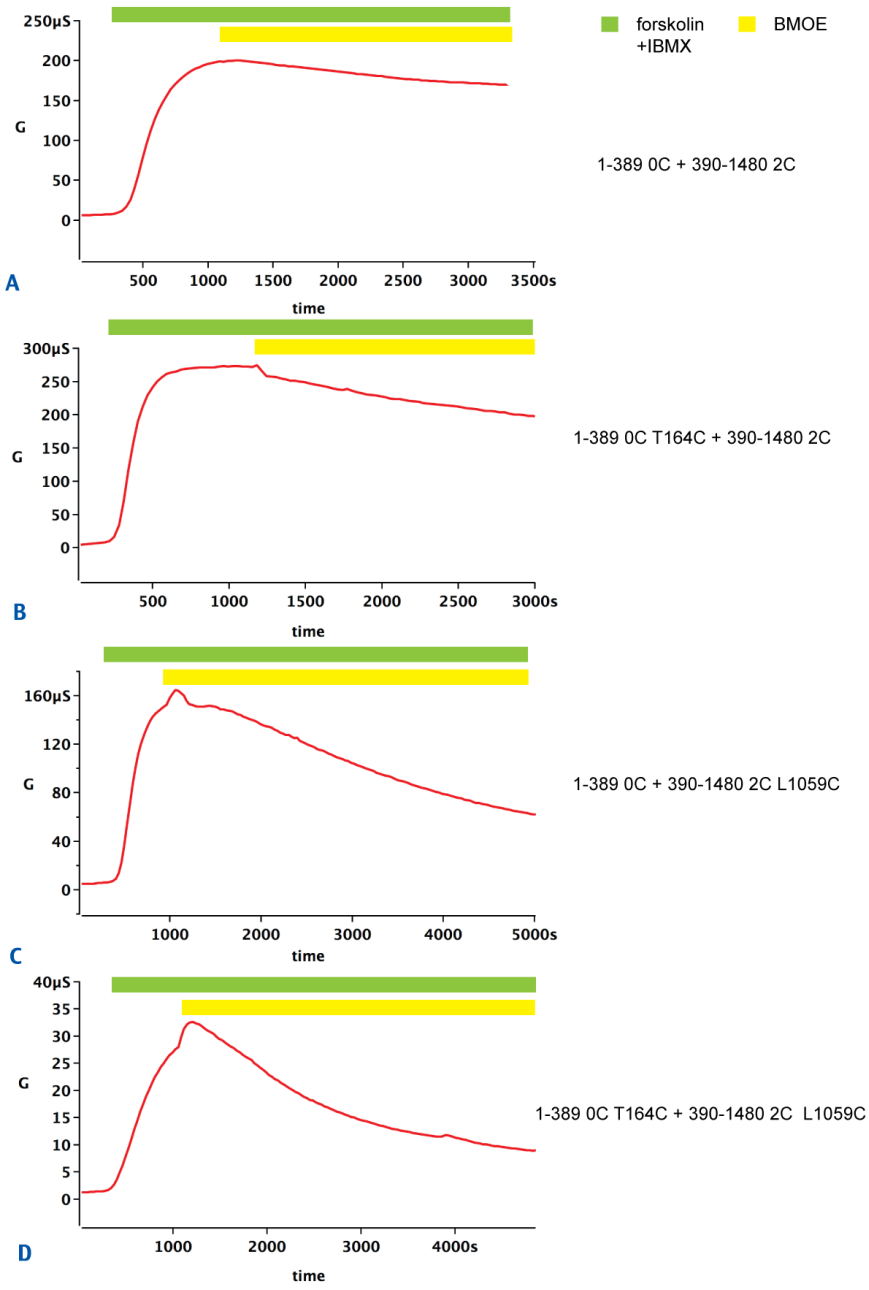

Figure 31. BMOE influence on the forskolin-induced conductance: examples of TEVC recordings for the pair of tested residues T164 and L1059.

Red traces show the changes of the whole cell conductance (G) of the oocytes expressing the background construct (A), single-cysteine mutants T164C (B) and L1059C (C), and the double-cysteine mutant T164C L1059C (D) recorded for over an hour. Oocytes were pre-stimulated with forskolin (the stimulation period is marked as green bars above the traces) before the crosslinker BMOE was added to the perfusion solution (the period of perfusion with BMOE is marked as yellow bars above the trace).

First, oocytes were superfused with the forskolin/IBMX solution; when the whole cell conductance reached a steady level, the crosslinker BMOE was added to the perfusion solution. Upon the forskolin stimulation, the whole cell conductance increased for all expressed constructs (Figure 31 A: 300-1000 s of the recording, Figure 31 B: 250-600 s, Figure 31C: 300-1000 s, Figure 31 D: 300-1200 s), reflecting the presence of functional CFTR in the cell membrane. The difference in the steady conductance levels reflects differences in the number and the activitiy of expressed CFTR channels in the cytoplasmic membrane. During the subsequent BMOE application, the conductance changed little for the oocytes expressing the background construct (Figure 31 A: 1100-3200 s of the recording) or the single-cysteine mutant T164C (Figure 31 B: 1200-3000 s), but decreased measurably for the oocytes expressing the single-cysteine L1059C and double-cysteine T164C L1059C mutant constructs (Figure 31 C: 1500-4100 s, Figure 31 D: 1200-3800 s). In these experiments, BMOE did not cause the transient conductance fluctuations, which were observed when BMOE was applied before the forskolin stimulation. Figure 32 summarizes the data.

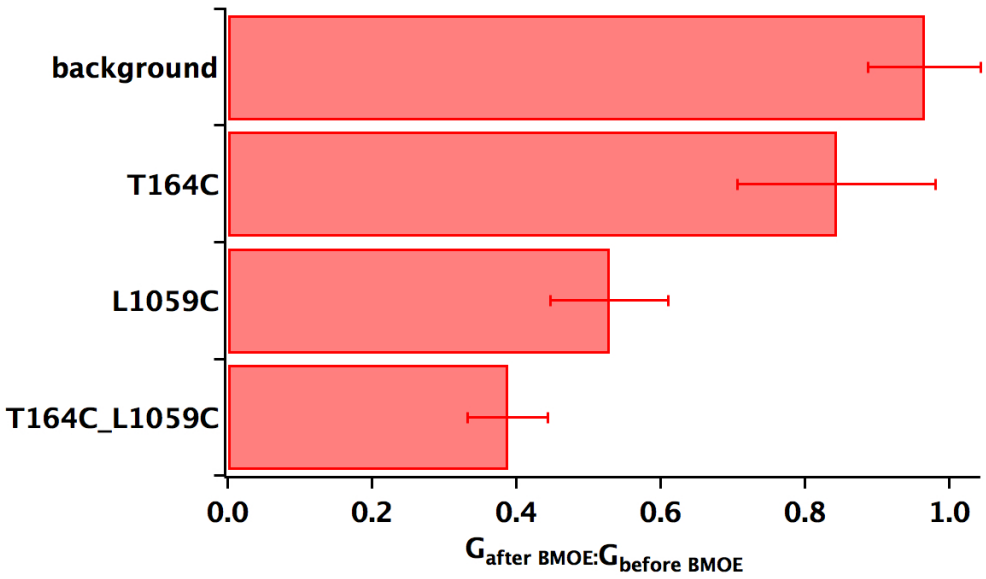

Figure 32. Effect of BMOE on the forskolin-induced conductance for the pair of tested residues T164 and L1059.

Each bar on the diagram represents a ratio of the whole-cell conductance of the pre-treated with forskolin oocytes after 30 min of the BMOE application ($G_{after\ BMOE}$) and before this application ($G_{before\ BMOE}$) averaged for 3-7 oocytes for the background construct, single-cysteine mutants T164C and L1059C and the double-cysteine mutant T164C L1059C. Error bars reflect the standard error of the mean.

BMOE did not change significantly the whole-cell conductance of the oocytes expressing the background construct (Figure 32, the first bar from the top) and decreased to only a minor extent the conductance of the oocytes expressing the single-cysteine mutant T164C (the second bar from the top). For the oocytes expressing single- and double-cysteine mutants with the engineered cysteine L1059C, a 50-60% conductance decrease upon BMOE application was observed (Figure 32, bottom two bars).

So, summarizing the results for the pair T164/L1059, it can be said that 10-15 min pretreatment with BMOE prevents response to the forskolin stimulation for the double-cysteine mutant, but not for the background, and somewhat impairs the response of the single-cysteines mutants. The crosslinker reduced the forskolin-induced conductance of the double-cysteine mutants and also to some extent for mutations of the single-cysteine mutant 1059. After 30 min, the crosslinker did not completely abolish the conductance of the double-cysteine mutant CFTR.

The stronger effect of BMOE on the double-cysteine mutants, compared to the single-cysteine ones suggests that linking position 164 in ICL1 to position 1059 in ICL4 traps these channels in a closed conformation.

3.2.1.2 Experimental data collected for the pair of residues I266 and A969

The next pair of tested residues was I266 in ICL2 of TMD1 and A969 in ICL3 of TMD2. Figure 33 demonstrates the proposed positions of these residues on the homology model. The corresponding cysteine mutations were introduced into the split CFTR background: the N-terminal cysteine-free fragment of the CFTR amino acid sequence from 1 to 389 residue (1-389 0C background) for the I266C mutation and the C-terminal half 390-1480 with two native cysteines, C590 and C592 (390-1480 2C background) for the A969C mutation. Figure 34 shows the traces obtained during TEVC recordings with oocytes expressing these mutants.

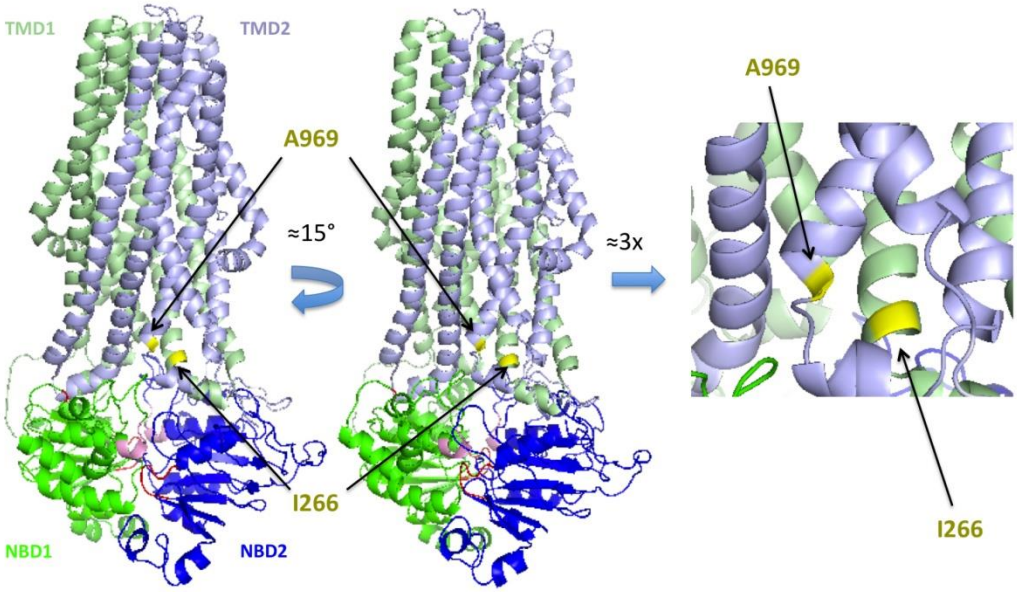

Figure 33. Positions of amino acid residues I266 and A969 predicted by the homology model.

Side views of the homology model show TMD1 (pale green), TMD2 (pale blue), NBD1 (bright green) and NBD2 (bright blue). Residues I266 and A969 are marked yellow.

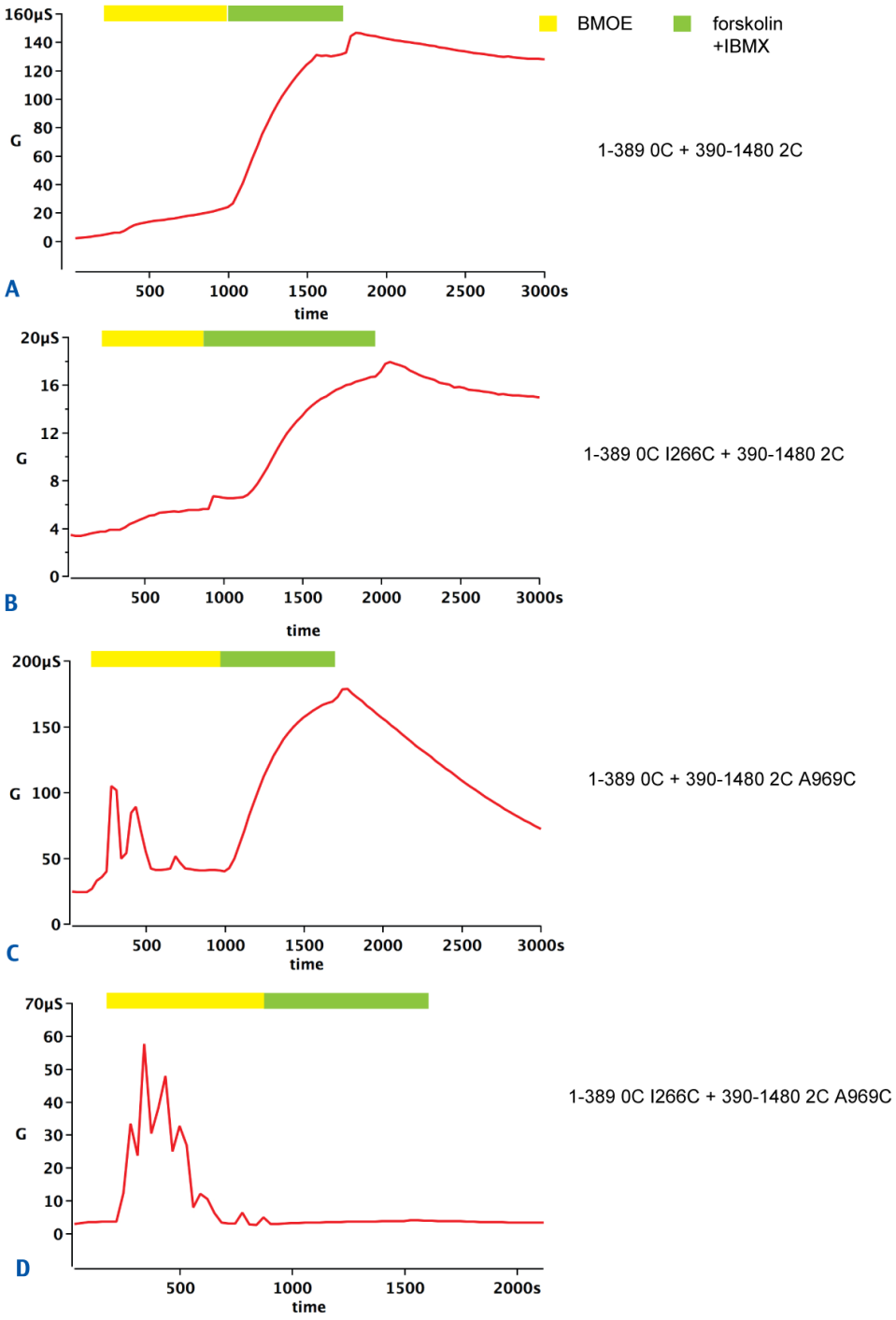

Figure 34. Response on the forskolin stimulation of CFTR pre-treated with BMOE. Examples of TEVC recordings for the pair of tested residues I266 and A969.

Red traces show the changes of the whole cell conductance (G) for the background construct (A), single-cysteine mutants I266C (B) and A969C (C), and the double-cysteine mutant I266C A969C (D) recorded for 35-40 min. During the experiments, the oocytes were superfused with the crosslinker solution (the perfusion period is marked as a yellow bar above the trace) before the forskolin stimulation (the stimulation period is marked as a green bar above the trace).

The whole cell conductance of the oocytes expressing the background construct and the single-cysteine mutants increased upon the forskolin stimulation (Figure 34 A: 1200-2100 s, Figure 34 B: 1200-2000 s, Figure 34 C: 1000-1700 s), but the conductance of the oocytes expressing the double-cysteine mutant did not change (Figure 34 D: 800-1800 s).

Figure 35 summarizes the data: after BMOE, forskolin-induced increase of whole-cell conductance was significantly larger ($P<0.01$) for the oocytes expressing the background (7-8 times, Figure 35, top bar) and single cysteine mutants (about 3-5 times, middle two bars) than for the double-cysteine mutant, whose conductance almost did not change (bottom bar).

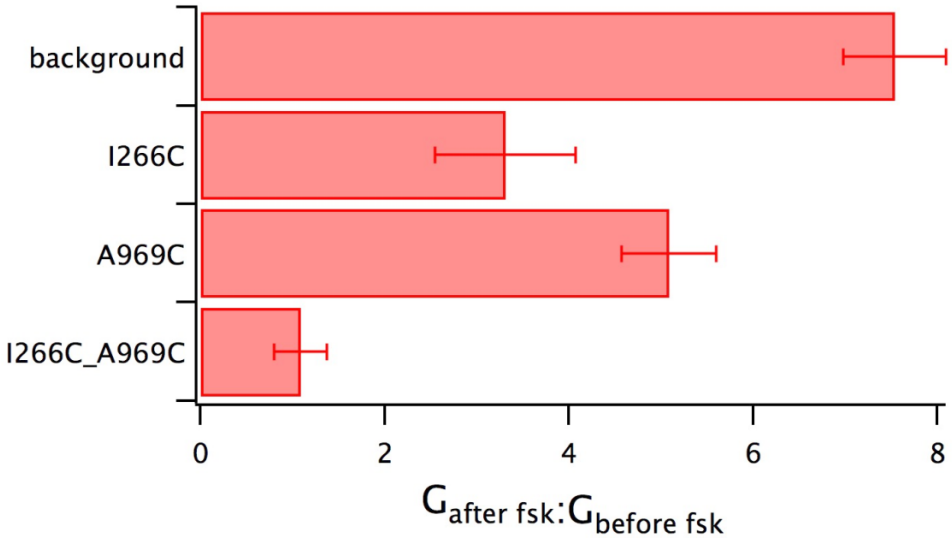

Figure 35. Effect of BMOE pre-treatment on the whole-cell conductance for the pair of tested residues I266 and A969.

Each bar on the diagram represents a ratio of the whole-cell conductance of the pre-treated with BMOE oocytes after the forskolin stimulation ($G_{after\ fsk}$) and before this stimulation ($G_{before\ fsk}$) averaged for 3-6 oocytes for each expressed construct. Error bars reflect the standard error of the mean.

Figure 36 demonstrates examples of traces obtained during TEVC experiments testing the crosslinker influence on the conductance pre-stimulated with forskolin.

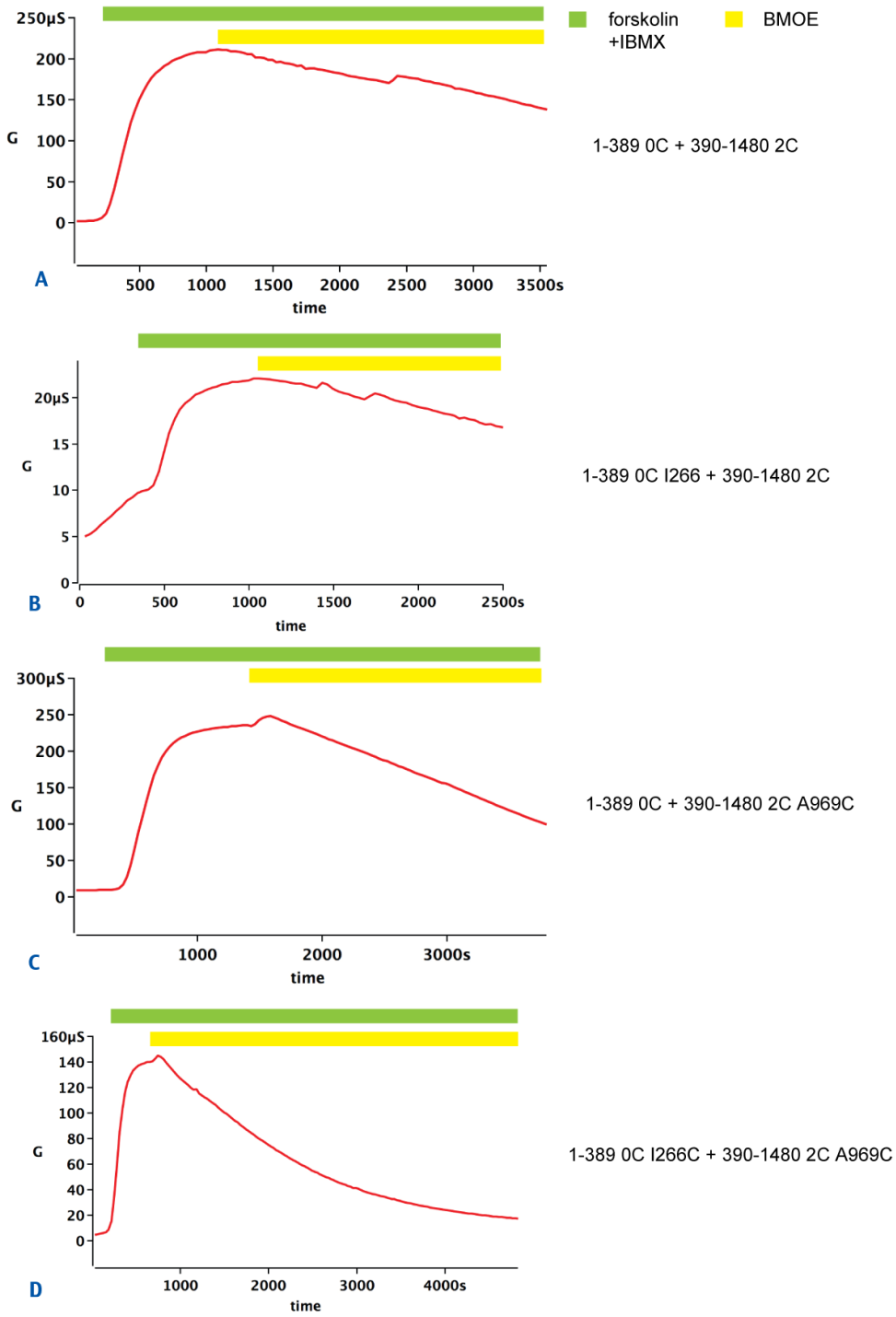

Figure 36. BMOE influence on the forskolin-induced conductance: examples of TEVC recordings for the pair of tested residues I266 and A969.

Red traces show the changes of the whole cell conductance (G) of the oocytes expressing the background construct (A), single-cysteine mutants I266C (B) and A969C (C), and the double-cysteine mutant I266C A969C (D) recorded for about 40 min. Oocytes were pre-stimulated with forskolin (the stimulation period is marked as green bars above the traces) before the crosslinker BMOE was added to the perfusion solution (the BMOE application period is marked as yellow bars above the trace).

After forskolin increased the whole cell conductance, BMOE application changed the conductance little for the oocytes expressing the background construct (Figure 36 A: 1100-3200 s) or the single-cysteine mutant I266C (Figure 36 B: 700-1500 s), but decreased it for the oocytes expressing the single or double mutants with the engineered cysteine A969C (Figure 36 C: 800-2000 s, Figure 36 D: 1200-2500 s).

Figure 37 summarizes the data.

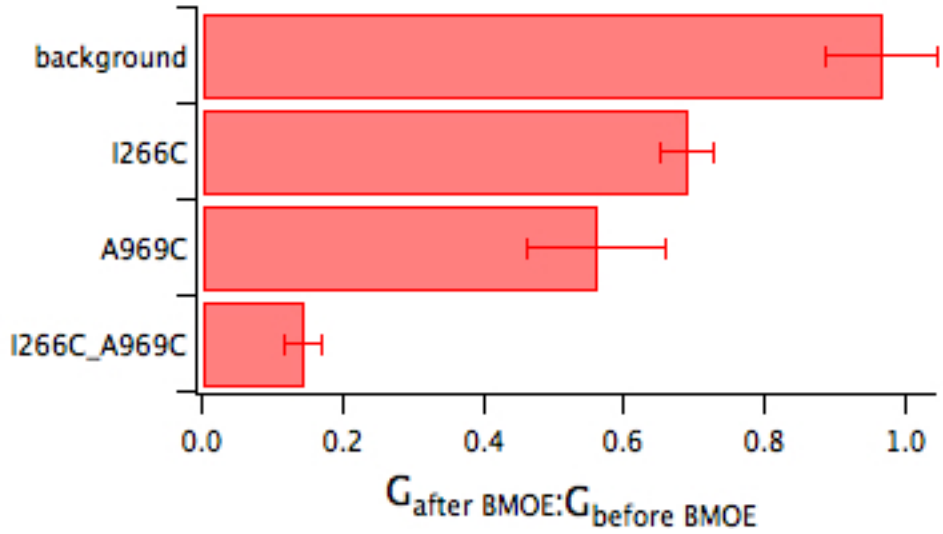

Figure 37. Effect of BMOE on the forskolin-induced conductance for the pair of tested residues I266 and A969.

Each bar on the diagram represents a ratio of the whole-cell conductance of the pre-treated with forskolin oocytes after 30 min of the BMOE application ($G_{after\ BMOE}$) and before this application ($G_{before\ BMOE}$) averaged for 3-6 oocytes for each expressed construct. Error bars reflect the standard error of the mean.

The more rapid and more complete conductance decrease by BMOE in the oocytes expressing the double-cysteine mutant compared to single-cysteine mutants argues that it results from crosslinking of the two target cysteines.

Gel electrophoresis was used to look for evidence of crosslinked proteins. The Western blot on Figure 38 visualizes protein electrophoresis results for mutants I266C and

A969C. PAGE was performed with membrane preparations of oocytes expressing single-cysteine mutants I266C, A969C, double-cysteine mutant I266C A969C, as well as the background construct and wild type CFTR.

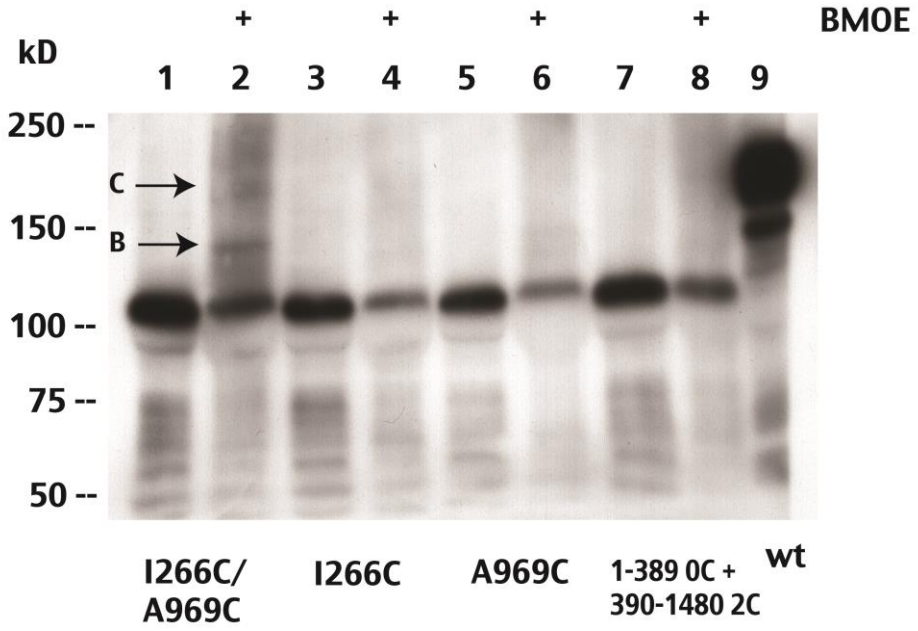

Figure 38. Western blot for I266C/A969C CFTR mutants.

Lanes 1, 2: double-cysteine mutant I266C/A969C; lanes 3, 4: single-cysteine mutant I266C; lanes 5, 6: single-cysteine mutant A969C; lanes 7, 8: background construct; lane 9 is a wild type CFTR used as a control. Preparations are made with application of the crosslinker (lanes 2, 4, 6, 8) or without it (lanes 1, 3, 5, 7, 9). Immunostaining was performed with anti-R-domain antibody G449. Arrows show additional bands, which appear only in case of the double-cysteine mutant I266C/A969C upon the crosslinker influence. The molecular weight of the bands corresponds to the band B (core glycosylated) and band C (fully glycosylated) of the full length CFTR (compare to lane 9).

Lanes 2, 4, 6, 8 represent samples of oocytes pre-treated with BMOE. Immunostaining was performed with anti-R-domain antibody G449 (see 2.5.2.1). Since the R-domain is a part of the C-terminal half (CFTR 390-1480 C590/C592), the N-terminal half (1-389 0C) on the blots is not visible.

The lane loaded with the prepararion from the pre-treated with BMOE oocytes expressing double-cysteine mutant I266C/A969C shows additional bands. The molecular weight of these bands (≈140 and ≈170 kDa) corresponds those of the wild type bands B

and C (lane 9). Immunostaining was performed with anti-R-domain antibody; and, since the R-domain is a part of the C-terminal half (390-1480) of the protein, only this half is visualized on the blots. It suggests that these additional bands correspond to the full glycosylated (C) and core glycosylated (B) crosslinked CFTR, which contains both halves of the CFTR molecule. The band with a molecular weight of about 100 kDa corresponds to the C-terminal half (390-1480) of CFTR, and the comparison with the crosslinked protein band reveals that only a small percentage of the protein was crosslinked. This might reflect the changing distance between the mutated residues depending on their relative orientation during the gating cycle, which influences the crosslinking yield. The lanes loaded with preparations containing CFTR with one or zero engineered cysteine (lanes 3-8) do not show additional bands reflecting that the crosslinking reaction did not take place.

To summarize the influence of BMOE to the pair of mutants I266C A969C, a conclusion can be made that BMOE almost completely prevented the response to forskolin for the double-cysteine mutant, but did not alter the response of the background, and allowed some response of the or single-cysteine mutants. The crosslinker measurably decreased the forskolin-induced current for all mutants with engineered cysteines, but the current was markedly lower for the double-cysteine mutant than for the single-cysteine mutants.

3.2.2 ICL1/ICL2 interface

Figure 39 shows predicted positions of residues G178 and V260 on a homology model for CFTR. The corresponding engineered cysteines were introduced into the full-length cysteine-depleted background containing two native cysteines, C590 and C592 (1-1480 2C background). Figure 40 demonstrates examples of traces obtained during TEVC recordings for the pair of mutants G178C and V260C.

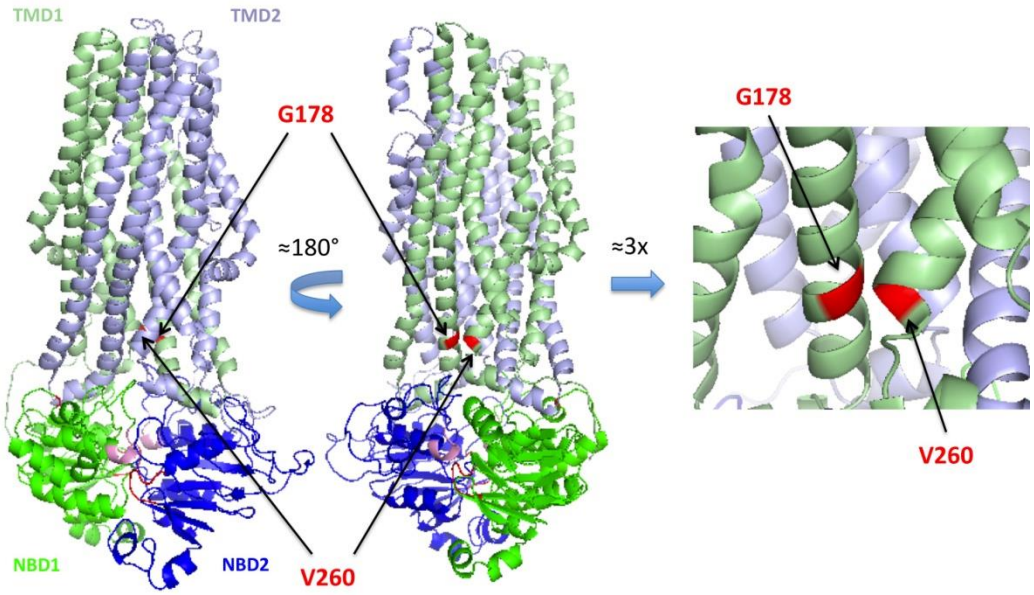

Figure 39. Positions of amino acid residues G178 and V260 predicted by the homology model.

Side views of the homology model show TMD1 (pale green), TMD2 (pale blue), NBD1 (bright green) and NBD2 (bright blue). Residues F178 and V260 are marked red.

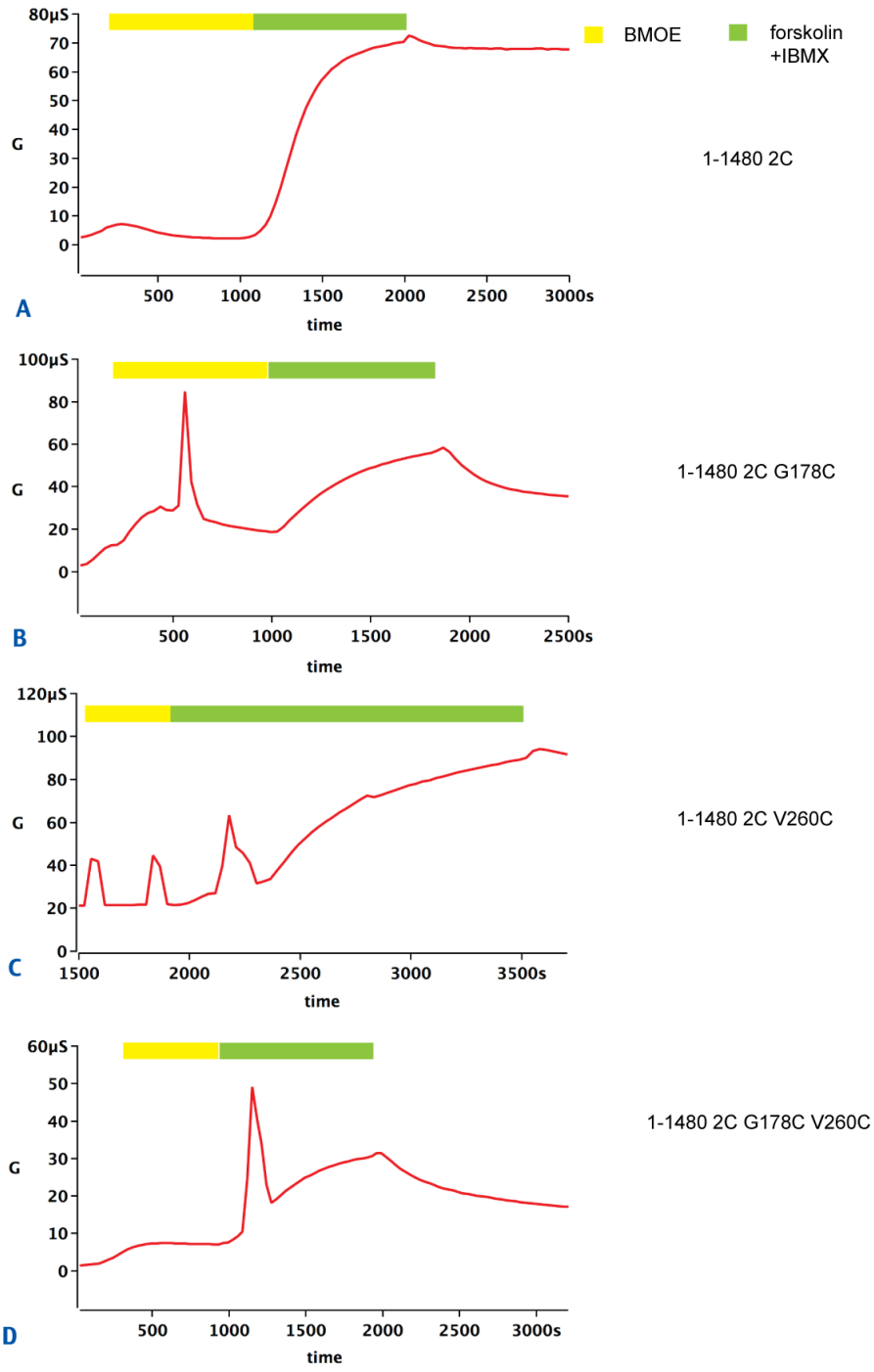

Figure 40. Response on the forskolin stimulation of CFTR pre-treated with BMOE. Examples of TEVC recordings for the pair of tested residues G178 and V260.

Red traces show the changes of the whole cell conductance (G) for the background construct, single-cysteine mutants G178C and V260C, and the double-cysteine mutant G178C V260C recorded for an hour. During the experiments, the oocytes were superfused with the crosslinker solution (the perfusion period is marked as a yellow bar above the trace) before the forskolin stimulation (which period is marked as a green bar above the trace).

Upon the forskolin stimulation, the whole cell conductance increased for all tested constructs (Figure 40 A: 1200-2100 s, Figure 40 B: 1000-1800 s, Figure 40 C: 2300-3500 s, Figure 40 D: 1300-2000 s), demonstrating that the CFTR function was not abolished by the crosslinker influence. The different conductance amplitudes reflect the different amount of expressed CFTR in the cell membrane.

Figure 41 summarizes the data. Forskolin increased the whole-cell conductance for all BMOE-pretreated constructs, however, significantly less strong than for the background/template CFTR (7-8 times, Figure 41, top bar). The forskolin-induced conductance increase was not significantly different for the mutants with engineered cysteines (Figure 41, bars 2-4 from the top).

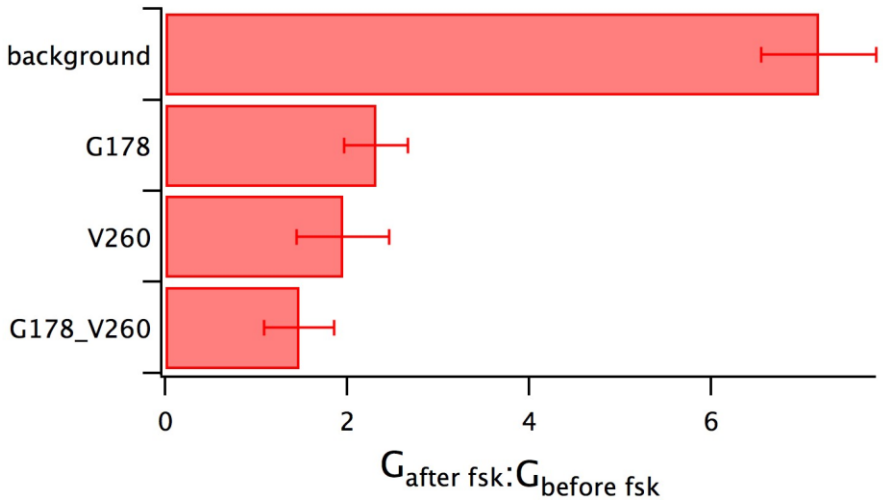

Figure 41. Effect of BMOE pre-treatment on the whole-cell conductance for the pair of tested residues G178 and V260.

Each bar on the diagram represents a ratio of the whole-cell conductance of the pre-treated with BMOE oocytes after the forskolin stimulation ($G_{after\ fsk}$) and before this stimulation ($G_{before\ fsk}$) averaged for 3-6 oocytes for each expressed construct. Error bars reflect the standard error of the mean.

Figure 42 shows examples of the traces obtained during TEVC experiments testing the crosslinker influence on the oocytes pre-stimulated with forskolin.

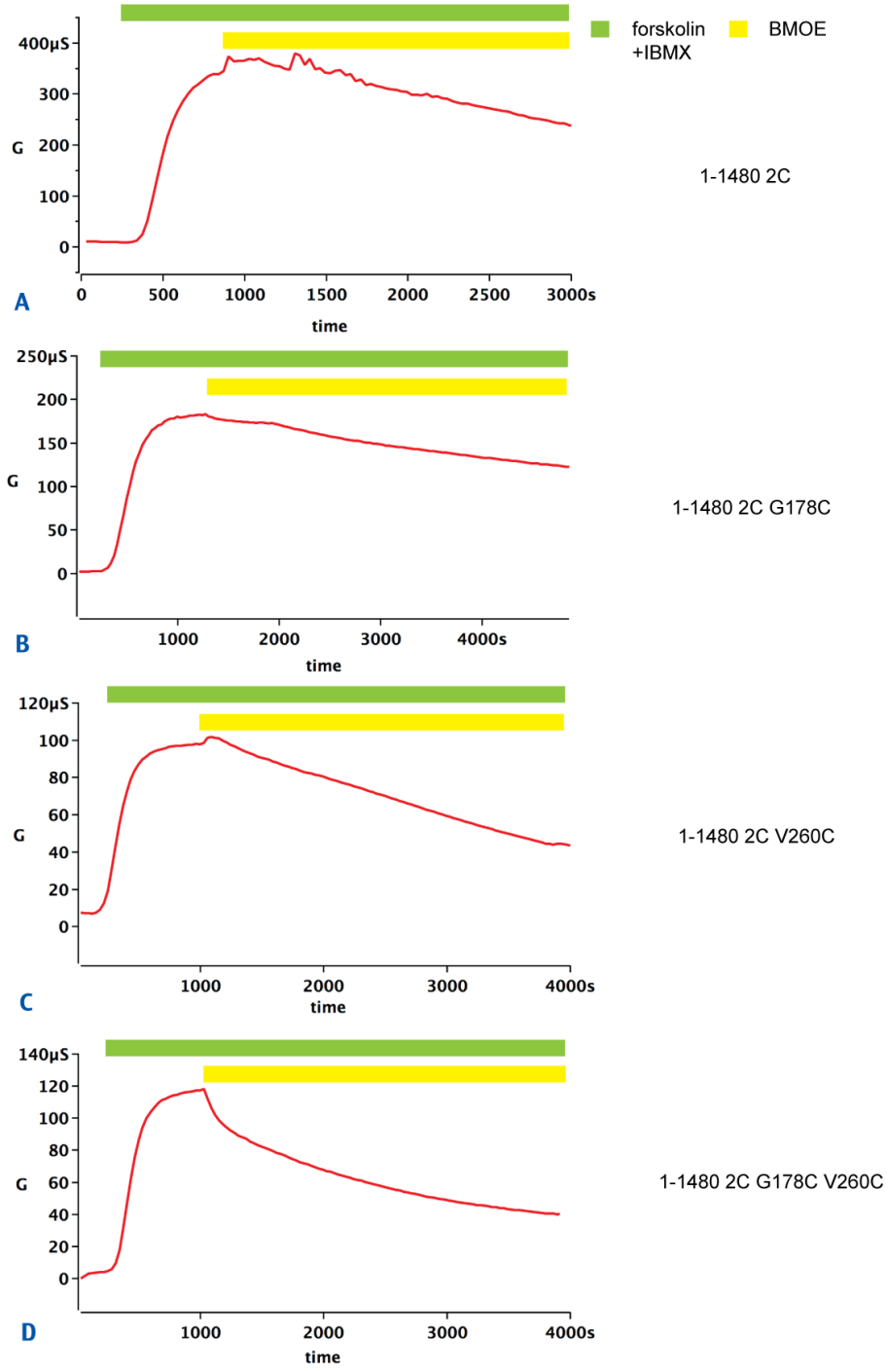

Figure 42. BMOE influence on the forskolin-induced conductance: examples of TEVC recordings for the pair of tested residues G178 and V260.

Red traces show the changes of the whole cell conductance (G) of the oocytes expressing the background construct (A), single-cysteine mutants G178C (B) and V260C (C), and the double-cysteine mutant G178C V260C (D) recorded for over an hour. Oocytes were pre-stimulated with forskolin (the stimulation period is marked as green bars above the traces) before the crosslinker BMOE was added to the perfusion solution (the BMOE application period is marked as yellow bars above the trace).

Upon the stimulation with forskolin, I observed the raise of the whole cell conductance for all expressed constructs (Figure 42 A: 300-1000 s of the recording, Figure 42 B: 300-1000 s, Figure 42 C: 300-800 s, Figure 42 D: 300-1000 s), which reflects the presence of functional CFTR in the cell membrane. Different amplitudes of this conductance increase reflect the amount of expressed CFTR.

During the subsequent BMOE application, the conductance almost did not change for the oocytes expressing the background construct and decreased for all oocytes expressing the mutants (Figure 42 A: 1100-3200 s of the recording, Figure 42 B: 1200-4100 s, Figure 42 C: 1200-4100 s, Figure 42 D: 1100-4000 s).

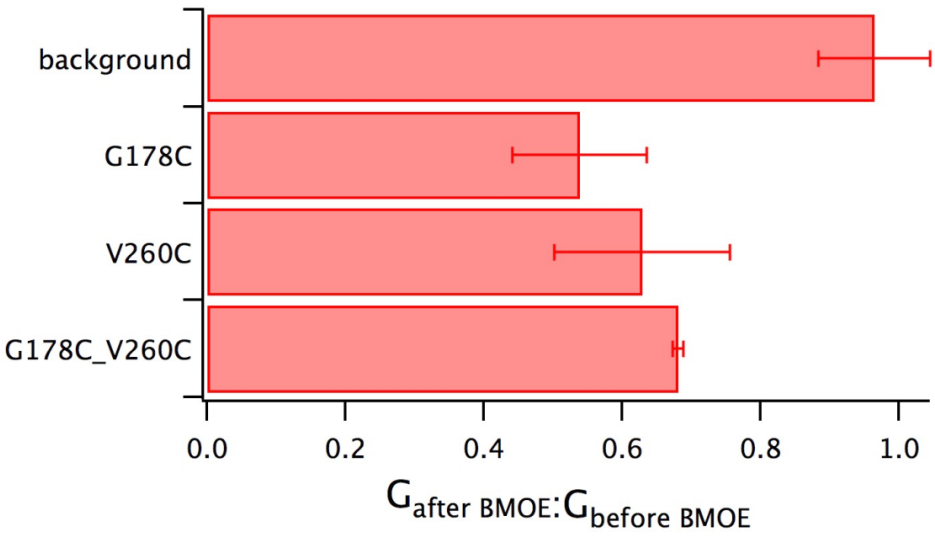

Figure 43. Effect of BMOE on the forskolin-induced conductance for the pair of tested residues G178 and V260.

Each bar on the diagram represents a ratio of the whole-cell conductance of the pre-treated with forskolin oocytes after 30 min of the BMOE application ($G_{after\ BMOE}$) and before this application ($G_{before\ BMOE}$) averaged for 3-6 oocytes for each expressed construct. Error bars reflect the standard error of the mean.

These data are summarized on Figure 43. BMOE did not change the whole-cell conductance of the oocytes expressing the background construct (Figure 43, top bar), but diminished it for the oocytes expressing mutants with engineered cysteines (35-50% decrease), but not significantly different for these three mutants (Figure 43, bars 2-4 from the top). BMOE influence appears to be stronger in case of G178C comparing to the double-cysteine mutant.

3.2.3 ICL3/ICL4 interface

This chapter presents experimental data for residues G971 and S1049. Figure 44 demonstrates positions of these residues on the homology model. Mutations G971C and S1049C were introduced into the full-length cysteine-depleted background containing two native cysteines, C590 and C592 (1-1480 2C background).

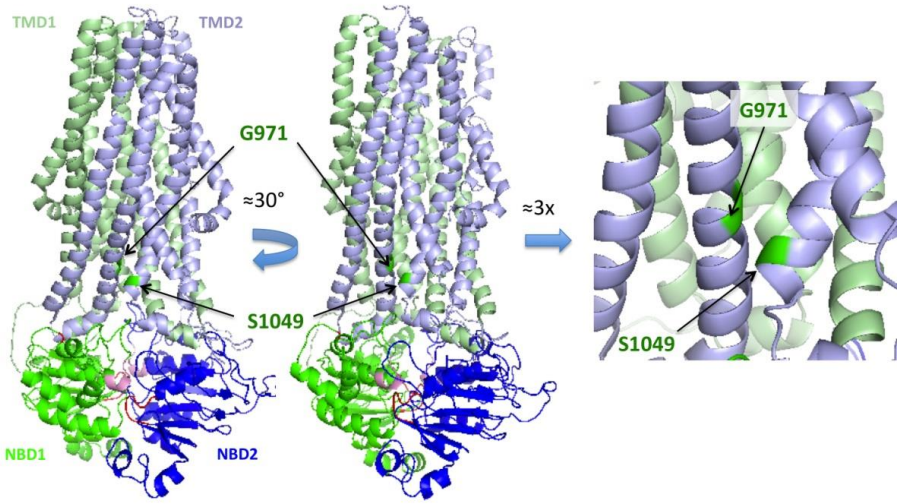

Figure 44. Positions of amino acid residues G971 and S1049 predicted by the homology model.

Side views of the homology model show TMD1 (pale green), TMD2 (pale blue), NBD1 (bright green) and NBD2 (bright blue). Residues G971 and S1049 are marked green.

Figure 45 illustrate TEVC recordings with oocytes expressing mutants G971C S1049C, G971C and S1049C, as well as the background CFTR construct 1-1480 2C as a control.

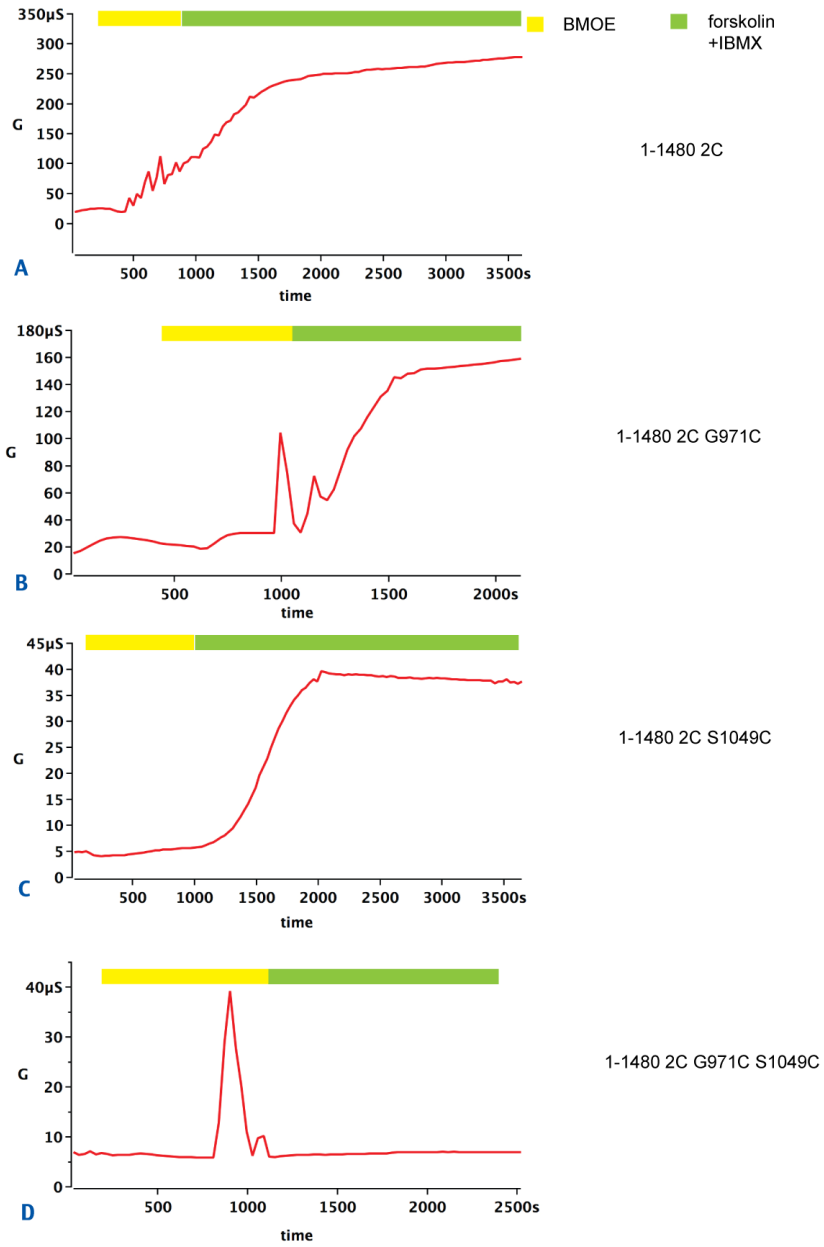

Figure 45. Response on the forskolin stimulation of CFTR pre-treated with BMOE. Examples of TEVC recordings for the pair of tested residues G971 and S1049.

Red traces show the changes of the whole cell conductance (G) for the background construct (A), the single-cysteine mutants G971C (B) and S1049C (C) and the double-cysteine mutant G971C S1049C (D) recorded for about 40 min. During the experiments, the oocytes were superfused with the crosslinker solution (the perfusion period is marked as a yellow bar above the trace) before the forskolin stimulation (which period is marked as a green bar above the trace).

After the BMOE pre-treatment, the forskolin stimulation increased the whole cell conductance of the oocytes expressing the background and both single-cysteine mutants (Figure 45 A: 1200-2100 s, Figure 45 B: 1000-1500 s, Figure 45 C: 1200-2000 s), but did not change the conductance for the double-cysteine mutant (Figure 45 D: 1200-2500 s).

Results are summarized on Figure 46.

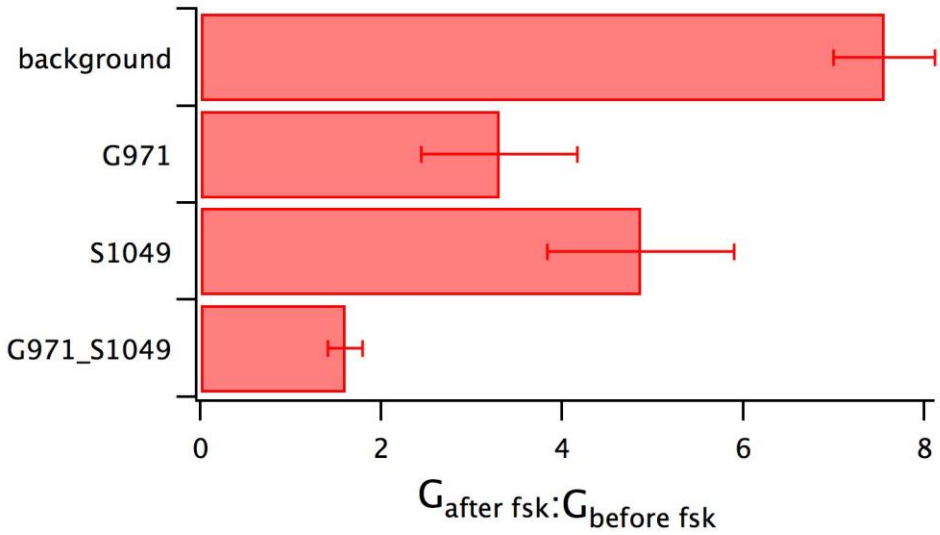

Figure 46. Effect of BMOE pre-treatment on the whole-cell conductance for the pair of tested residues G971 and S1049.

Each bar on the diagram represents a ratio of the whole-cell conductance of the pre-treated with BMOE oocytes after the forskolin stimulation ($G_{after\ fsk}$) and before this stimulation ($G_{before\ fsk}$) averaged for 3-7 oocytes for each expressed construct. Error bars reflect the standard error of the mean.

Forskolin increased the whole-cell conductance of the oocytes expressing the background construct (Figure 46, top bar) 7-8 times, which is significantly higher ($P<0.01$) than of oocytes expressing single-cysteine mutants (3-5 times, Figure 46, bars 2 and 3 from the top). In the double-cysteine mutant, forskolin had no significant activating effect (Figure 46, bottom bar).

Figure 47 illustrates TEVC experiments testing the crosslinker influence on oocytes pre-stimulated with forskolin for the mutants G971C and S1049C.

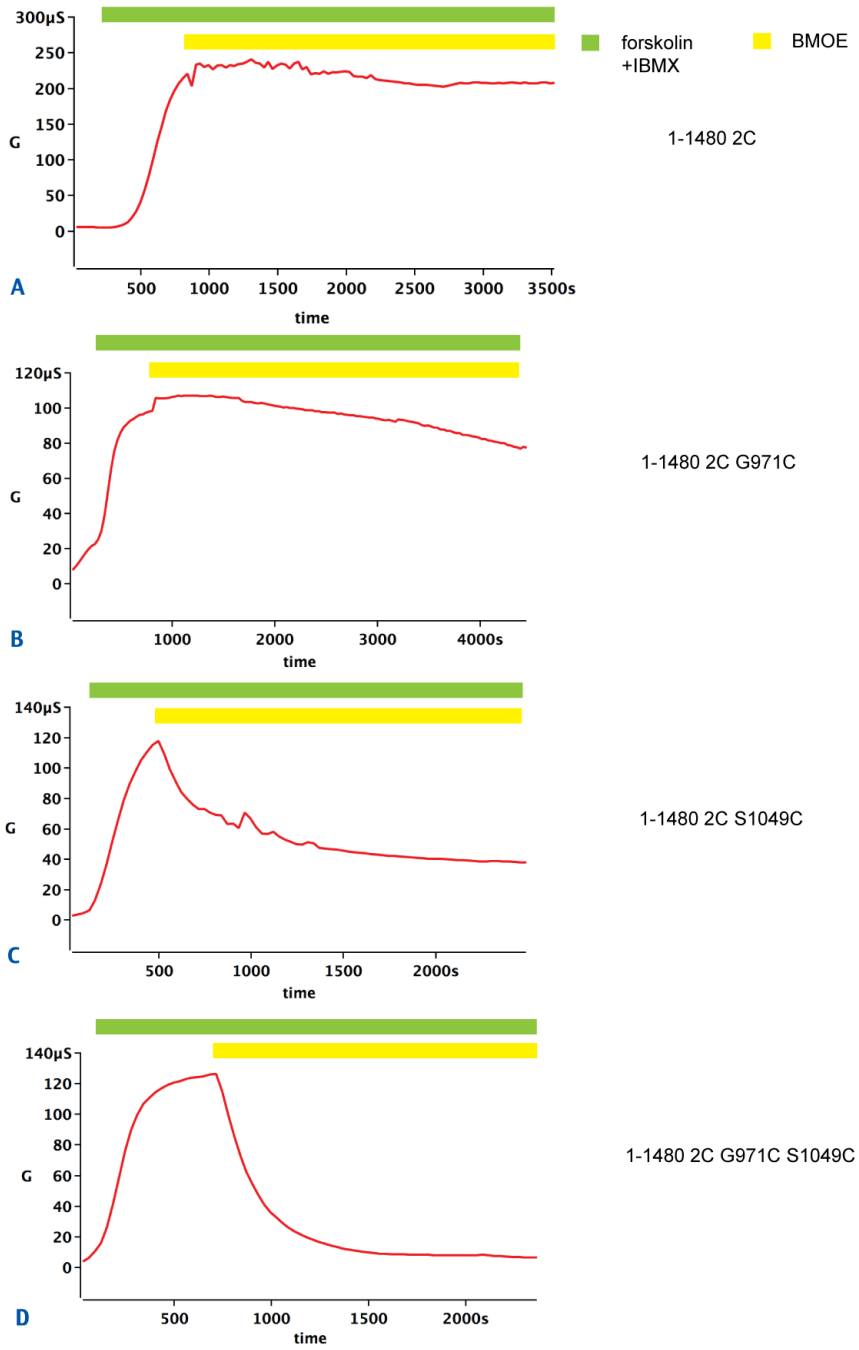

Figure 47. BMOE influence on the forskolin-induced conductance: examples of TEVC recordings for the pair of tested residues G971 and S1049.

Red traces show the changes of the whole cell conductance (G) of the oocytes expressing the background construct (A), single-cysteine mutants G971C (B) and S1049C (C), and the double-cysteine mutant G971C S1049C (D) recorded for about 40 min. Oocytes were pre-stimulated with forskolin (the stimulation period is marked as green bars above the traces) before the crosslinker BMOE was added to the perfusion solution (the BMOE application period is marked as yellow bars above the trace).

During the forskolin application, the whole cell conductance increased for all expressed constructs (Figure 47 A: 300-1000 s of the recording, Figure 47 B: 250-800 s, Figure 47 C: 200-500 s, Figure 47 D: 200-700 s). The amplitude differences of this increase reflect different expression level of CFTR.

BMOE almost did not change the conductance for the oocytes expressing the background construct (Figure 47 A: 1100-3200 s of the recording) as well as for the single-cysteine mutant G971C (Figure 47 B: 800-2500 s), but decreased it for the oocytes expressing the mutants with the engineered cysteine S1049C, both single- and double-cysteine mutants (Figure 47 C: 500-2500 s, Figure 47 D: 700-2500 s).

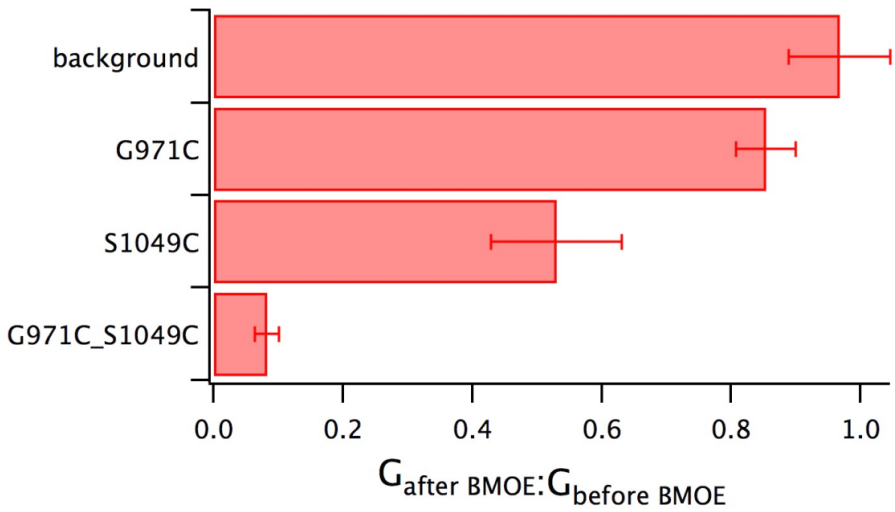

Figure 48. Effect of BMOE on the forskolin-induced conductance for the pair of tested residues G971 and S1049.

Each bar on the diagram represents a ratio of the whole-cell conductance of the pre-treated with forskolin oocytes after 30 min of the BMOE application ($G_{after\ BMOE}$) and before this application ($G_{before\ BMOE}$) averaged for 3-7 oocytes for each expressed construct Error bars reflect the standard error of the mean.

Figure 48 summarizes the results. The whole-cell conductance of the oocytes expressing the background construct almost did not change upon BMOE. For the single-cysteine mutant G971C, the conductance reduction after ~30 min was about 10%. The whole-cell conductance of the oocytes expressing the mutants with the engineered cysteine S1049C decreased even stronger (Figure 48, bars 3 and 4 from the top). In case of the

single-cysteine mutant, the conductance decreased to about 50% after ~35 min of the incubation, and for the double-cysteine mutant the conductance decrease was about 90% after 30 min. So, BMOE compromised the response on forskolin for the single-cysteine mutants and strongly diminished the forskolin-induced current for the double-cysteine mutant.

3.3 Probing of possible interactions for NBD/TMD interfaces

3.3.1 NBD1/TMD2 interface

Residues F508 and R1070 on the NBD1/TMD2 interface were proposed to interact, and Figure 49 demonstrates their positions on the homology model. The corresponding cysteine mutations were introduced into the split CFTR background: mutation F508C was introduced into N-terminal 1-633 native part of the CFTR sequence (1-633 wt), and mutation R1070C was introduced into the C-terminal cysteine free part 634-1480 (634-1480 0C). Figure 50 shows traces obtained during TEVC recordings with the first perfusion protocol for the pair of mutant residues F508C and R1070C in the split CFTR background (1-633 wt (containing all 9 native cysteines) co-expressed with 634-1480 0C).

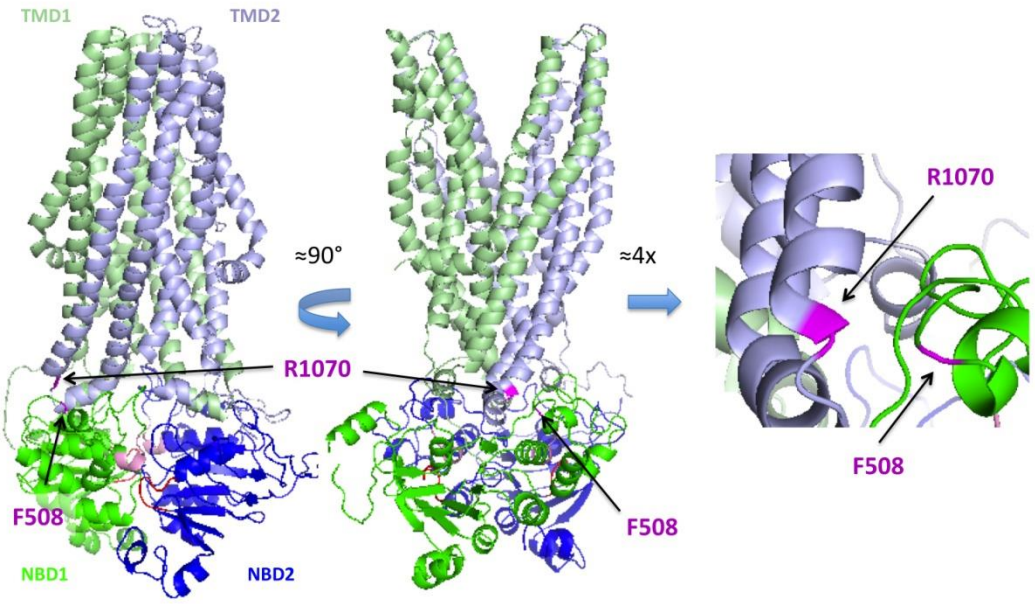

Figure 49. Positions of amino acid residues F508 and R1070 predicted by the homology model.

Side views of the homology model show TMD1 (pale green), TMD2 (pale blue), NBD1 (bright green) and NBD2 (bright blue). Residues F508 and R1070 are marked magenta.

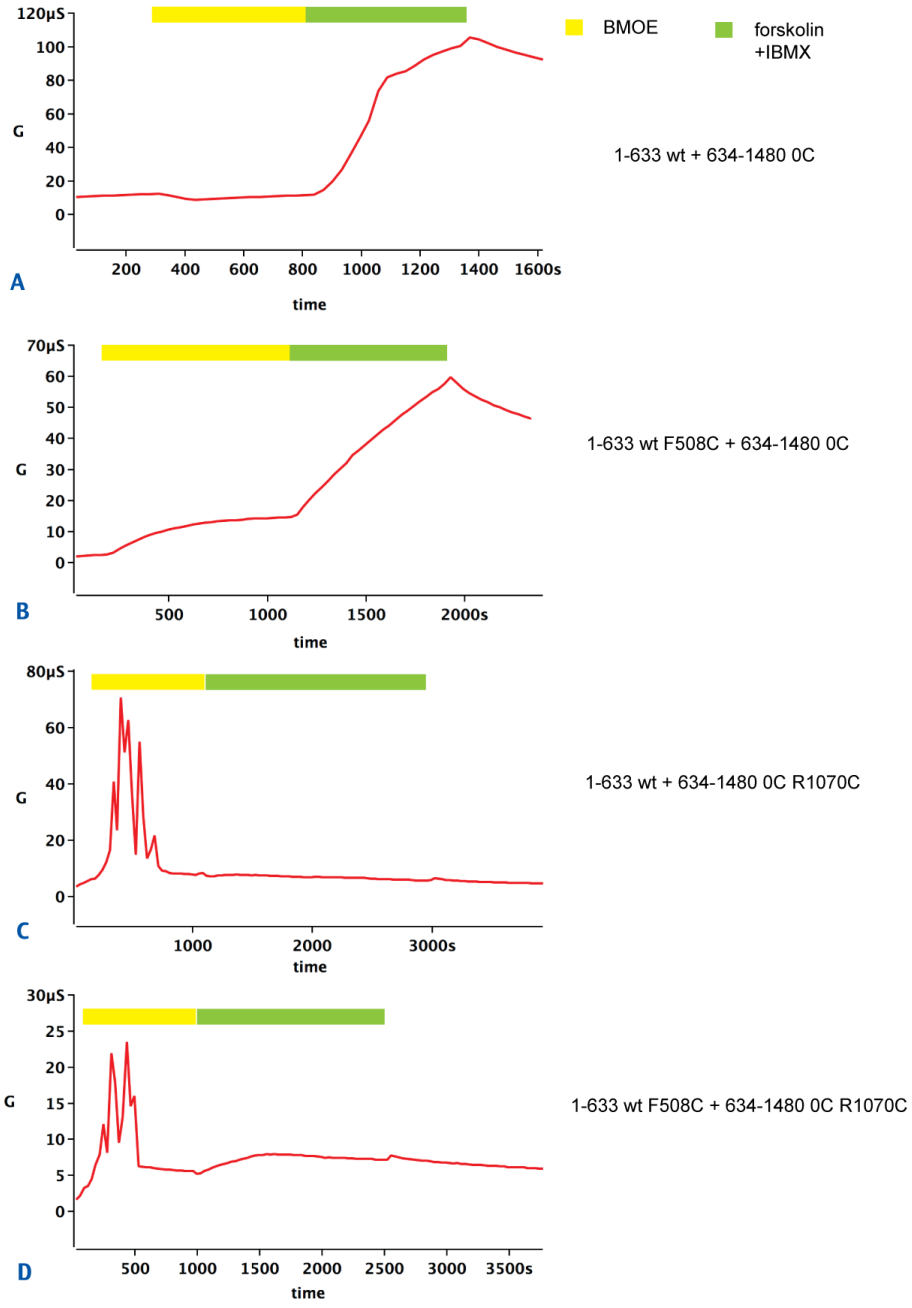

Figure 50. Response on the forskolin stimulation of CFTR pre-treated with BMOE. Examples of TEVC recordings for the pair of tested residues F508 and R1070.

Red traces show the changes of the whole cell conductance (G) for the background construct (A), the single-cysteine mutants F508C (B) and R1070C (C) and the double-cysteine mutant F508C R1070C (D) recorded for about 40 min. During the experiments, the oocytes were superfused with the crosslinker solution (the perfusion period is marked as a yellow bar above the trace) before the forskolin stimulation (which period is marked as a green bar above the trace).

Conductance fluctuations upon the BMOE application were observed (Figure 50 A: 450-1200 s of the recording, Figure 50 C: 500-1000 s, Figure 50 D: 200-500 s); the subsequent forskolin stimulation increased the conductance for the background (Figure 50 A: 1200-2100 s) and the single-cysteine mutant F508C (Figure 50 B: 1200-1900 s), but not for the mutants R1070C, both single- and double-cysteine mutants (Figure 50 C: 1200-2500 s, Figure 50 D: 500-2500 s).

Figure 51 summarizes the data. Forskolin increased 7-8 times the whole-cell conductance of the oocytes expressing the background (Figure 51, top bar), significantly higher ($P<0.01$) than for the cysteine mutants: the conductance increased about 3 times for the cells expressing F508C (Figure 51, bar 2 from the top) and almost did not change for the oocytes expressing R1070C (Figure 51, bar 2 vs. bars 3 and 4 from the top). It is remarkable that BMOE resulted in the same conductance depletion in the single and double mutant carrying R1070C.

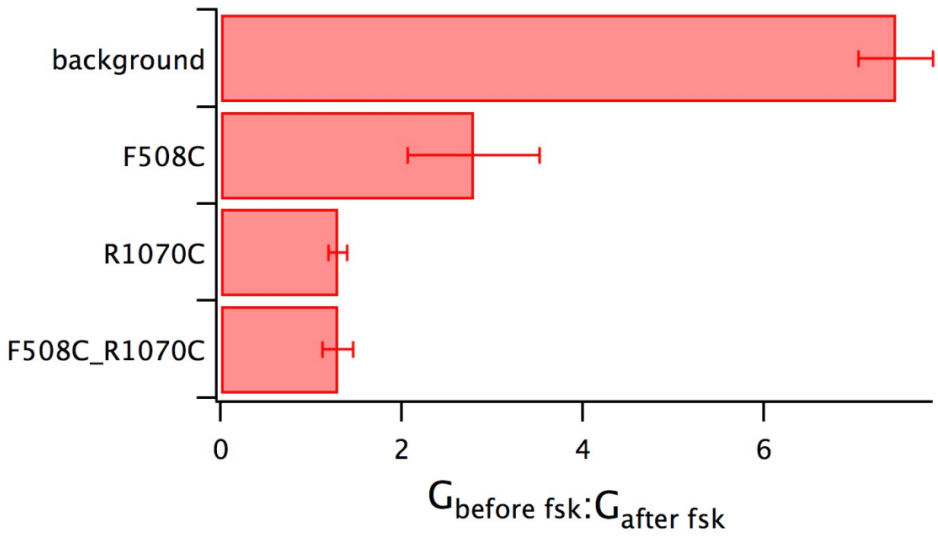

Figure 51. Effect of BMOE pre-treatment on the whole-cell conductance for the pair of tested residues F508 and R1070.

Each bar on the diagram represents a ratio of the whole-cell conductance of the pre-treated with BMOE oocytes after the forskolin stimulation ($G_{after\ fsk}$) and before this stimulation ($G_{before\ fsk}$) averaged for 3-6 oocytes for each expressed construct. Error bars reflect the standard error of the mean.

Figure 52 demonstrates examples of the traces obtained during TEVC recordings testing the crosslinker influence on the pre-stimulated with forskolin oocytes.

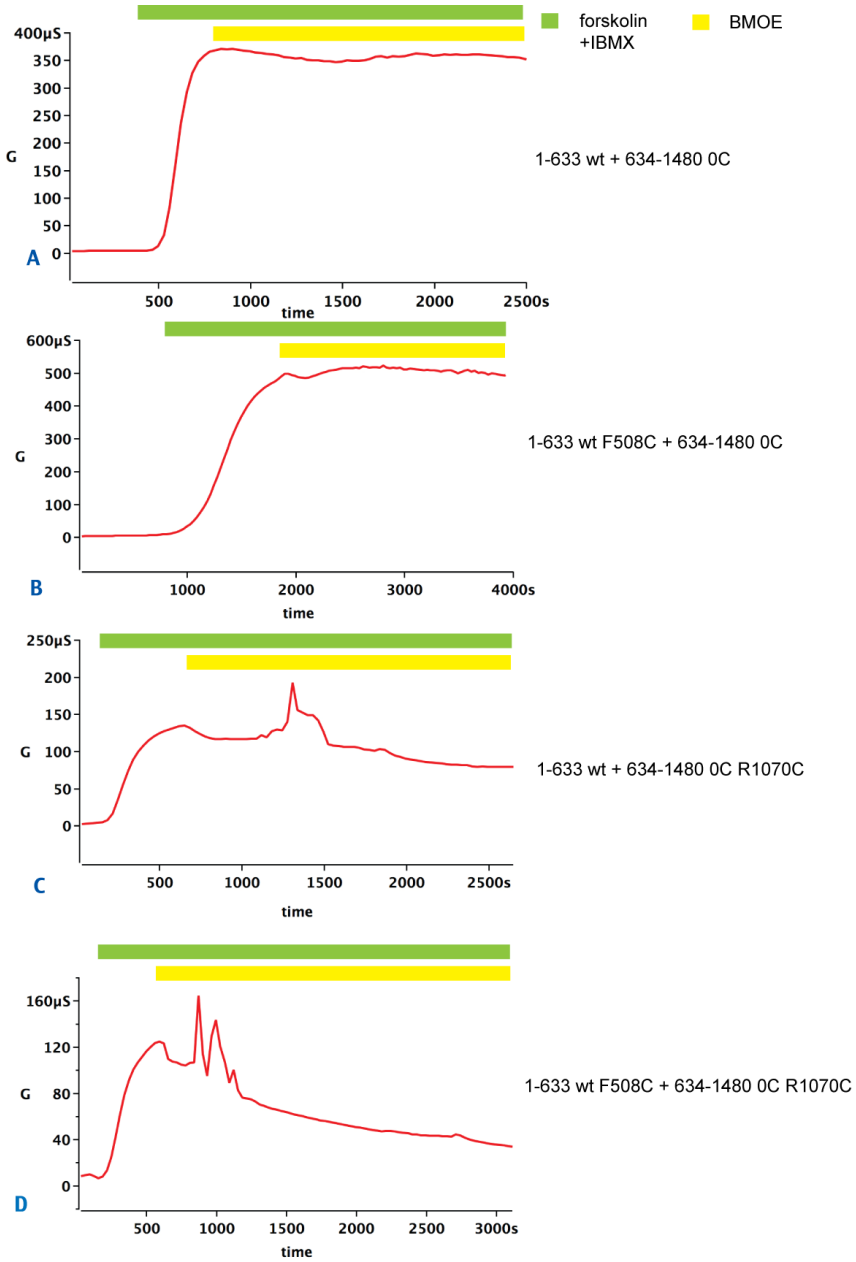

Figure 52. BMOE influence on the forskolin-induced conductance: examples of TEVC recordings for the pair of tested residues F508 and R1070.

Red traces show the changes of the whole cell conductance (G) of the oocytes expressing the background construct (A), single-cysteine mutants F508C (B) and R1070C (C), and the double-cysteine mutant F508C R1070C (D) recorded for about 40 min. Oocytes were pre-stimulated with forskolin (the stimulation period is marked as green bars above the traces) before the crosslinker BMOE was added to the perfusion solution (the BMOE application period is marked as yellow bars above the trace).

Upon the stimulation with forskolin, the whole cell conductance increased for all expressed constructs (Figure 52 A: 300-1000 s of the recording, Figure 52 B: 250-800 s, Figure 52 C: 200-500 s, Figure 52 D: 200-700 s), the amplitude differences reflect different expression level of CFTR.

The forskolin-induced conductance almost did not change for the oocytes expressing the background construct (Figure 52 A: 1000-2500 s of the recording) and the oocytes expressing the single-cysteine mutant F508C (Figure 52 B: 1800-3800 s), but decreased the conductance in oocytes expressing the mutants with the engineered cysteine R1070C, both single- and double-cysteine mutants (Figure 52 C: 700-1800 s, Figure 52 D: 700-2500 s).

Figure 53 summarizes the data.

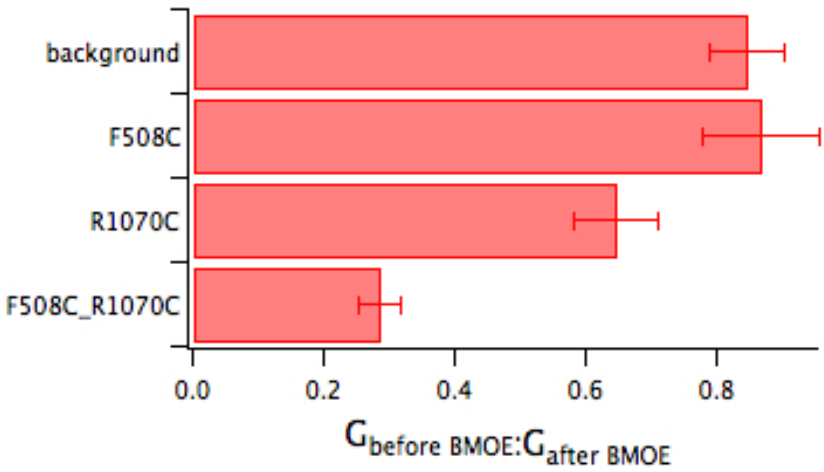

Figure 53. Effect of BMOE on the forskolin-induced conductance for the pair of tested residues F508 and R1070.

Each bar on the diagram represents a ratio of the whole-cell conductance of the pre-treated with forskolin oocytes after 30 min of the BMOE application ($G_{after\ BMOE}$) and before this application ($G_{before\ BMOE}$) averaged for 3-7 oocytes for each expressed construct. Error bars reflect the standard error of the mean.

BMOE almost did not change the whole-cell conductance of the oocytes expressing the background construct and the oocytes expressing the single-cysteine mutant F508C (Figure 53, top two bars) and decreased the whole-cell conductance of the oocytes expressing the mutants with the engineered cysteine R1070C (Figure 53, two bottom bars):

~40% conductance decrease for the single-cysteine mutant R1070C and ~70% conductance decrease for the double-cysteine mutant F508C R1070C was observed. In this case, a significant difference was expected if the crosslinking reaction between F508C and R1070C could occur.

In summary, the crosslinker somewhat decreased the response on forskolin for F508C mutant, but it was indistinguishable from the effect on the background/template CFTR. Mutants with the R1070C mutation were significantly affected by the crosslinker. The forskolin-induced current was smaller by a factor of more than 2 after BMOE application on the double-cysteine mutant. This indicates that BMOE affects the conductance by crosslinking stronger than if it reacts with only one cysteine.

4. Discussion

The present work aimed to identify points of possible inter- and intradomain interactions in CFTR and their involvement in conformational changes occurring during the channel gating cycle. Homology models for CFTR suggested amino acid residues expected to be involved in such interactions (see 1.2.2 and 1.3). The existence of these inter- and intradomain contacts was tested by means a cysteine-specific crosslinking method, where the corresponding channel state was assayed by two-electrode voltage-clamp (TEVC) technique.

After mutation of the selected pairs of target residues to cysteines, application of the bifunctional cysteine-specific crosslinker to the mutant CFTR channels allows investigation of the crosslinker influence on channel function. Conductance changes caused by the crosslinker in double-cysteine mutants, but not single-cysteine mutants, reflect the effect of crosslinking the target positions, perhaps trapping the channel in a fixed state. This implies that the tested residues approach each other to the distance spanned by the crosslinker's spacer arm.

4.1 Conductance fluctuations upon the crosslinker influence

Fluctuations of the whole cell conductance were observed in *Xenopus* oocytes upon sulfhydryl-specific reagents BMOE and NEM before the forskolin stimulation for all studied constructs and also intact oocytes. The amplitude of these fluctuations approached the size of the maximal CFTR conductance of the cell, suggesting activity of some channels allowing passing of millions of ions per second. The oscillatory character of these

conductance changes suggests possible activation of Ca^{2+}-dependent Cl^- channels (CaCC) by IP3-gated oscillatory release of Ca^{2+} from intracellular stores (Fewtrell 1993, Berridge 1994).

The CaCC channels are normally expressed in *Xenopus* oocytes and activated by increased cytosolic concentration of Ca^{2+}, which can be a result of Ca^{2+} release from intracellular stores (Miledi 1982, Barish 1983).

In the presented here experiments, IP3-receptors appear to be triggered by disturbances of the oocyte membrane upon BMOE or NEM application, which led to oscillatory Ca^{2+} release and resulted in conductance changes. The absence or decrease of these conductance fluctuations upon the forskolin stimulation is in agreement with the finding that activated CFTR reduces activation of CaCC in *Xenopus* oocytes (Kunzelmann, et al. 1997).

4.2 Cysteine-specific crosslinking of mutant CFTR: possible intramolecular interactions

4.2.1 ICL/ICL interfaces

In experiments with CFTR carrying mutants T164C (in ICL1) and L1059C (in ICL4), pre-treatment with the cysteine-specific crosslinker BMOE prevented the conductance increase in response to the forskolin stimulation for the double-cysteine mutant, whereas the single-cysteines mutants and the background constructs still showed this response. When BMOE was applied after the forskolin stimulation, the crosslinker decreased the forskolin-induced current significantly stronger for the double-cysteine mutants comparing to the single-cysteine ones.

Similar results were obtained for the pairs of residues I266/A969 (belonging to ICL2 and ICL3, respectively) and G971/S1049 (belonging to ICL3 and ICL4, respectively): BMOE applied before forskolin prevented the conductance increase for the double-cysteine mutant, BMOE applied after the forskolin stimulation decreased the forskolin-induced current. This effect was significantly stronger for the double-cysteine mutants comparing to the single-cysteine ones.

A possible explanation for the observed conductance changes is the formation of a covalent bond between two engineered cysteines by the crosslinker molecule. In this case, the crosslinked double-cysteine mutant cannot change its conformation upon the stimulation to allow the chloride ions to flow through the channel. As this reaction is only possible when the distance between two residues does not exceed 8 Å (the distance between two maleimide groups of BMOE), this implies the corresponding spatial proximity of the tested residues.

In case of the single-cysteine mutants, the observed conductance decrease was significantly smaller then for the double-cysteine mutants. This decrease also might be explained by the covalent reaction of the crosslinker with one engineered cysteine: the presence of the crosslinker molecule could lead to steric hindrance of intramolecular movements, which are necessary for the channel opening. This can result in decreased whole cell conductance. Such steric hindrance might also be a cause of conductance changes in case of the double-cysteine mutants: two crosslinker molecules might react with two engineered cysteines and result in diminished conductance. However, biochemical experiments for the double-cysteine mutant I266C/A969C give some additional evidence that the formation of a covalent bond between these engineered cysteines does take place: Western blot analysis shows that BMOE causes appearance of a band additional to those visualizing the CFTR halves containing one mutation (Figure 38). The molecular weight of this additional band is in the range of that for a full-length CFTR, suggesting that this band corresponds to the product of the crosslinking reaction: two halves of the CFTR molecule each carrying one engineered cysteine joined together by the crosslinker molecule. This means that these residues do approach each other to the distance of about 8 Å. This

biochemical evidence relates electrophysiological events observed during TEVC experiments to the crosslinking reaction between two engineered cysteines.

The obtained data suggest the spatial proximity of residues T164/L1059, I266/A969 and G971/S1049 in the closed state, as the crosslinker influence kept the channel in the closed state (or led to its failure to re-open, as the channels are opening and closing all the time before exposure to the crosslinker). However, a homology model of the human CFTR (Mornon, Lehn und Callebaut 2009), which was constructed on the basis of different MsbA structures, represents the channel in an inward-facing conformation corresponding the CFTR closed channel state (Figure 54) and predicts following distances between the mentioned residues (their Cα-atoms): about 3-4 Å between T164 and L1059, about 7-8 Å between I266 and A969, and about 17 Å between G971 and S1049 (Figure 55). This predicted proximity of residues T164 and L1059, as well as I266 and A969, would be in agreement with the data suggesting that the crosslinking of these pairs stabilize the closed state of the channel. However, the predicted distance between the residues G971 and S1049 in the closed state does not support the proposed crosslinking of the corresponding double-cysteine mutant stabilizing the closed state. A possible explanation for the diminished conductance in this case could be the reaction of both engineered cysteines with the crosslinker molecule and therefore stronger steric influence on the channel state. It is also possible that the crosslinking reaction between residues G971 and S1049 does not occur in the closed, but in the open state, trapping though the channel in a conformation, which fails to re-open. The faster decrease of the forskolin-induced current upon BMOE for G971C S1049C (Figure 47 D) comparing to T164C L1059C (Figure 31 D) and I266C A969C (Figure 36 D) could be explained that the crosslinking between G971C and S1049C appears to be facilitated when the channel is open. This supports the suggestion that the crosslinking reaction between G971C and S1049C could occur in the open CFTR state.

Intramolecular distances similar to those proposed by a homology model of the human CFTR (Mornon, Lehn und Callebaut 2009) are observed in the crystal structure of the heterodimeric ABC transporter TM287/288 in its closed (inward-facing) state (Hohl, et al. 2012): 6-7 Å between residues V96 (TM287) and I223 (TM288), which correspond to

T164 and L1059 of human CFTR according to the mentioned in 1.3 multiple sequence alignment performed in the laboratory by Dr. W. Labeikowsky; 4-7 Å between L199 (TM287) and H133 (TM288), which correspond to I266 and A969 of CFTR; 17-19 Å between D135 and G213 in TM288, corresponding to G971 and S1049 of CFTR.

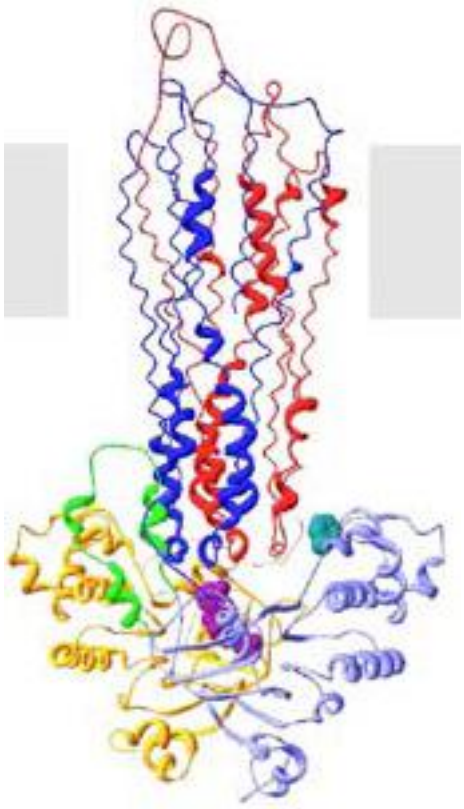

Figure 54. Homology model for CFTR representing the inward-facing conformation of CFTR (Mornon, Lehn and Callebaut 2009).

The model was constructed on the basis of the X-ray structures of the ABC transporter MsbA (Ward, et al. 2007). TMD1 and NBD1 are colored dark and light blue, respectively; TMD2 and NBD2 are colored red and orange, respectively.

A

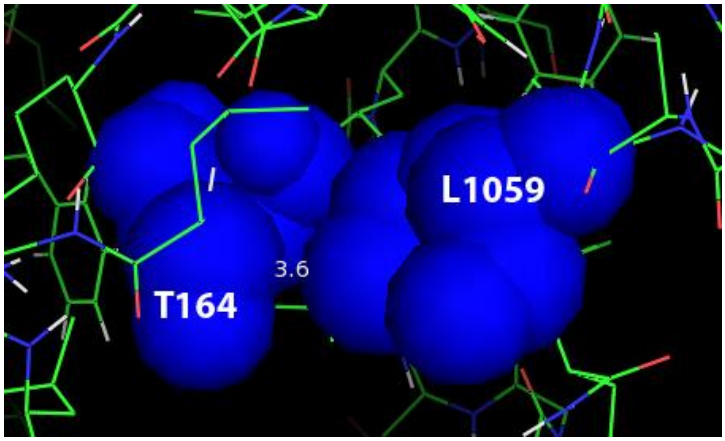

B

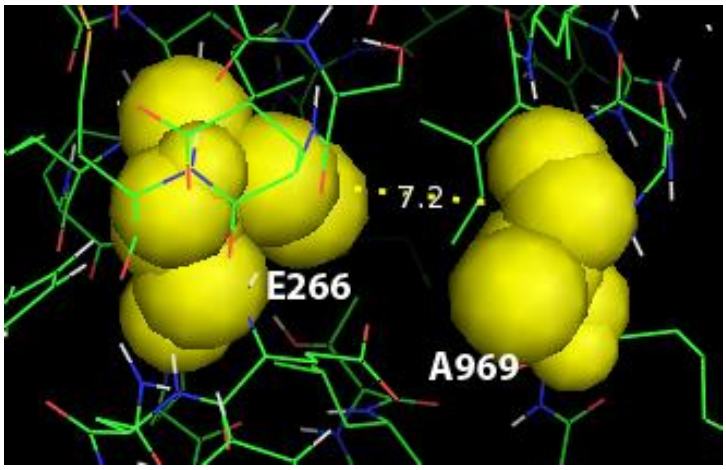

C

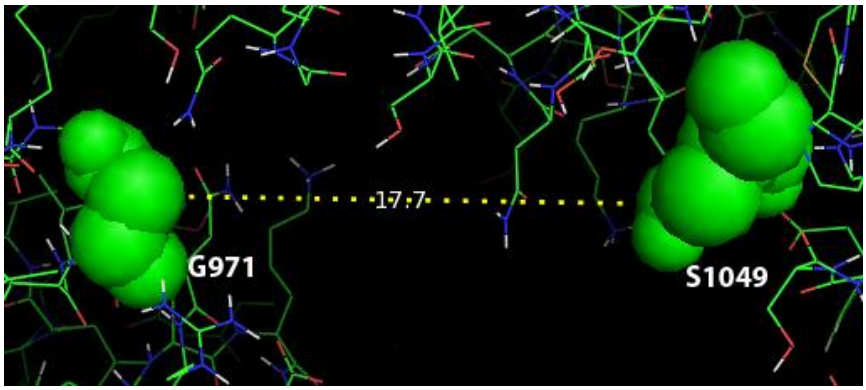

Figure 55. Distances (Å) between residues (Cα-atoms) T164 and L1059 (A), I266 and A969 (B), and G971 and S1049 (C), predicted by the homology model for CFTR representing the closed channel state (Mornon, Lehn and Callebaut 2009).

For the pair of residues G178/V260, the forskolin response for single- and double-cysteine mutants diminished after the BMOE pre-treatment, but not significantly different for all these mutants. Decrease of the forskolin-induced conductance upon BMOE was also not significantly different for single- and double-cysteine mutants. One possible explanation for this could be that residues 178 and 260 do not approach each other to a distance sufficient for a crosslinking reaction with BMOE. The mentioned homology model for CFTR (Mornon, Lehn und Callebaut 2009), representing the closed channel state (Figure 54), predicts a distance of about 18-19 Å between these residues in the closed state, which is too far to be joined by BMOE. A similar distance (19-22 Å) is observed in the structure of TM287/288 (Hohl, et al. 2012) between residues S110 and R193 (TM287), which correspond to residues G178 and V260 of human CFTR according to the alignment.

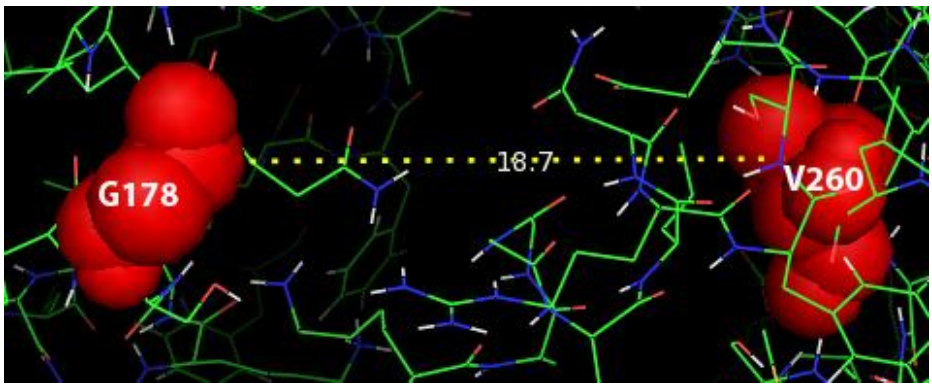

Figure 56. Distances (Å) between residues (Cα-atoms) G178 and V260 predicted by the homology model for CFTR representing the closed channel state (Mornon, Lehn and Callebaut 2009).

Another explanation is that the modification of either of these residues by the crosslinking leads to diminished overall conductance by steric effects that lower the open probability somewhat. This supports a prediction made by the homology model for CFTR (Mornon, Lehn und Callebaut 2008) of a possible steric hindrance with the main chain of ICL2, which could be caused by substitution of G178 with another residue. This steric hindrance might be caused by the substitution of G178 with cysteine as well as by the reaction of BMOE with each of these engineered cysteines. The significance of this residue

might find the experimental support in the stronger BMOE influence on the conductance of CFTR carrying G178C comparing even with the corresponding double-cysteine mutant (see 3.2.2). The last could be explained that the second mutation (V260C) replaces a branched amino acid residue valine with unbranched cysteine, which might have a positive influence on the mentioned steric issues.

4.2.2 ICL4/NBD1 interface

For the pair of residues F508/R1070, TEVC experiments showed similar results for the double- and the single-cysteine mutants with engineered cysteine R1070C: BMOE prevented response on the forskolin stimulation for both of these mutants, whereas the single-cysteines mutant F508C still showed the response on forskolin, as well as the background construct.

Similarly, when BMOE was applied after the forskolin stimulation, the crosslinker decreased the forskolin-induced current almost completely again for both mutants with R1070C, the single- and the double-cysteine one. Comparing to these data, our previous results for the pair of residues F508/L1065 (Jaksekovic, et al. 2008) showed that BMOE decreased the forskolin-induced current almost completely only for the double-cysteine mutant, whereas the single-cysteine mutant L1065C still kept the forskolin-induced current even under the BMOE influence.

The observed lack of significant difference between the BMOE effect on the double- and single-cysteine mutants with engineered cysteine R1070C could be related to conformational changes caused by the crosslinker molecule reacted with this residue leading to the relative stabilization of the closed channel state. This might reflect the significance of this residue for the intramolecular rearrangements during the gating cycle. The question, whether the crosslinking reaction between F508C and R1070C does take place, or whether the BMOE effect on the double-cysteine mutant should be related to the

steric rearrangements, still remains open. To distinguish between the crosslinking and steric hindrance in this case, biochemical experiments similar to those performed for the pair of residues I266/A969 could be helpful. Appearance of an additional band on the Western blot would support the presence of the crosslinking product. These findings would suggest NBD1/ICL4 interaction, confirming the domain-swapping architecture in CFTR, and would be in agreement with the crosslinking data of Serohijos at al. (Serohijos, et al. 2008). In that study, a homology model of CFTR (Figure 6) was constructed based on the known structure of the ABC exporter Sav1866 (Dawson and Locher 2006). To define the contacting sites between ICL4 and NBD1, pairs of cysteines were introduced at positions on this interface that are in close proximity according to the homology model. The study showed that F508 could be crosslinked to cysteines introduced at several positions in ICL4, including L1065, F1068, G1069, and F1074, reflecting the central role of this residue in this interface and in the interdomain interaction (Serohijos, et al. 2008).

4.2.3 ICL1/NBD2 and ICL2/NBD2 interfaces

Mutations on the ICL1/NBD2 and ICL2/NBD2 interfaces diminished the CFTR expression in *Xenopus* oocytes (ICL1: L172C, D173C, K174C; ICL2: A274C, Y275C) or completely depleted it (ICL1: I175C; NBD2: R1283C, Y1307C, D1341C). Interestingly, mutations of residues Y275, Y1307, I175 and R1283 were described in patients with CF (http://www.genet.sickkids.on.ca, Romey, et al. 1994, Cheadle, Meredith und al-Jader 1992). This suggests the significance of these positions for the normal channel expression and/or function.

4.3 Outlook

The approach applied in this work can gain structural information about CFTR as well as other channels and is a useful tool to study influence of structural rearrangements on the channel function *in vivo*. Electrophysiogical experiments combined with biochemical data can deliver strong evidence of structural proximity and functional interaction of amino acid residues belonging to different structural units of a protein. Further biochemical experiments would be useful to distinguish, whether the inferred crosslinking reaction between residues occurs, or whether altered conductance is a result of steric hindrance caused by attachment of the crosslinker molecule to a single cysteine. In the former case, the appearance of an additional band on a Western Blot could confirm the presence of the crosslinking product.

The obtained data confirm some predicted intramolecular interactions based on homology models, indicating that the models are therefore suitable for planning future experiments and drug discovery approaches.

References

Albrecht, C., et al. "A novel missense mutation in ABCA1 results in altered protein trafficking and reduced phosphatidylserine translocation in a patient with Scott syndrome." *Blood* 106 (2005): 542–549.

Aller, S. G., et al. "Structure of P-glycoprotein reveals a molecular basis for poly-specific drug binding." *Science* 323 (2009): 1718-1722.

Ambudkar, S. V., I. W. Kim, D. Xia, and Z. E. Sauna. "The A-loop, a novel conserved aromatic acid subdomain upstream of the Walker A motif in ABC transporters, is critical for ATP binding." *FEBS Lett.* 580 (2006): 1049-1055.

Andersen, D. H. "Cystic fibrosis of the pancreas and its relation to celiac disease: a clinical and pathological study." *Am. J. Dis. Child.* 56 (1938): 344–399.

Anderson, D. H., and R. G. Hodges. "Celiac syndrome; Genetics of cystic fibrosis of the pancreas with a consideration of etiology." *Am. J. Dis. Child.* 72 (1946): 62-80.

Anderson, M. P., D. P. Rich, R. J. Gregory, A. E. Smith, and M. J. Welsh. "Generation of cAMP-activated chloride currents by expression of CFTR." *Science* 251 (1991): 679-682.

Anderson, M. P., et al. "Demonstration that CFTR is a chloride channel by alteration of its anion selectivity." *Science* 253 (1991): 202-205.

Anderson, M. P., H. A. Berger, D. P. Rich, R. J. Gregory, A. E. Smith, and M. J. Welsh. "Nucleoside triphosphates are required to open the CFTR chloride channel." *Cell* 67 (1991): 775-784.

Anfenson, M. "The school-age child with cystic fibrosis." *J. Sch. Health.* 50, no. 1 (1980): 26-28.

Atwell, S., et al. "Structures of a minimal human CFTR first nucleotide-binding domain as a monomer, head-to-tail homodimer, and pathogenic mutant." *Prot. Eng. Des. Sel.* 23, no. 5 (2010): 375-384.

Barish, M. E. "A transient calcium dependent chloride current in the immature Xenopus oocyte." *J. Physiol.* 342 (1983): 309–325.

Bear, C. E., et al. "Purification and functional reconstitution of the cystic fibrosis transmembrane conductance regulator (CFTR)." *Cell* 68 (1992): 809-818.

Bear, C. E., F. Duguay, A. L. Naismith, N. Kartner, J. W. Hanrahan, and J. R. Riordan. "Cl channel activity in Xenopus oocytes expressing the cystic fibrosis gene." *J. Biol. Chem.* 266 (1991): 19142-19145.

Berger, H. A., et al. "Identification and regulation of the CFTR-generated chloride channel." *J. Clin. Invest.* 88 (1991): 1422-1431.

Berger, H. A., S. M. Travis, and M. J. Welsh. "Regulation of the cystic fibrosis transmembrane conductance regulator Cl channels by specific kinases and protein phosphatases." *J. Biol. Chem.* 268 (1993): 2037-2047.

Berridge, M. J., Dupont, G. "Spatial and temporal signalling by calcium." *Curr. Opin. Cell. Biol.* 6 (1994): 267-274.

Brown, T., and E. L. Schwind. "Update and review: Cystic fibrosis." *J. Genet. Couns.* 8, no. 3 (1999): 137-162.

Cheadle, J. P., A. L. Meredith, and L. N. al-Jader. "A new missense mutation (R1283M) in exon 20 of the cystic fibrosis transmembrane conductance regulator gene." *Hum. Mol. Genet.* 1, no. 2 (1992): 123-125.

Chen, J.-M., et al. "A combined analysis of the cystic fibrosis transmembrane conductance regulator: implications for structure and disease models." *Mol. Biol. Evol.* 18, no. 9 (2001): 1771-1788.

Cheng, S. H., D. P. Rich, J. Marshall, R. J. Gregory, M. J. Welsh, and A. E. Smith. "Phosphorylation of the R domain by cAMP-dependent protein kinase regulates the CFTR chloride channel." *Cell* 66 (1991): 1027-1036.

Cheng, S. H., R. J. Gregory, J. Marshall, S. Paul, D. W. Souza, and G. A. et al. White. "Defective intracellular transport and processing of CFTR is the molecular basis of most cystic fibrosis." *Cell* 63 (1990): 827-34.

Cheung, K., C. Leung, G. Leung, and P. Wong. "Synergistic effects of cystic fibrosis transmembrane conductance regulator and aquaporin-9 in the rat epididymis." *Biol. reprod.* 68, no. 5 (2003): 1505-1510.

Childs, S., and V. Ling. "The MDR superfamily of genes and its biological implications." *Important Adv. Oncol.*, 1994: 21–36.

Cole, K. S. "Dynamic electrical characteristics of the squid axon membrane." *Arch. Sci. Physiol.* 3 (1949): 253-258.

Cotten, J. F., L. S. Ostedgaard, and M. R., Welsh, M. J. Carson. "Effect of cystic fibrosis-associated mutations in the fourth intracellular loop of cystic fibrosis transmembrane conductance regulator." *J. Biol. Chem.* 271 (1996): 21279-21284.

Csanády, L., K. W. Chan, A. C. Nairn, and D. C. Gadsby. "Functional roles of nonconserved structural segments in CFTR's NH2-terminal nucleotide binding domain." *J. Gen. Physiol.* 125 (2005): 43–55.

Csanády, L., K. W. Chan, D. Seto-Young, D. C. Kopsco, A. C. Nairn, and D. C. Gadsby. "Severed Channels Probe Regulation of Gating of Cystic Fibrosis Transmembrane Conductance Regulator by Its Cytoplasmic Domains." 116, no. 3 (2000): 477-500.

Cui, L., et al. "Domain Interdependence in the Biosynthetic Assembly of CFTR." *J. Mol. Biol.* 365, no. 4 (2006): 981-994.

Dascal, N. "Voltage clamp recordings from Xenopus oocytes." *Curr. Protoc. Neurosci.*, 2000: 6.12.1-6.12.20.

Davidson, A. L., E. Dassa, C. Orelle, and J. Chen. "Structure, function, and evolution of bacterial ATP-binding cassette systems." *Microbiol. Mol. Biol. Rev.* 72, no. 2 (2008): 317–364.

Davidson, H., M. S. Taylor, A. Doherty, A. C. Boyd, and D. J. Porteous. "Genomic sequence analysis of Fugu rubripes CFTR and flanking genes in a 60 kb region conserving synteny with 800 kb of human chromosome 7." *Genome Res.* 10 (2000): 1194-1203.

Dawson, R. J., and K. P. Locher. "Structure of a bacterial multidrug ABC transporter." *Nature* 443 (2006): 180-185.

Dawson, R.J., K. Hollenstein, and K.P. Locher. "Uptake or extrusion: crystal structures of full ABC transporters suggest a common mechanism." *Mol. Microbiol.* 65 (2007): 250–257.

Dean, M. *The Human ATP-Binding Cassette (ABC) Transporter Superfamily.* Bethesda (MD): National Center for Biotechnology Information (US), 2002.

Dean, M., A. Rzhetsky, and R. Allikmets. "The human ATP-binding cassette (ABC) transporter superfamily." *Genome Res.* 11 (2001): 1156–1166.

Dean, M., and R. Allikmets. "Evolution of ATP-binding cassette transporter genes." *Curr. Opin. Genet. Dev.* 5, no. 6 (1995): 779–785.

Dean, M., and T. Annilo. "Evolution of the ATP-binding cassette (ABC) transporter superfamily in vertebrates." *Annu. Rev. Genomics Hum. Genet.* 6 (2005): 123–142.

Di Sant'Agnese, P. A., R. C. Darling, G. A. Perera, and E. Shea. "Abnormal electrolytic composition of sweat in cystic fibrosis of the pancreas. Clinical significance and relationship of the disease." *Pediatrics* 12 (1953): 549.

Diamond, G., T. F. Scanlin, M. A. Zasloff, and C. L. Bevins. "A cross-species analysis of the cystic fibrosis transmembrane conductance regulator. Potential functional domains and regulatory sites." *J. Biol. Chem* 266 (1991): 22761-22769.

DOI:10.2210/pdb3gd7/pdb. n.d.

Drumm, M. L., et al. "Chloride conductance expressed by F508 and other mutant CFTRs in Xenopus oocytes." *Science* 254 (1991): 1797-1799.

Du, K., M. Sharma, and G. L. Lukacs. "The DeltaF508 cystic fibrosis mutation impairs domain-domain interactions and arrests post-translational folding of CFTR." *Nature Struct. Mol. Biol.* 12 (2005): 17–25.

Farber, S. "Some organic digestive disturbances in early life." *J. Michigan Med. Soc.* 44 (1945): 406.

Fewtrell, C. "Ca2+ oscillations in non-excitable cells." *Annu. Rev. Physiol.* 55 (1993): 427-454.

Fiedler, M. A., Z. K. Nemecz, and G. E. Shull. "Cloning and sequence analysis of rat cystic fibrosis transmembrane conductance regulator." *Am. J. Physiol* 262 (1992): L779-L784.

Fragoso, M. A., V. Fernandez, R. Forteza, S. H. Randell, M. Salathe, and G. E. Conner. "Transcellular thiocyanate transport by human airway epithelia." *J. Physiol.* 561 (Pt 1) (2004): 183-194.

Gabriel, S. E., K. N. Brigman, B. H. Koller, R. C. Boucher, and M. J. Stutts. "Cystic fibrosis heterozygote resistance to cholera toxin in the cystic fibrosis mouse model." *Science* 266 (1994): 107-109.

Gadsby, D. C. "Ion channels versus pumps: the principle difference, in principle." *Nat. Rev. Mol. Cell Biol.* 10 (2009): 344–352.

Gadsby, D. C., and A. C. Nairn. "Regulation of CFTR channel gating." *Trends Biochem. Sci.* 19 (1994): 513-518.

Gadsby, D. C., P. Vergani, and L. Csanády. "The ABC protein turned chloride channel." *Nature* 440 (2006): 477-483.

Gelfi, C., P.G. Righetti, L. Cremonesi, and M. Ferrari. "Detection of point mutations by capillary electrophoresis in liquid polymers in temporal thermal gradients." *Electrophoresis* 15 (1994): 1506-1511.

Goffeau, A., B. Hertogh, and P.V. Baret. "ABC Transporters." In *Encyclopedia of Biological Chemistry. Vol. 1*, 1-5. 2004.

Gregory, R. J., et al. "Maturation and function of cystic fibrosis transmembrane conductance regulator variants bearing mutations in putative nucleotide-binding domains 1 and 2." *Mol. Cell. Biol.* 11 (1991): 3886-3893.

Gulyas-Kovacs, A., S.W. Lockless, and D.C. Gadsby. "Combining homology modeling and statistical coupling analysis to predict structure-function relationships in the CFTR chloride channel." *Poster presented at the Biophysical Society Annual Meeting.* Baltimore, MD, March 2007.

Hamosh, A., S. C. Fitz-Simmons, M. Jr. Macek, M. R. Knowles, B. J. Rosenstein, and G. R. Cutting. "Comparison of the clinical manifestations of cystic fibrosis in black and white patients." *J. Pediatr.* 132, no. 2 (1998): 255-259.

Hanrahan, J. W., Tabcharani, J. A., Grygorczyk, R. "Patch clamp studies of apical membrane chloride channels." In *Cystic Fibrosis: Current Topics*, by J. A. Dodge, D. J. H. Brock and J. H. Widdicombe, 93-137. New York: Wiley, 1993.

He, L., et al. "Multiple Membrane-Cytoplasmic Domain Contacts in the Cystic Fibrosis Transmembrane Conductance Regulator (CFTR) Mediate Regulation of Channel Gating." *J. Biol. Chem.* 283, no. 39 (2008): 26383–26390.

Higgins, C. F. "ABC transporters: from micro-organisms to man." *Annu. Rev. Cell. Biol.* 8 (1992): 67–113.

Higgins, C. F., et al. "A family of related ATP binding subunits coupled to many distinct biological processes in bacteria." *Nature* 323 (1986): 448-50.

Hiles, I. D., M. P. Gallagher, D. J. Jamieson, and C. F. Higgins. "Molecular characterization of the oligopeptide permease of Salmonella typhimurium." *J. Mol. Biol.* 195 (1987): 125-42.

Hodgkin, A. L., A. F. Huxley, and B. Katz. "Measurement of current-voltage relations in the membrane of the giant axon of Loligo." *J. Physiol.* 116 (1952): 424-448.

Hohl, M., C. Briand, M. G. Grütter, and M. A. Seeger. "Crystal structure of a heterodimeric ABC transporter in its inward-facing conformation." *Nat. Str. Mol. Biol.* 19, no. 4 (2012): 395-402.

Holland, I. B., S. P. C. Cole, K. Kuchler, and C. F. Higgins. *ABC Proteins: From Bacteria to Man.* London: Academic Press, 2003.

Hollenstein, K., D. C. Frei, and K. P. Locher. "Structure of an ABC transporter in complex with its binding protein." *Nature* 446 (2007): 213-216.

Hollenstein, K., R.J. Dawson, and K.P. Locher. "Structure and mechanism of ABC transporter proteins." *Curr. Opin. Struct. Biol.* 17 (2007): 412-418.

Horowitz, B., S. S. Tsung, P. Hart, P. C. Levesque, and J. R. Hume. "Alternative splicing of CFTR Cl channels in heart." *Am. J. Physiol.* 264 (1993): H2214-H2220.

http://www.genet.sickkids.on.ca. n.d.

Huang, S. Y., D. Bolser, H. Y. Liu, T. C. Hwang, and X. Q. .. Zou. "Molecular modeling of the heterodimer of human CFTR's nucleotide-binding domains using a protein-protein docking approach." *J. Mol. Graph. Model.* 27 (2009): 822-828.

Hung, L. W. et al. "Crystal structure of the ATP-binding subunit of an ABC transporter." *Nature* 396 (1998): 703–707.

Hyde, S. C., et al. „Structural model of ATP-binding proteins associated with cystic fibrosis, multidrug resistance and bacterial transport.“ *Nature* 346 (1990): 362-365.

Jacquemin, E. "Progressive familial intrahepatic cholestasis. Genetic basis and treatment." *Clin. Liver. Dis.* 4 (2000): 753–763.

Jaksekovic, I., A. Gulyas-Kovacs, A.B. Patel, R. Ram, and D.C. Gadsby. "The role of F508 and L1065 in the interaction between NBD1 and intracellular loop 4 of CFTR." *Poster presented at the Biophysical Society Annual Meeting.* Long Beach, CA, February 2008.

Jones, P. M., and A. M. George. "The ABC transporter structure and mechanism: perspectives on recent research." *Cell. Mol. Life Sci.* 61, no. 6 (2004): 682-699.

Kirk, K. L., and D. C. Dawson. *The Cystic Fibrosis Transmembrane Conductance Regulator.* New York, NY, USA: Kluwer Academic/Plenum Publishers, 2003.

Kleizen, B., T. van Vlijmen, H. R. de Jonge, and I. Braakman. "Folding of CFTR is predominantly cotranslational." *Mol. Cell* 20 (2005): 277–287.

Knowles, M., J. Gatzy, and R. Boucher. "Increased bioelectric potential difference across respiratory epithelia in cystic fibrosis." *N. Engl. J. Med.* 305 (1981): 1489.

Kopito, R. R. "Biosynthesis and Degradation of CFTR." *Physiol. Rev.* 79, Suppl. (1999): S167–S173.

Kulka, M., M. Gilchrist, M. Duszyk, and A. D. Befus. "Expression and functional characterization of CFTR in mast cells." *J. Leukoc. Biol.* 71 (1 2002): 54-64.

Kunzelmann, K., M. Mall, M. Briel, A. Hipper, and R., et al. Nitschke. "The cystic fibrosis transmembrane conductance regulator attenuates the endogenous Ca2+ activated Cl− conductance of Xenopus oocytes." *Pflügers Arch.* 435 (1997): 178–181.

Kuzumoto, M., A. Takeuchi, H. Nakai, C. Oka, A. Noma, and S. Matsuoka. "Simulation analysis of intracellular Na(+) and Cl(-) homeostasis during beta1-adrenergic stimulation of cardiac myocyte." *Prog. Biophys. Mol. Biol.* 96 (2007): 171-186.

Laemmli, U. K. "Cleavage of structural proteins during the assembly of the head of bacteriophage T4." *Nature* 227 (1970): 680–685.

Levesque, P. C., P. J. Hart, J. R. Hume, J. L Kenyon, and B. Horowitz. "Expression of cystic fibrosis transmembrane regulator Cl- channels in heart." *Circulation Research* 71 (1992): 1002-1007.

Lewis, H. A., et al. "Structure and dynamics of NBD1 from CFTR characterized using crystallography and hydrogen-deuterium exchange mass spectrometry." *J. Mol. Biol.* 396, no. 2 (2010): 406-430.

Lewis, H. A., et al. "Structure and dynamics of NBD1 from CFTR characterized using crystallography and hydrogen-deuterium exchange mass spectrometry." *EMBO J.* 23 (2010): 406-430.

Lewis, H. A., et al. "Structure of nucleotide binding domain 1 of the cystic fibrosis transmembrane conductance regulator." *EMBO J.* 23 (2004): 282-293.

Lewis, H. A., X. Zhao, C. Wang, J. M. Sauder, I. Rooney, and B. W. et al. Noland. "Impact of the deltaF508 mutation in first nucleotide-binding domain of human cystic fibrosis transmembrane conductance regulator on domain folding and structure." *J. Biol. Chem.* 280 (2005): 1346–1353.

Linsdell, P. "Mechanism of chloride permeation in the cystic fibrosis transmembrane conductance regulator chloride channel." *Exp. Physiol.* 99 (2006): 123–129.

Linton, K. J. "Structure and Function of ABC Transporters." *Physiology* 22, no. 2 (2007): 122-130.

Linton, K. J., and C. F. Higgins. "The Escherichia coli ATP-binding cassette (ABC) proteins." *Mol. Microbiol.* 28 (1998): 5–13.

Locher, K. P., A. T. Lee, and D. C. Rees. "The E. coli BtuCD structure: A framework for ABC transporter architecture and mechanism." *Science* 296 (2002): 1091–1098.

Locher, K.P. "Review: structure and mechanism of ATP-binding cassette transporters." *Phil. Trans. R. Soc.* 364 (2009): 239–245.

Marshall, J., et al. "Stoichiometry of recombinant cystic fibrosis transmembrane conductance regulator in epithelial cells and its functional reconstitution into cells in vitro." *J. Biol. Chem.* 269 (1994): 2987-2995.

Marshall, J., K. A. Martin, M. Picciotto, S. Hockfield, A. C. Nairn, and L. K. Kaczmarek. " Identification and localization of a dogfish homolog of human cystic fibrosis transmembrane conductance regulator ." *J. Biol. Chem* 266 (1991): 22749-22754.

Martinez-Mir, A., et al. "Retinitis pigmentosa caused by a homozygous mutation in the Stargardt disease gene ABCR." *Nat. Genet.* 18 (1998): 11–12.

Mendoza, J. L., and P. J. Thomas. "Building an understanding of cystic fibrosis on the foundation of ABC transporter structures." *Bioenerg. Biomembr. J.* 39 (2007): 499-505.

Mense, M., P. Vergani, D. M. White, G. Altberg, A. C. Nairn, and D. C. Gadsby. "In vivo phosphorylation of CFTR promotes formation of a nucleotide-binding domain heterodimer." *EMBO J.* 25 (2006): 4728-4739.

Miledi, R. "A calcium-dependent transient outward current in Xenopus laevis oocytes." *Proc. Natl. Acad. Sci. USA* 215 (1982): 491–497.

Miller, C. "CFTR: break a pump, make a channel." *Proc. Natl. Acad. Sci. USA* 107 (2010): 959-960.

Mimura, C. S., A. Admon, K. A. Hurt, and G. Ferro-Luzzi Ames. "The nucleotide-binding site of HisP, a membrane protein of the histidine permease, identification of amino acid residues photoaffinity labelled by 8-azido ATP." *J. Biol. Chem.* 265 (1990): 19535-19542.

Mornon, J.-P., P. Lehn, and I. Callebaut. "Atomic model of human cystic fibrosis transmembrane conductance regulator: Membrane-spanning domains and coupling interfaces." *Cell. Mol. Life Sci.* 65 (2008): 2594 – 2612.

Mornon, J.-P., P. Lehn, and I. Callebaut. "Molecular models of the open and closed states of the whole human CFTR protein." *Cell. Mol. Life Sci.* 66, no. 21 (2009): 3469-3486.

Norimatsu, Y., A. Ivetac, C. Alexander, J. Kirkham, and N. O'Donnell. "Cystic Fibrosis Transmembrane Conductance Regulator: A Molecular Model Defines the Architecture of the Anion Conduction Path and Locates a "Bottleneck" in the Pore." *Biochemistry* 51 (2012): 2199−2212.

Ostedgaard, L. S., et al. "Processing and function of CFTR-ΔF508 are species-dependent." *PNAS* 104 (2007): 15370–15375.

Pinkett, H. W., A. T. Lee, P. Lum, K. P. Locher, and D. C. Rees. "An inward-facing conformation of a putative metal-chelate-type ABC transporter." *Science* 315 (2006): 373–377.

Ponte-Sucre, A. *ABC Transporters in Microorganisms.* Caister Academic Press, 2009.

Qu, B. H., E. H. Strickland, and P. J. Thomas. "Localization and suppression of a kinetic defect in cystic fibrosis transmembrane conductance regulator folding." *J. Biol. Chem.* 272 (1997): 15739–15744.

Quinton, P.M. "Chloride impermeability in cystic fibrosis." *Nature* 301 (1983): 421.

Rees, D. C., E. Johnson, and O. Lewinson. "ABC transporters: the power to change." *Nat. Rev. Mol. Cell Biol.* 10 (2009): 218–227.

Rees, D. M., A. G. Leslie, and J. E. Walker. "The structure of the membrane extrinsic region of bovine ATP synthase." *Proc. Natl. Acad. Sci. USA* 106, no. 51 (2009): 21597-21601.

Reyes, C., and J. Chang. "Structure of the ABC transporter MsbA in complex with ADP-Vanadate and Lipopolysaccharide." *Science* 308 (2005): 1028-1031.

Rich, D. P., et al. "Expression of cystic fibrosis transmembrane conductance regulator corrects defective chloride channel regulation in cystic fibrosis airway epithelial cells." *Nature* 347 (1990): 358-363.

Rich, D. P., R. J. Gregory, M. P. Andeson, P. Manavalan, A. E.. Smith, and M. J. Welsch. "Effect of deleting the R-domain on CFTR generated chloride channels." *Science* 253 (1991): 205-207.

Riordan, J. R., et al. "Identification of the Cystic Fibrosis Gene: Cloning and Characterization of Complementary DNA." *Science* 245 (1989): 1066-1073.

Romey, M. C., M. Desgeorges, P. Malzac, J. Sarles, J. Demaille, and M. Claustres. "Homozygosity for a novel missense mutation (I175V) in exon 5 of the CFTR gene in a family of Armenian descent." *Hum. Mol. Gen.* 3, no. 4 (1994): 661-662.

Rosenberg, M. F., A. B. Kamis, L. A. Aleksandrov, R. C. Ford, and J. R. Riordan. "Purification and Crystallization of the Cystic Fibrosis Transmembrane Conductance Regulator (CFTR)." *J. Biol. Chem.* 279, no. 37 (2004): 39051-39057.

Rosenberg, M. F., Callaghan, R., S. Modok, C. F. Higgins, and R. C. Ford. "Three-dimensional structure of P-glycoprotein: the transmembrane regions adopt an asymmetric configuration in the nucleotide-bound state." *J. Biol. Chem.* 280 (2005): 2857–2862.

Seibert, F. S., P. Linsdell, T. W. Loo, J. W. Hanrahan, D. M. Clarke, and J. R. Riordan. "Disease-associated mutations in the fourth cytoplasmic loop of cystic fibrosis transmembrane conductance regulator compromise biosynthetic processing and chloride channel activity." *J. Biol. Chem.* 271 (1996): 15139-15145.

Seibert, F. S., P. Linsdell, T. W. Loo, J. W. Hanrahan, J. R. Riordan, and D. M. Clarke. "Cytoplasmic loop three of cystic fibrosis transmembrane conductance regulator contributes to regulation of chloride channel activity." *J. Biol. Chem.* 271 (1996): 27493-27499.

Serohijos, A. W., et al. "Phenylalanine-508 mediates a cytoplasmic–membrane domain contact in the CFTR 3D structure crucial to assembly and channel function." *Proc. Nat. Acad. Sci. USA* 105, no. 9 (2008): 3256-3261.

Sheppard, D. N., S. M. Travis, H. Ishihara, and M. J. Welsh. "Contribution of proline residues in the membrane-spanning domains of cystic fibrosis transmembrane conductance regulator to chloride channel function." *J. Biol. Chem.* 271, no. 25 (1996): 14995-15001.

Short, D. B., et al. "An apical PDZ protein anchors the cystic fibrosis transmembrane conductance regulator to the cytoskeleton." *J. Biol. Chem.* 273, no. 31 (1998): 19797-19801.

Shrimpton, A. E., D. Borowitz, and P. Swender. "Cystic fibrosis mutation frequencies in upstate New York." *Hum. Mutat.* 10, no. 6 (1997): 436-442.

Shumaker, H., H. Amlal, R. Frizzell, C. D. Ulrich, and M. Soleimani. "CFTR drives Na+-nHCO3 cotransport in pancreatic duct cells: a basis for defective HCO3 secretion in CF." *Am J Physiol Cell Physiol*, 1999: 276: C16-C25.

Singer, T. D., S. J. Tucker, W. S. Marshall, and C. F. Higgins. "A divergent CFTR homologue: highly regulated salt transport in the euryhaline teleost F. heteroclitus." *Am. J. Physiol* 274 (1998): C715-C723.

Stemmer, W. P., Crameri, A., Ha, K. D., Brennan, T. M., Heyneker, H. L. "Single-step assembly of a gene and entire plasmid from large numbers of oligodeoxyribonucleotides." *Gene* 164 (1995): 49–53.

Stühmer, W. *Electrophysiological recording from Xenopus oocytes.* Vol. 207, in *Methods in enzymology*, by B. Rudy and L. Iverson, 319-339. San Diego: Academic press, Inc. , 1992.

Stutts, M. J., et al. "CFTR as a cAMP-dependent regulator of sodium channels." *Science* 269 (1995): 847-50.

Sullivan, L. P., D. P. Wallace, and J. J. Grantham. "Epithelial transport in polycystic kidney disease." *Physiol. Rev.* 78, no. 4 (1998): 1165-1191.

Tabcharani, J. A., X. B. Chang, J. R. Riordan, and J. W. Hanrahan. "Phosphorylation-regulated Cl¬ channel in CHO cells stably expressing the cystic fibrosis gene." *Nature* 352 (1991): 628–631.

Tang, L., M. Fatehi, and P. Linsdell. "Mechanism of direct bicarbonate transport by the CFTR anion channel." *J. Cyst. Fibros.* 8, no. 2 (2009): 115-121.

Tata, F., et al. "Cloning the mouse homolog of the human cystic fibrosis transmembrane conductance regulator gene." *Genomics* 10, no. 2 (1991): 301-307.

Tebbutt, S. J., C. J. Wardle, D. F. Hill, and A. Harris. "Molecular analysis of the ovine cystic fibrosis transmembrane conductance regulator gene." *Proc. Natl. Acad. Sci. USA* 92, no. 6 (1995): 2293-2297.

Thibodeau, P. H., C. A. Brautigam, M. Machius, and P. J. Thomas. "Side chain and backbone contributions of Phe508 to CFTR folding." *Nat. Struct. Mol. Biol.* 12 (2005): 10-16.

Thomas, P. J., B. H. Qu, and P. L. Pedersen. "Defective protein folding as a basis of human disease." *Trends Biochem. Sci.* 20 (1995): 456-459.

Tousson, A., B. A. Van Tine, A. P. Naren, G. M. Shaw, and L. M. Schwiebert. "Characterization of CFTR expression and chloride channel activity in human endothelia." *Am. J. Physiol.* 275, no. 6 Pt 1 (1998): C1555-C1564.

Tucker, S. J., D. Tannahill, and C. F. Higgins. " Identification and developmental expression of the Xenopus laevis cystic fibrosis transmembrane conductance regulator gene." *Hum. Mol. Genet* 1 (1992): 77-82.

Vergani, P., S. W. Lockless, A. C. Nairn, and D. C. Gadsby. "CFTR channel opening by ATP-driven tight dimerization of its nucleotide-binding domains." *Nature* 433, no. 7028 (2005): 876-880.

Walker, J. E., M. Saraste, M. J. Runswick, and N. J. Gay. "Distantly related sequences in the a- and 13-subunits of ATP synthase, myosin, kinases and other ATP requiring enzymes and a common nucleotide binding fold." *EMBO J* 1 (1982): 945-51.

Wang, W., and P. Linsdell. "Conformational change opening the CFTR chloride channel pore coupled to ATP-dependent gating." *Biochim. Biophys. Acta* 1818 (2012): 851–860.

Ward, A., C.L. Reyes, J. Yu, C.B. Roth, and G. Chang. "Flexibility in the ABC transporter MsbA: Alternating access with a twist." *Proc. Natl. Acad. Sci. USA* 48, no. 104 (2007): 19005-19010.

Ward, C. L., S. Omura, and R. R. Kopito. "Degradation of CFTR by the ubiquitin-proteasome pathway." *Cell* 83 (1995): 121–127.

Welsh, M. J., L. -C. Tsui, F. Boat, and A. L. Beaudet. "Cystic fibrosis." In *The Metabolic and Molecular Basis of inherited Disease.*, by C. R. Scriver, A. L. Beaudet, W. S. Sly and D. Valle, 3799-3876. New York.: McGraw-Hill Inc., 1995.

Zaitseva, J., S. Jenewein, T. Jumpertz, I. B. Holland, and L. Schmitt. "H662 is the linchpin of ATP hydrolysis in the nucleotide-binding domain of the ABC transporter HlyB." *EMBO J.* 24 (2005): 1901-1910.

Zeitlin, P. L., et al. "CFTR protein expression in primary and cultured epithelia." *Proc. Natl. Acad. Sci. USA* 89, no. 1 (1992): 344-347.

Zhang, Z. R., G. Cui, X. Liu, B. Song, D.C. Dawson, and N.A. McCarty. "Determination of the functional unit of the cystic fibrosis transmembrane conductance regulator chloride channel: One polypeptide forms one pore." *J. Biol. Chem.* 280, no. 1 (2005): 458–468.

Zielenski, J., et al. "Genomic DNA sequence of the Cystic Fibrosis Transmembrane Conductance Regulator (CFTR) Gene." *Genomics* 10, no. 1 (1991): 214-228.

Zielenski, J., et al. "Identification of mutations in exons 1 through 8 of the cystic fibrosis transmembrane conductance regulator (CFTR) gene." *Genomics* 10, no. 1 (1991): 229–235.